AD-A100 905 AVCO EVERETT RESEARCH LAB INC EVERETT MA F/G 20/5
MODE MEDIUM INTERACTION. A THEORETICAL STUDY.(U)
SEP 80 A BALLANTYNE, C DUZY F49620-79-C-0195
UNCLASSIFIED AFOSR-TR-81-0519 NL

1 OF 2
AD A
100905

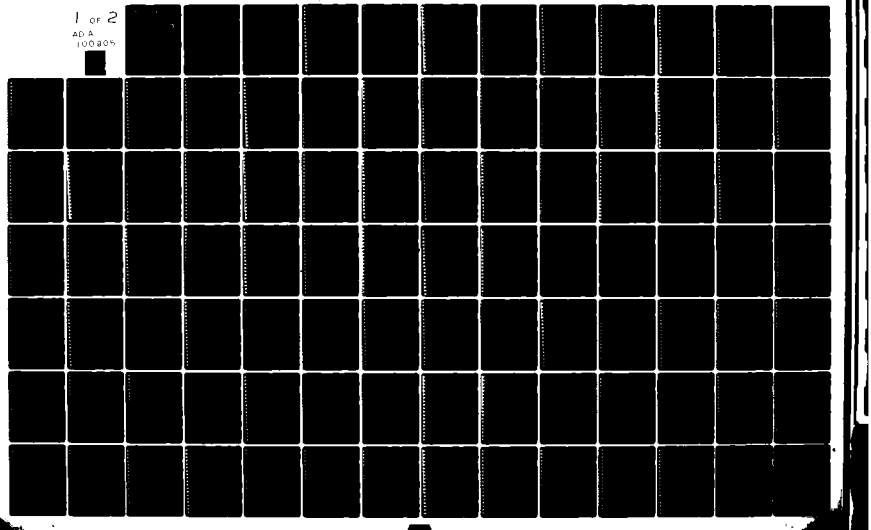

LEVEL II

(1)

MODE MEDIUM INTERACTION: A THEORETICAL STUDY

Avco Everett Research Laboratory, Inc.
a Subsidiary of Avco Corporation
2385 Revere Beach Parkway
Everett, MA 02149

September 1980
Final Technical Report for Period 1 July 1979 – 30 June 1980

F49620-79-C-0195

Sponsored by

AIR FORCE OFFICE OF SCIENTIFIC RESEARCH (AFSC)
UNITED STATES AIR FORCE
Bolling Air Force Base, D.C. 20332

UNCLASSIFIED

SECURITY CLASSIFICATION OF THIS PAGE (When Data Entered)

REPORT DOCUMENTATION PAGE	READ INSTRUCTIONS BEFORE COMPLETING FORM
1. REPORT NUMBER: AFOSR-TR-81-0519	2. GOVT ACCESSION NO.: AD-A100 905	3. RECIPIENT'S CATALOG NUMBER
4. TITLE (and Subtitle): Mode Medium Interaction: A Theoretical Study.	5. TYPE OF REPORT & PERIOD COVERED: Final Technical Report. 1 Jul 79 - 30 Jun 80.
	6. PERFORMING ORG. REPORT NUMBER
7. AUTHOR(s): A. Ballantyne, C. Duzy	8. CONTRACT OR GRANT NUMBER(s): F49620-79-C-0195
9. PERFORMING ORGANIZATION NAME AND ADDRESS: Avco Everett Research Laboratory, Inc. 2385 Revere Beach Parkway Everett, MA 02149	10. PROGRAM ELEMENT, PROJECT, TASK AREA & WORK UNIT NUMBERS: 61102F 2301/A7
11. CONTROLLING OFFICE NAME AND ADDRESS: Air Force Office of Scientific Research United States Air Force/NP Bolling Air Force Base, D.C. 20332	12. REPORT DATE: September 1980
	13. NUMBER OF PAGES: 173
14. MONITORING AGENCY NAME & ADDRESS(if different from Controlling Office)	15. SECURITY CLASS. (of this report): Unclassified
	15a. DECLASSIFICATION/DOWNGRADING SCHEDULE

16. DISTRIBUTION STATEMENT (of this Report)

Approved for public release; distribution unlimited.

17. DISTRIBUTION STATEMENT (of the abstract entered in Block 20, if different from Report)

18. SUPPLEMENTARY NOTES

19. KEY WORDS (Continue on reverse side if necessary and identify by block number)

CO_2 Laser	Transfer Function	Chemical Laser	Unstable Resonator
Brillouin Scattering	Instability	Supersonic Laser	Modes
Acoustic Noise	Acoustic Instability	Perturbed Resonator	Gain Saturation
Alignment Sensitivity	Electron-Discharge Laser	Mode-Medium Interaction	Saturated Gain
			Diffraction

20. ABSTRACT (Continue on reverse side if necessary and identify by block number)

An instability in the output of a high-power unstable-resonator cw CO_2 laser is analyzed in terms of the perturbative effect of an acoustic wave which is induced by laser heating. The alignment sensitivity of such a laser is also explained in terms of a temperature gradient along the gas-flow direction, which is transverse to the laser axis. We extend our instability analysis to a simple one-dimensional model of a supersonic laser, which we

DD FORM 1 JAN 73 1473 EDITION OF 1 NOV 65 IS OBSOLETE

UNCLASSIFIED 048450

SECURITY CLASSIFICATION OF THIS PAGE (When Data Entered)

81 6 29 205

(20)
determine to be stable. Finally, we present a new computational technique to determine the intensity distribution and output coupling of the modes of an unstable resonator whose gain is saturated by a variable amount by the flux of the lowest-loss mode. The intensity distribution of this lowest-loss mode is determined self consistently.

FOREWORD

The following authors contributed to the work described in this report: A. Ballantyne, C. Duzy, A. Flusberg, D. Korff, M.J. Smith, and M. Tekula.

TABLE OF CONTENTS

LIST OF ILLUSTRATIONS

SECTION I

INTRODUCTION

Understanding the performance of high-power lasers requires a model of the system response to external perturbations. In the case of small perturbations about some equilibrium value the system response can be characterized by a (frequency-dependent) transfer function.

As the simplest example of such a transfer function, consider the problem of relaxation oscillations in a conventional laser. The system can be described by the following set of equations:

$$\frac{\partial \phi}{\partial \tau} = c\ (g - g_c)\phi \tag{1}$$

$$\frac{\partial g}{\partial t} = -\frac{g}{\tau}\left(1 + \frac{\phi}{\phi_s}\right) + P \tag{2}$$

where

ϕ = system flux

g = system gain/unit length

ϕ_s = saturation flux

τ = upper state deactivation time

c = speed of light

g_c = cavity coupling

P = external pumping

Let us now assume steady-state pumping with a small perturbation, i.e.,

$$P = P_o + P_1, \tag{3}$$

where P_o is the steady-state component and P_1 is the perturbation. Similarly, if

$$\phi \equiv \phi_o + \phi_1 \tag{4}$$

$$g \equiv g_o + g_1 \tag{5}$$

$$r \equiv 1 + \phi_o/\phi_s \tag{6}$$

we have the following equations (after Laplace transforming, denoted by $\tilde{\phi}(s)$, etc.)

$$\begin{pmatrix} s & -cg_o \\ \frac{r-1}{\tau} & s + \frac{r}{\tau} \end{pmatrix} \begin{pmatrix} \tilde{\phi}_1/\phi_o \\ \tilde{g}_1/g_o \end{pmatrix} = \begin{pmatrix} 0 \\ \tilde{P}_1 \end{pmatrix} \tag{7}$$

In this case

$$\begin{pmatrix} \tilde{\phi}_1/\phi_o \\ \tilde{g}_1/g_o \end{pmatrix} = \begin{pmatrix} s & -cg_o \\ \frac{r-1}{\tau} & s - \frac{r}{\tau} \end{pmatrix} \begin{pmatrix} o \\ \tilde{P}_o \end{pmatrix} \equiv \mathbf{A}^{-1} \begin{pmatrix} \\ \tilde{P}_1 \end{pmatrix} \tag{8}$$

The transfer function matrix, $\mathbf{A}^{-1}$, is given by

$$\mathbf{A}^{-1} = \frac{1}{s(s + \frac{r}{\tau} + cg_o\,(\frac{r-1}{\tau})} \begin{pmatrix} s + \frac{r}{\tau}\,cg_o \\ -\,(\frac{r-1}{\tau}) \quad s \end{pmatrix} \tag{9}$$

If any singularities occur with Real $s > 0$, the system has an instability.

In this case, the roots occur at

$$s = -\frac{2r}{\tau} \pm i\sqrt{\frac{2g_o(r-1)}{\tau}} \tag{10}$$

i.e., at a frequency

$$\omega_o = \sqrt{\frac{2g_o(r-1)}{\tau}} \tag{11}$$

with a damping factor of

$$\Gamma = 2r/\tau \tag{12}$$

and no instability obtains.

In this report we will show that a realistic transfer function for high-power lasers must include the acoustic, or thermodynamic degrees of freedom as well. The reason for this inclusion can be seen in schematic form in Figure 1.

Gain and flux perturbations lead to density perturbations via local heating. This, in turn, causes refractive index fluctuations and flux perturbations which close the cycle.

We will show below three separate examples of this expanded approach to the system transfer function and system stability. The first two deal with CO_2 EDLs, although the formalism can be generalized to other types of lasers. The third deals explicitly with the chemical laser.

We shall see that when the thermodynamic degrees of freedom are included, the possibility of a system instability exists. In fact, such an instability has actually been found experimentally in the case of a cw CO_2 electron-discharge laser (EDL).

We shall now briefly outline the remainder of this report. Section II contains a discussion of an instability arising from the transfer of energy from an initially oscillating cavity mode to a different transverse mode by an acoustic wave. The approach to this problem is the solution of a perturbed propagator equation, i.e., an integral equation for the change in the electromagnetic wave after a round-trip traversal of the acoustically perturbed cavity. Two simplifying assumptions made in this

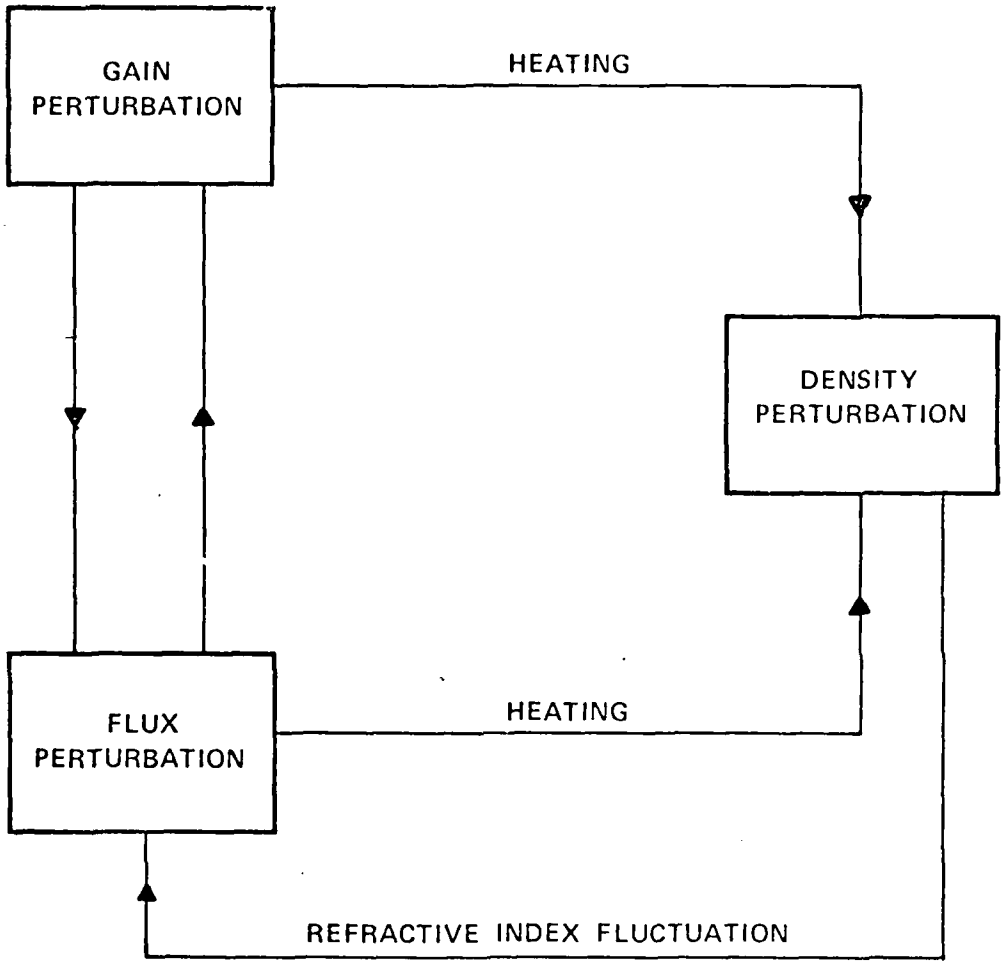

J6185

Figure 1. Schematic Indication of the Coupling of Flux, Gain, and Thermodynamic Degrees of Freedom

section are that (a) the initially oscillating mode has a uniform transverse fluence distribution and (b) that both electromagnetic modes have the same natural frequency of oscillation. It is shown that the oscillatory heating which occurs can result in an unstable interaction between the two electromagnetic waves and the acoustic wave, i.e., a perturbation whose amplitude increases exponentially.

In Section III we discuss a different type of instability: alignment sensitivity. Variations in the gas density along the flow direction lead to both gain variations and slight changes in the propagation direction of a light mode. We show that this can result in extreme cavity alignment sensitivity.

In Section IV we return to the mode-medium interaction problem of Section II, which is now reformulated in the language of Brillouin scattering (differential treatment). We show the equivalence of the differential and integral formulations of the mode-medium interaction. We focus, however, on an alternative instability mechanism. We show that an acoustic wave of frequency ω_A tends to resonantly couple an initially oscillating mode to a new transverse mode whose natural frequency is offset by ω_A from the natural frequency of the intial mode. This is just the ordinary Brillouin effect. We derive equations of motion for the amplitude of the new mode and for the acoustic wave. The secular equation for the system is derived. It is shown to be unstable in the limit of negligible gain-flux oscillations (that is, with a ratio of cavity flux to saturation flux $<< 1$, so that gain saturation may be ignored). A brief discussion is given of the nonlinear saturation of this process.

An idealization of the mode-medium interaction theory of Sections II and IV is the implicit assumption that the net loss (= loss minus gain) of two cavity modes may be very nearly equal. (See Appendix A.) At the beginning of this program it was realized that no self-consistent calculation of the eigenmodes of a loaded (i.e., gain-saturated), unstable resonator of moderate Fresnel number, such as a cw electron-discharge laser, existed. Such a calculation, which clearly is quite relevant to this program, is described for the first time in Section V. Using a new computational technique developed at AERL, we have solved for the self-consistent eigenmodes of an unstable resonator whose gain is saturated by the presence of a strong oscillating mode (the "fundamental" mode). We find that the fluence distributions of the various eigenmodes are modified by the saturation, and that the eigenvalues are shifted from their empty-resonator values. In particular, the empty-resonator loss degeneracy which exists at certain half-integral values of Fresnel number disappears in the presence of a saturated gain, i.e., different modes are found to have different losses. This is a significant new result which

suggests that it is not advantageous to avoid half-integral values of Fresnel numbers in the design of an unstable resonator which will be operated in the saturated-gain regime. From the point of view of our program, the results of this section suggest that the model of Sections II and IV, which assumes that at least some modes have nearly equal net loss, is somewhat simplistic. However, the nonuniformity of the gas density has been neglected in this section; it is possible that when the nonuniformity is taken into account the net losses of several modes may be very nearly equal.

In Section VI we extend our instability-theory techniques to a relatively simple model of a supersonic chemical laser (HF/DF). The model corresponds to a one-dimensional flowfield. The fluid-mechanic, chemical and optical coupling equations are obtained and Laplace transformed. The stability of the system is studied by use of the Routh Criterion, which allows the sign of the roots of a polynomial equation to be determined. Numerical calculations for typical operating conditions of the model laser show that it is stable. The important result of this model is that it determines the transfer function of the system. The transfer function can be used to predict the magnitude of the laser response to any external perturbation.

Finally, in Appendix A, we discuss the acoustically perturbed optical resonator in a more rigorous fashion. Using the integral-operator formalism, we derive the equation satisfied by the amplitudes of the various eigenmodes in the presence of the acoustic perturbation. We reformulate, in the language of quantum mechanical perturbation theory, the difference between the instability mechanisms discussed in Sections II and IV; both follow from the present treatment. We suggest an alternative model to explain the experimentally observed flux modulation in the electron-discharge laser: one in which only a single eigenmode oscillates, but an acoustic standing wave both modulates the cavity loss and is driven by nonuniform heating caused by the nonuniformity of the eigenmode and changes of the cavity flux.

SECTION II

A THREE-WAVE LASER INSTABILITY

A. INTRODUCTION

It has been known for some time[1] that high-power CO_2 cw Electric Discharge Lasers (EDL) exhibit output instabilities. This is evidenced via a spontaneous oscillation of the output flux usually resulting in full modulation.

An example of such behavior for a typical CO_2 cw EDL is shown in Figure 2. To the left of point "a" the output is stable, while to the right of point "b" the instability has already built up. Between "a" and "b" the output may be considered linearly unstable, and periodic in nature. This suggests the possible success of a linearized model, with the (linear) instability evidencing itself via an exponentially growing root of the characteristic equation of the system.

Corroboration of such a model may be obtained by reviewing interferograms of the laser taken with flux extraction (Figure 3). Also shown is the laser output flux versus time with the points corresponding to the three interferograms as indicated. We note the presence of low amplitude density (or acoustic) standing waves between anode and cathode where the instability in the output flux is already evident. It is as if the laser were being acoustically-Q-switched.

Further evidence of an acoustic connection can be found in the period of the output oscillations. Typical oscillations of a gain-flux system, such as are found in relaxation of a gain-switched spike, are of the order of a few microseconds. As can be seen from Figures 2 and 3, the period of the oscillations is of the order of 50 μsec. For typical anode-cathode separation of about 5 cm, with an acoustic mode number ~ 5 (Cf. Figure 3), the acoustic time is typically

$$t \sim \frac{(5\ \text{cm}/5)}{3 \times 10^4\ \text{cm/sec}} \sim 35\ \mu\text{sec}$$

---

1. Yoder, M.J. and Ahouse, D.R., Appl. Phys. Lett., 27, 673 (1975).

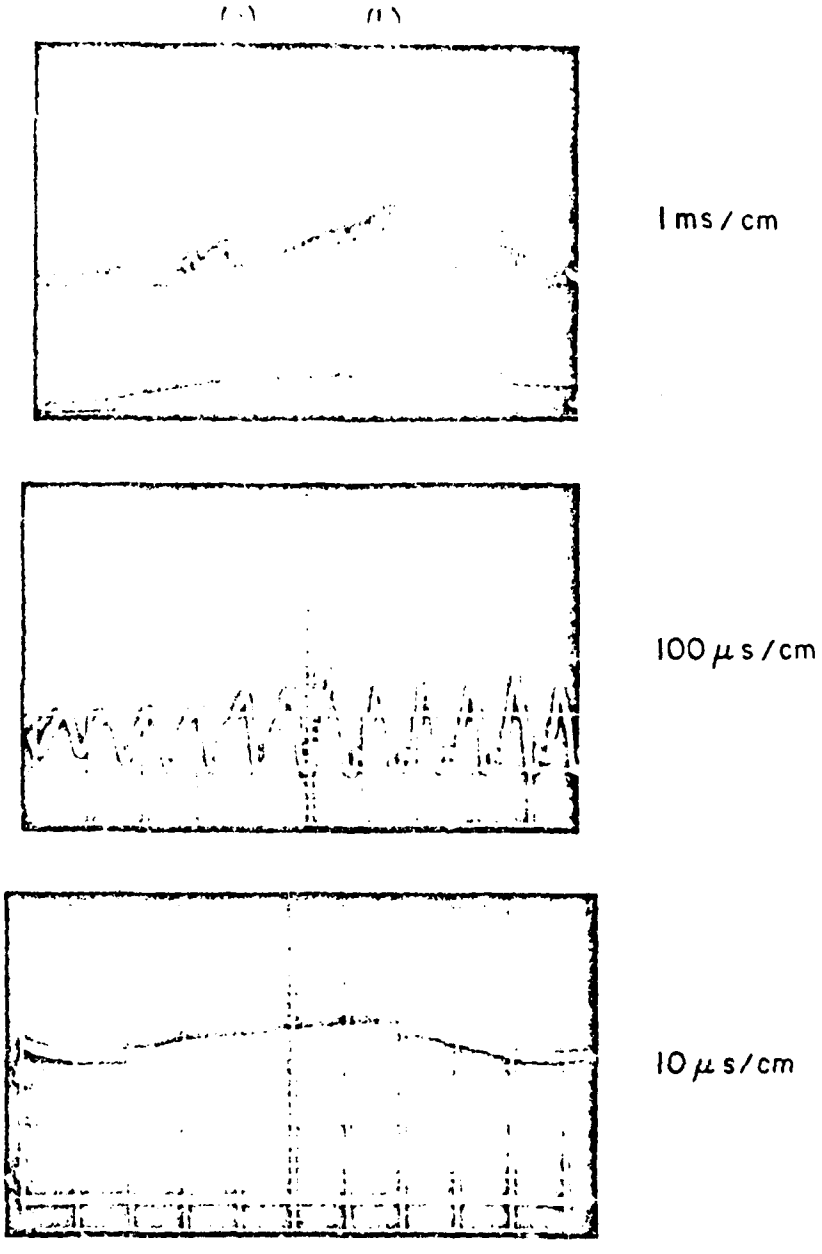

Figure 2. Evidence of Linear Instability. The upper trace in the top figure is the flux and the bottom is sustainer current. The first three msec show a dc output whereupon the flux begins to oscillate. At this point there is a floating zero level due to detector sensitivity. The lower figures are expanded time scales at incipient breakup of flux.

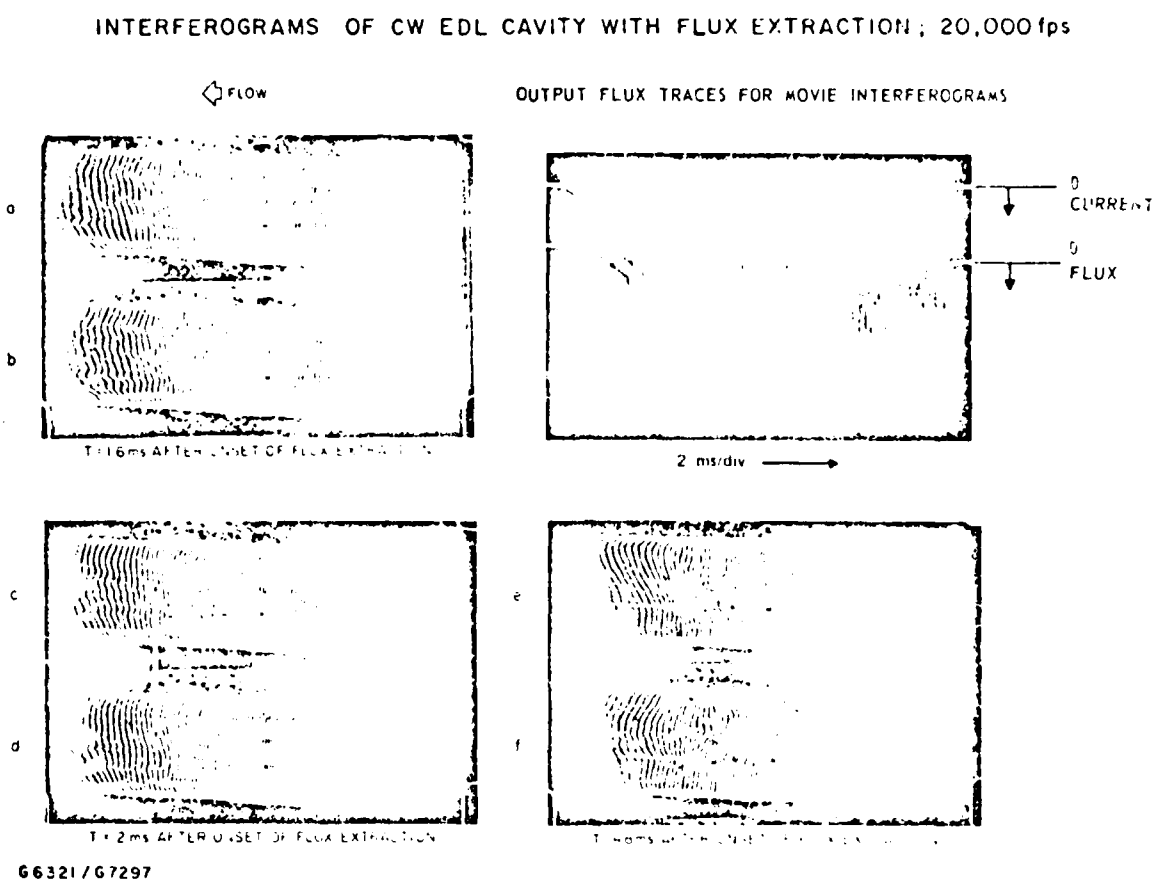

Figure 3. Mach Zender Interferograms of the Flow. The output flux trace is shown as the lower curve in the upper right with positive downward. The flux is stable up to about 2 msec whereupon the Q-switching occurs. The three interferograms are before, at, and after onset of full scale oscillators. Each picture shows two exposures separated by 25 μsec. The large scale waves evident at 4.8 msec are a result of the oscillations and not the cause as they do not appear earlier. At 2 msec notice the presence of a standing transverse wave of a few fringes and about 3 or 4 cycles. It is this wave that produces the oscillations in the flux.

In this section, we will describe a model of flux-gain-acoustic (density) coupling which admits an instability and derive an analytic expression for the unstable root in certain limiting cases. A subsequent paper will present a more rigorous formulation, comparison with experiment, and experimental methods of removing the instability.

B. THE MODEL

A schematic model of the CO_2 CWEDL is shown in Figure 4. The flow, anode-cathode, and optical axis directions are along the x, y, z axes, as shown in Figure 4.

The anode is below and the cathode above, the plane of the paper. Furthermore, we take the plane z = 0 as lying midway between the mirrors. Assuming that the change of the medium is negligible in a round trip photon time (2 L/c) we may write the following integral equation for the complex amplitude

$$u\left(x, y, z = 0, t_o + \frac{2L}{c}\right) =$$

$$\int K_{op}\ (x, x'; y, y', z = 0, s, t_o)\ u\ (x', y', z = 0, t_o)\ dx'dy' \tag{13}$$

In Eq. (13) u represents the amplitude for either the left or right going flux; the propagation operator K_{op} is a function of the state of the medium; and s denotes the path taken by a ray from (x', y', z' = 0) to (x, y, z = 0).

In the presence of small perturbations, we make the decomposition

$$K_{op} = K_{op\ (o)} + K_{op\ (1)}\ (t) \tag{14}$$

for the propagator and

$$u = \exp\{i(k_o z - \omega_o t)\}[u_o(x, y, z) + u_1(x, y, z, t)] \tag{15}$$

for the complex amplitude, where k_o, ω_o are the wavenumber and angular frequency of the light. both u_o and u, are assumed to vary slowly over a distance comparable to a wavelength. By definition of u_o, $K_{op\ (o)}$ and of what constitutes a laser mode we have

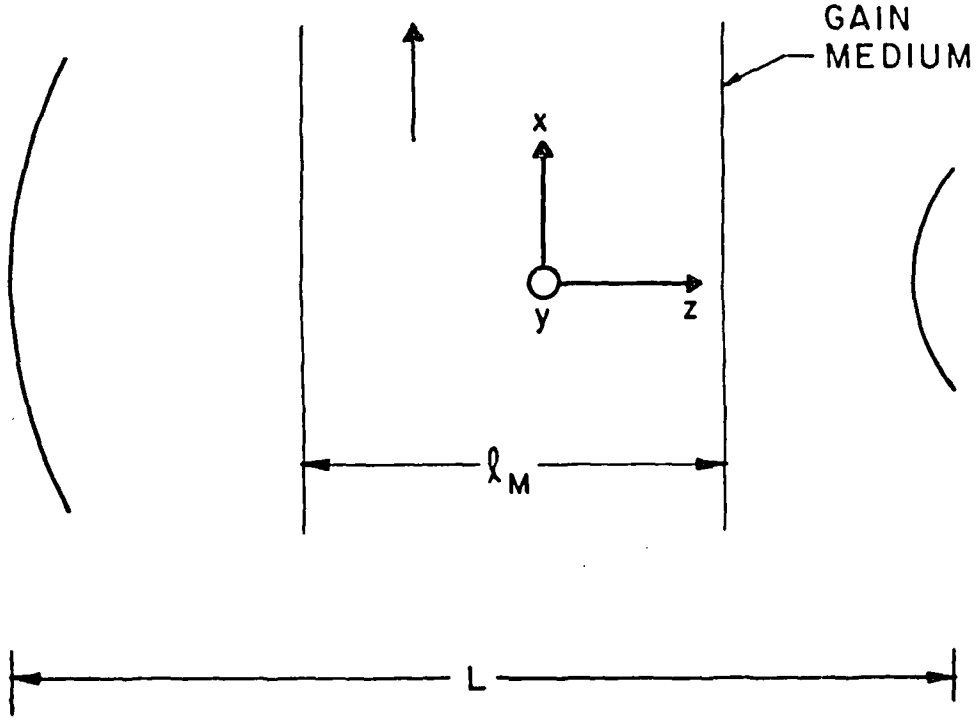

J6184

Figure 4. A Schematic Description of the CO_2 CWEDL

$$u_o\,(x,\ y,\ z = 0,\ t_o + \frac{2L}{c}) =$$

$$\int K_{op\ (o)}\ (x,\ x',\ y,\ y';\ z = 0)\ u_o\ (x',\ y',\ z' = 0)\ dx'dy' \tag{16}$$

Keeping terms to first order in Eq. (13) and using Eqs. (14) - (16) we have

$$\left[u_o(t_o + \frac{2L}{c}) + u_1\ (t_o + \frac{2L}{c})\right] \exp\{- i\omega_o(\frac{2L}{c})\} = \int K_{op\ (o)}\ u_o\ dx'dy'$$

$$+ \int K_{op\ (1)}\ u_o\ dx'dy' + \int K_{op\ (o)}\ u_1\ dx'dy' \tag{17}$$

If $2L\omega_o/c = n\pi$ where n is an integer (i.e., we have a longitudinal mode) then

$$u_1(x,\ y,\ z = 0,\ t_o + \frac{2L}{c}) = \int K_1(t_o)\,u_o\ dx'dy' + \int K_o\ u_1(t_o)\,dx'dy' \tag{18}$$

Expanding the left-hand side of Eq. (18) in a Taylor series, we obtain

$$u_1(x,\ y,\ z = 0,\ t) + \frac{2L}{c}\,\dot{u}_1 \approx \int K_1\ u_o\ dx'dy' + \int K_o\ u_1\ dx'dy' \tag{19}$$

or

$$\frac{2L}{c}\,\frac{\partial u_1}{\partial t} = \int [K_o - \delta(x-x')\ \delta\ (y-y')]\ u_1\ (x',\ y',\ z' = 0,\ t_o)\,dx'dy'$$

$$+ \int K_1\ (x,\ x';\ y,\ y')\ u_o\ dx'dy' \tag{20}$$

In physical terms the second term on the right-hand side of Eq. (29) represents scattering "into" u_1, whereas the first term is leakage "out of" u_1. If u_1 is an approximate eigenmode of the loaded resonator with eigenvalue close to unity, the first term on the right-hand side will be second order and can be dropped. We investigate the meaning of this condition in greater detail in Appendix A. We have then

$$\frac{\partial u_1}{\partial t} = \frac{c}{2L} \int K_1(x, x', y, y')\, u_o\, dx'dy' \qquad (21)$$

In most applications it is the flux perturbation which is experimentally of interest and which couples to gain and density perturbations in the medium. To obtain the flux equation corresponding to Eq. (21) we multiply both sides by u_o^* and take the real part of both sides. We obtain

$$\frac{\partial}{\partial t} (u_o^* u_1 + u_o u_1^*) = \frac{c}{2L} \left[u_o^* \int K_1\, u_o\, dx'dy' + c.c. \right] \qquad (22)$$

We note that

$$\phi = \phi_o + \phi_1 = |u_o + u_1|^2 = u_o^2 + (u_o^* u_1 + u_o u_1^*) + O\,(|u_1|^2) \qquad (23)$$

so that

$$\phi_1 = u_o^* u_1 + u_o u_1^* \qquad (24)$$

We now assume that the lowest mode u_o is independent of x,y (i.e., spatially uniform), so that u_o may be taken outside the integral on the right hand side of Eq. (22). This will be most valid for small equivalent Fresnel numbers, but is a reasonable first approximation in any case.

$$\frac{\partial \phi}{\partial t} = \frac{\partial \phi_1}{\partial t} = \frac{c}{2L}\, \phi_o \left[\int K_1\, dx'dy' + c.c. \right] \qquad (25)$$

As we have noted K_1 will be directly related to the perturbations of the medium. We now turn to expressing K_1 in terms of density and gain perturbations.

Assuming the medium reacts slowly in a time 2L/c, the propagator K_{op} can be written in the form

$$K_{op}(x, y; x', y'; z = 0, s, t) = \qquad (26)$$

$$\frac{i}{2\lambda L} \exp\left\{ i\, \frac{2\pi}{\lambda} \int_{x',y'}^{x,y} n(x, y; x', y'; t, z' = 0, s)\, d\, s \right\}$$

Where the path is the line segmented geometric path from (x', y') to (x,y) and n is the complex refractive index. An illustration for the typical points is given below in Figure 5.

For the unperturbed medium, we have, simply

$$K_{op\ (o)} = \frac{i}{2\lambda L} \exp\left\{ i \frac{2\pi}{\lambda} \int_{(x',y')}^{(x,y)} n_o \, ds \right\} \tag{27}$$

Hence, if

$$n = n_o + n_1 \tag{28}$$

$$K_{op\ (1)} = K_{op} - K_{op\ (o)} = K_{op\ (o)} \left[\exp\left\{ i \frac{2\pi}{\lambda} \int n_1 \, ds \right\} - 1 \right] \tag{29}$$

For sufficiently small values of n_1 (less than one fringe displacement on an interferogram) we may expand the exponential in Eq. (29) to obtain

$$K_{op\ (1)} \approx i \frac{2\pi}{\lambda} \left[\int_{(x',y')}^{(x,y)} n_1 \, ds \right] K_{op\ (o)} \tag{30}$$

Substituting Eq. (30) into Eq. (25) there results for either the left or right running flux

$$\frac{\partial \phi_1}{\partial t} = \frac{c\phi_o}{2L} \frac{2\pi i}{\lambda} \left[\int K_{op\ (o)} \left\{ \int_{(x'y')}^{(x,y)} n_1 \, ds \right\} dx'dy' - \int K_{op}{}^{*}{}_{(o)} \left\{ \int_{(x',y')}^{(x,y)} n_1{}^{*} \, ds \right\} dx'dy' \right] \tag{31}$$

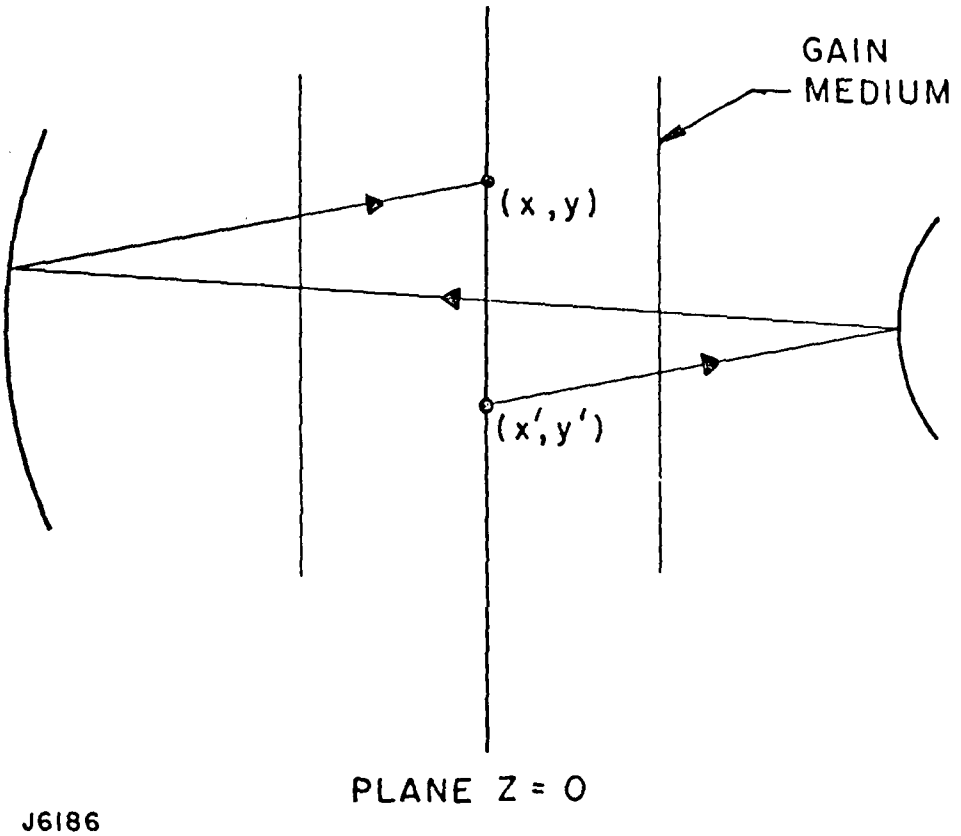

Figure 5. Illustrating the Propagator via which the Medium at (x',y') on the Nth Pass Influences the Light Amplitude at (x,y) on the (N + 1)st Pass

If the left and right flux are equal, Eq. (31) can be considered as the equation for the total flux. The right-hand side of Eq. (31) may be transformed by writing

$$\int K_{op}\,(x,\, x';\, y,\, y') \int_{(x',y')}^{(x,y)} n_1(s,\, t)\, ds$$

$$\equiv \int K_2(x,\, y;\, x',\, y')\; n_1\,(x',\, y',\, t)\; dx'dy' \qquad (32)$$

(definition of K_2)

If n_1 is assumed to be independent of z, then K_2 will be a property of the unperturbed laser (i.e., independent of n_1). As we shall see below, there exist excellent reasons for making this assumption. Finally, writing

$$n_1 = n_{1_R} + i\, n_{1_I} \qquad (33)$$

there results

$$\frac{\partial \phi_1}{\partial t} = \frac{c\phi_o}{2L}\,\frac{2\pi}{\lambda}\left[i\int (K_2 - K_2^*)\; n_{1_R}\; dx'dy' - \int (K_2 + K_2^*)\; n_{1_I}\; dx'dy'\right] \qquad (34)$$

We now define

$$\alpha_R(x,\, x';\, y,\, y') \equiv \frac{i2\pi\beta_g}{\lambda\rho_a}\quad (K_2 - K_2^*) \qquad (35)$$

$$\alpha_I(x,\, x';\, y,\, y') \equiv \quad K_2 - K_2^* \qquad (36)$$

where β_g is the Gladstone-Dale constant for the medium and ρ_a is the density of the gas mixture at one atmosphere pressure. Noting that, by definition

$$n_{1_R} = \frac{\beta_g \rho_1}{\rho_a} \tag{37}$$

and

$$-\frac{2\pi}{\lambda} n_{1_I} = g_1 \tag{38}$$

we have, finally

$$\frac{\partial \phi_1}{\partial t}(x, y, t) = \frac{c\phi_o}{2L}\left[\int \alpha_R(x, x'; y, y')\, \rho_1(x', y', t)\, dx'dy' + \int \alpha_I(x, x'; y, y')\, g_1(x', y', t)\, dx'dy'\right] \tag{39}$$

To appreciate the physical content of Eq. (39), we transform, spatially as follows:

(a) In the y (anode-cathode) direction we take a finite Fourier cosine transform.

(b) In the x direction we perform an exponential Fourier transform. Since the steady-state flux, ϕ_o, is nonzero only over a finite region, we get convolutions. To finesse this problem we smooth in k_x-space over a region 2/b, where b is the length of the flow channel. That is, we define

$$\phi_{1K} = \frac{1}{2/b} \int_{K_x - 1/b}^{K_x + 1/b} \phi_1(K_x)\, dx \tag{40}$$

We may now cast Eq. (39) in the form

$$\frac{d\phi_{1m,k}}{dt} = \frac{c\phi_o}{2L} \sum_{m',K'} \left(\alpha_{Rmm',KK'}\, \rho_{1m'K'} + \alpha_{Imm'KK'}\, g_{1m'K'}\right) \tag{41}$$

We now postulate that one acoustic mode will be favored above all others, and that this mode has no variation on a scale less than b (in the flow direction) and has m = ℓ, say, in the y direction. The reason for this assumption, as well as a prescription for estimating ℓ, will be given below.

Equation (41) now becomes the pair of equations.

$$\frac{d\phi_{1_{o,o}}}{dt} = \frac{c\phi_o}{2L}\left[\alpha_{R_{o\ell,oo}}\frac{\rho_{1_{\ell,o}}}{\rho_o} + 2\ell_M\, g_{1_{o,o}}\right] \tag{42}$$

(where ℓ_M is the medium thickness)

$$\frac{d\phi_{1_{\ell,o}}}{dt} = \frac{c\phi_o}{2L}\left[\alpha_{R_{\ell\ell,oo}}\frac{\rho_{1_{\ell,o}}}{\rho_o} + 2\ell_M\, g_{1_{\ell,o}}\right] \tag{43}$$

In Eqs. (42) and (43) we have tacitly assumed

$$\alpha_{Imm';oo} = \delta_{mm'} \tag{44}$$

since the main effect of a gain variation is to change the flux in the same spatial manner. We note further that Eq. (42) is an equation for the rate of change of the output flux and as such

$$\alpha_{R_{o\ell,oo}}\,\rho_{1_{\ell,o}} \equiv -g_{c_1} \tag{45}$$

can be considered to be a time varying modulation of the cavity coupling. Equation (40), on the other hand, describes the variation of the "ℓ"th Fourier component of the flux distribution. The following physical interpretation can be given to Eq. (40). When the laser is turned on there will be some acoustic noise (density fluctuations) between anode and cathode which can be expanded in a Fourier series. Each acoustic mode constitutes a phase diffraction grating for the incident flux ϕ_o. In Appendix B we will show that the following statements can be made about the scattered light:

a. The acoustic gain and optical modes will have a transverse variation with period a/n, where "a" is the anode-cathode separation, and n is given by

$$n^2 = a^2/\lambda L \tag{46}$$

b. A plane wave scattered by an acoustic wave will, after one trip, produce a flux oscillation with the same transverse wavelength as the original acoustic wave.

c. The variation of the acoustic perturbation in the optical propagation direction can be neglected.

Furthermore, we note that if we take u_o as a constant for the lowest mode, then the higher Fourier components $u_{1\ell}$ (recall $\phi_{1\ell} = u_o^* u_{1\ell} + u_o u_{1\ell}^*$) are orthogonal to u_o and it is reasonable to assume that the higher-order modes are representable by sines and consines to the same extent that the lowest order mode is representable by a constant. This simple picture, incidentally, allows us to make a realistic estimate of the influence coefficient $\alpha_{R\ell\ell,oo}$ (henceforth referred to as α) in Eq. (43).

Technically, the quantity α enters into the model equations as the influence coefficient from a sinusoidal density variation on one pass to a sinusoidal flux variation on the next pass of the laser radiation.

The radiation diffracts through the standing acoustic wave, which acts as a phase grating, and completes a round trip, reinforcing the density wave. Thus reinforcement arises by having the perturbed radiation in the same physical shape (same spatial Fourier component) as the density wave. The reinforcement is accomplished via heating.

The perturbation in the amplitude of the scattered light (due to diffraction) is

$$u_1 \sim (e^{i\delta} - 1)\, u_o \sim i\, u_o \delta \tag{47}$$

Where u_o is the incident amplitude and δ is the (sinusoidally, spatially varying) change in the optical path. The change in the flux, ϕ, is given by

$$\Delta\phi_1 \sim u_o^* u_1 + u_o u_1^* \sim |u_o|^2 \delta = \phi_o \delta \tag{48}$$

Hence, in one pass

$$\frac{\Delta\phi_1}{\phi_o} \sim \delta \sim \frac{2\pi\beta_g}{\lambda} \frac{\delta\rho}{\rho_a} \ell_m \tag{49}$$

Where ℓ_m is the optical length through the medium, β_g is the Gladstone-Dale constant, and ρ_a is the density of the medium at one atmosphere

The equation in which α enters is of the form

$$\frac{\partial \phi_{1\ell}}{\partial t} = \frac{c}{2L} \left(2\ell_m g_{1\ell} + \alpha \frac{\rho_{1\ell}}{\rho_o}\right) \phi_o \tag{50}$$

From this equation, the change in one pass due to a density perturbation is given by

$$\frac{\Delta\phi_{1\ell}}{\phi_o} \sim \frac{2L/c \frac{\partial \phi_{1\ell}}{\partial t}}{\phi_o} \sim \alpha \frac{\rho_{1\ell}}{\rho_o} \tag{51}$$

By comparing Eqs. (49) and (51) we obtain

$$\alpha \approx \frac{2\pi \beta_g \rho_o \ell_m}{\lambda \rho_a} \tag{52}$$

We now proceed to a consideration of the gain and heating equations necessary to complete the model. The gain equation for the flowing CO_2 medium is ($\phi_s \equiv$ saturation flux)

$$\left(\frac{\partial g}{\partial t} + v \frac{\partial g}{\partial x}\right) \approx - \frac{g}{\tau} - \frac{g\phi}{\tau \phi_s} + P \tag{53}$$

Where τ is the effective deactivation time from the upper lasing level of the CO_2 molecule, including the effects of the nitrogen in the gas mix, and P is the pumping.

Once again, we consider the perturbed form of Eq. (53) (v is the mean flow velocity)

$$\frac{\partial g_1}{\partial t} + v \frac{\partial g_1}{\partial x} \approx - \frac{g_1}{\tau} - \frac{g_1 \phi_o}{\tau \phi_s} - \frac{g_o \phi_1}{\tau \phi_s} \tag{54}$$

The effect of the flowing term is to damp the growth of any perturbations with a damping time of the order of the convection time through the cavity. This is of the order of b/v where b is the beam dimension in the direction of flow. Hence, Eq. (54) becomes

$$\frac{\partial g_1}{\partial t} \approx - \frac{r g_1}{\tau} - \frac{v g_1}{b} - \frac{g_o (r-1)}{\tau} \frac{\phi_1}{\phi_o} \tag{55}$$

Where $r \equiv 1 + \frac{\phi_o}{\phi_s}$

The ℓth component of Eq. (55) will be of the form

$$\frac{\partial g_{1\ell}}{\partial t} + \frac{v}{b} g_{1\ell} = - \frac{r g_{1\ell}}{\tau} - \frac{g_o (r-1)}{\tau} \frac{\phi_{1\ell}}{\phi_o} \tag{56}$$

To complete the coupled set of equations we use the fact that perturbations in the gain and flux amount to a perturbation in the heating profile in the medium. This, in turn, will affect the density perturabations, completing the loop.

The acoustic equations for a flowing medium and non-isentropic flow can be obtained from the equations of momentum, continuity, and from the first law of thermodynamics. In Appendix C we show that the heating equation is of the form

$$\left(\frac{\partial}{\partial t} + v \frac{\partial}{\partial x}\right)\left(\left(\frac{\partial}{\partial t} + v \frac{\partial}{\partial x}\right)^2 - c_s^2 \nabla^2\right) p_1 = (\gamma - 1) \nabla^2 P_1 \tag{57}$$

Where P_1 is the perturbation in the power per unit volume given by

$$P_1 = \frac{\nu_1}{\nu} (g_o \phi_1 + g_1 \phi_o) + \frac{\nu_3}{\nu} g_1 \phi_s \tag{58}$$

where

$$\nu \equiv \nu_3 - \nu_1, \tag{59}$$

and ν_3, ν_1 represent the upper and lower frequencies of the lasing transition. Combining Eqs. (57) - (59) with the prescription (Cf. Appendix C),

$$v \frac{\partial}{\partial x} \sim \frac{v}{b} \tag{60}$$

(where b is the dimension of the beam in the direction of the flow) we obtain

$$\left(\frac{\partial}{\partial t} + \frac{v}{b}\right)\left[\left(\frac{\partial}{\partial t} + \frac{v}{b}\right)^2 - c_s^2\, \nabla^2\right]\rho_1 =$$
$$(\gamma-1)\ \nabla^2\left[\frac{\nu_1}{\nu}\ (g_o\phi_1 + g_1\phi_o) + \frac{\nu_3}{\nu}\ g_1\phi_s\right] \tag{61}$$

For the ℓth component we have

$$\nabla^2 \sim \partial_y^2 \sim \left(\frac{\ell\pi}{a}\right)^2 \tag{62}$$

Where "a" is the anode-cathode spacing. Hence,

$$\left(\frac{\partial}{\partial t} + \frac{v}{b}\right)\left[\left(\frac{\partial}{\partial t} + \frac{v}{b}\right)^2 - c_s^2\left(\frac{\ell\pi}{a}\right)^2\right]\rho_{1\ell}$$
$$= (\gamma-1)\left(\frac{\ell\pi}{a}\right)^2\left[\frac{\nu_1}{\nu}\ (g_o\phi_{1\ell} + g_{1\ell}\phi_o) + \frac{\nu_3}{\nu}\ g_{1\ell}\phi_s\right] \tag{63}$$

Equations (43), (56), and (63) constitute one set of coupled equations. To find the normal modes of the system we use Laplace transforms of our variables $\rho_{1\ell}$, $g_{1\ell}$ and $\phi_{1\ell}$

$$\tilde{\phi}_{1\ell}(S) = \int_o^\infty \phi_{1\ell}(t)e^{-St}\, dt \tag{64}$$

etc. This allows us to make the replacement

$$\frac{\partial}{\partial t}\ \phi_1(t) \to S\ \tilde{\phi}_1(S), \text{ etc.} \tag{65}$$

In matrix form our coupled equations become

$$\mathbb{A}\begin{pmatrix} \tilde{\phi}_{1\ell}/\phi_o \\ \tilde{g}_{1\ell}/g_o \\ \tilde{\rho}_{1\ell}/\rho_o \end{pmatrix} = 0 \tag{66}$$

Where

$$\mathbb{A} \equiv \begin{pmatrix} S & -cg_o \frac{\ell_m}{L} & -\frac{c\alpha}{2L} \\ \frac{r-1}{\tau} & S + \frac{r}{\tau} + \frac{\nu}{b} & 0 \\ (\gamma-1)\left(\frac{\ell\pi}{a}\right)^2 \frac{\nu_1}{\nu} \frac{g_o\phi_o}{\rho_o} & (\gamma-1)\left(\frac{\ell\pi}{a}\right)^2 \frac{g_o\phi_o}{\rho_o}\left(\frac{\dot{\nu}_1}{\nu} + \frac{\nu_3}{\nu(r-1)}\right) & (S+\frac{\nu}{b})\left[\left(S+\frac{\nu}{b}\right)^2 + c_S^2\left(\frac{\ell\pi}{a}\right)^2\right] \end{pmatrix} \quad (67)$$

Equation (66) contains both the normal modes and the instability criteria for the system. The normal modes can be found from the secular equation

$$|\mathbb{A}(S)| = 0 \quad (68)$$

Equation (68) can be rewritten in the form

$$\sum_{n=0}^{5} \gamma_n S^n = 0 \quad (69)$$

where γ_n are functions of the system parameters. The roots of Eqs. (68) and (69) are the normal modes. An instability obtains if one of the roots has a real part greater than zero. The condition that no root has a real part greater than zero can be formulated as a condition on the coefficients γ_n (the Routh-Hurwitz conditions). We now proceed to a determination of the stability boundary (Eq. (98)).

C. STABILITY BOUNDARY

Equations (67) - (69) yield the following values for γ_n:

$$\gamma_o = S_v(S_A^2 + S_{RA}^2)(S_B^2 + S_{RB}^2) - \frac{c\alpha}{2L}(\gamma - 1)\left(\frac{\ell\pi}{a}\right)^2 \frac{g_o\phi_o}{\rho_o} \quad (70)$$

$$\gamma_1 = (S_A^2 + S_{RA}^2)(S_B^2 + S_{RB}^2) + 2S_v\left[S_A(S_B^2 + S_{RB}^2) + S_B(S_A^2 + S_{RA}^2)\right] + \frac{c\alpha}{2L}(\gamma - 1)\left(\frac{\ell\pi}{a}\right)^2 \frac{\nu_1}{\nu} \frac{q_o\phi_o}{\rho_o} \quad (71)$$

$$\gamma_2 = S_v(S_A^2 + S_B^2 + S_{RA}^2 + S_{RB}^2) + 2\left[S_A(S_B^2 + S_{RB}^2) + S_B(S_A^2 + S_{RA}^2)\right] \quad (72)$$

$$\gamma_3 = 2S_v(S_A + S_B) + S_A^2 + S_B^2 + S_{RA}^2 + S_{RB}^2 \quad (73)$$

$$\gamma_4 = S_v + 2(S_A + S_B) \quad (74)$$

$$\gamma_5 = 1 \quad (75)$$

In Eqs. (70) - (75), S_v represents the acoustic damping and is given by

$$S_v = \frac{\nu}{b} \quad (76)$$

where b is the length of the beam in the direction of the flow channel, S_A, S_{RA} represents the damping component and the frequency of the (unperturbed) acoustic root and are given by

$$S_A = \frac{\nu}{b} \quad (77)$$

$$S_{RA} = C_S\left(\frac{\ell\pi}{a}\right) \quad (78)$$

S_B, S_{RB} represent the damping component and the frequency of the (unperturbed) gain-flux (relaxation oscillation) mode and are given by

$$S_B = r/2\tau \qquad (r = 1 + \phi_o/\phi_s) \quad (79)$$

$$S_{RB} = \left[\frac{(r-1)cq_o}{\tau}\right]^{1/2} \quad (80)$$

The Routh-Hurwitz conditions require that for stability the following conditions obtain:

$$\gamma_n > 0 \qquad (n = 1...5) \tag{81}$$

$$\frac{\gamma_4\gamma_3 - \gamma_2\gamma_5}{\gamma_4} > 0 \tag{82}$$

$$\gamma_2 - \gamma_4 \left(\frac{\gamma_4\gamma_1 - \gamma_0\gamma_5}{\gamma_4\gamma_3 - \gamma_2\gamma_5}\right) > 0 \tag{83}$$

$$\left(\gamma_1 - \frac{\gamma_0\gamma_5}{\gamma_4}\right) - \frac{\gamma_0\left(\gamma_3 - \frac{\gamma_2\gamma_5}{\gamma_4}\right)}{\gamma_2 - \left(\frac{\gamma_4\gamma_1 - \gamma_0\gamma_5}{\gamma_4\gamma_3 - \gamma_2\gamma_5}\right)\gamma_4} > 0 \tag{84}$$

To make the algebra tractable we take the leading terms in Eqs. (70) - (75). In determining the leading terms, we note that for typical systems

$$S_{RB}^2 >> S_{RA}^2 >> S_v^2,\ S_B^2 \tag{85}$$

Then we take

$$\gamma_0 \approx S_v\, S_{RA}^2\, S_{RB}^2 - \frac{P\alpha}{\tau} \tag{86}$$

$$\gamma_1 \approx S_{RA}^2\, S_{RB}^2 + 2S_v^2\, S_{RB}^2 + P\alpha\,\frac{\nu_1}{\nu} \tag{87}$$

$$\gamma_2 \approx 3S_v\, S_{RB}^2 \tag{88}$$

$$\gamma_3 \approx S_{RB}^2 \tag{89}$$

$$\gamma_4 \approx 3S_v + 2S_B \tag{90}$$

$$\gamma_5 = 1 \tag{91}$$

where

$$P \equiv \frac{c\alpha}{2L}(\gamma - 1)\left(\frac{\ell\pi}{a}\right)^2 \frac{q_o^* t_o}{\rho_o} \tag{92}$$

Now Eq. (84) is equivalent to the condition

$$\gamma_0\gamma_2\gamma_3\gamma_4 + 2\gamma_0\gamma_1\gamma_4^2 - \gamma_0\gamma_3^2\gamma_4^2 + \gamma_1\gamma_2\gamma_4(\gamma_3\gamma_4 - \gamma_2) - \gamma_1^2\gamma_4^3 > 0 \tag{93}$$

Inserting Eqs. (86) - (91) in Eq. (93) and using the conditions of Eq. (85) we obtain, after some tedious algebra,

$$(3S_v + 2S_B)\left\{4S_v S_B S_{RA}^2 S_{RB}^6 + \frac{2P\alpha S_B S_{RB}^4}{\tau}\left(1 + 3\frac{\nu_1}{\nu} S_v\tau\right)\right\} > 0 \tag{94}$$

Or, if $\alpha < 0$,

$$P|\alpha| < \frac{2(S_v\tau) S_{RA}^2 S_{RB}^2}{1 + 3(S_v\tau)\frac{\nu_1}{\nu}} \tag{95}$$

The Eqs. (81) - (83) are trivially satisfied except for the condition that $\gamma_o > 0$. If $\alpha > 0$, this imposes the condition that

$$P\alpha < (S_v\tau) S_{RA}^2 S_{RB}^2 \tag{96}$$

Combining Eqs. (95) and (96), we have

$$\frac{-2}{P}\frac{S_v\tau S_{RA}^2 S_{RB}^2}{1 + 3S_v\tau\frac{\nu_1}{\nu}} < \alpha < \frac{S_v\tau S_{RA}^2 S_{RB}^2}{P} \tag{97}$$

as our stability criterion.

Utilizing the definitions contained in Eqs. (76) - (80) and Eq. (92), we have, alternatively

$$-2\frac{\phi_A}{\phi_S}\cdot\frac{2L}{b}\cdot\frac{v}{C_S}\cdot\frac{1}{1+3\frac{\nu_1}{\nu}\cdot\frac{v\tau}{b}}<\pm\frac{2\pi\beta g}{\lambda}\frac{\rho_o}{\rho_a}\ell_m(\gamma-1)<\frac{\phi_A}{\phi_S}\cdot\frac{2L}{b}\cdot\frac{v}{C_S} \tag{98}$$

where

$$\phi_A \equiv \rho_o C_S^3 \tag{99}$$

D. DISCUSSION

Equation (98) can be put in a more useful form. We note that

$$\phi_S = \phi_{SA}\left(\frac{\rho_o}{\rho_A}\right)^2 \tag{100}$$

$$\tau = \tau_A\frac{\rho_A}{\rho_o} \tag{101}$$

$$\phi_A = \phi_{AA}\frac{\rho_o}{\rho_A} \tag{102}$$

Where τ_A, ϕ_{SA}, ϕ_{AA} denote the values of τ, ϕ_S, ϕ_A at a pressure of one atmosphere. For a value of $\alpha_R < 0$ (for which the left side of the inequality of Eq. (98) obtains) the limiting value of ρ_o/ρ_A, which we denote by $(\rho_o/\rho_A)_{cr}$ will be given by

$$\left(\frac{\rho_o}{\rho_A}\right)_{cr} = -\frac{3}{2}\frac{\nu_1}{\nu}\frac{v\tau_o}{b}+\frac{1}{2}\left[\left(\frac{3\nu_1}{\nu}\frac{v\tau_o}{b}\right)^2+\frac{8}{\pi}\cdot\frac{\phi_{AA}}{\phi_{SA}}\cdot\frac{L}{\ell_m}\cdot\frac{v}{C_S}\cdot\frac{\lambda}{(\gamma-1)Fr\,b}\right]^{1/2} \tag{103}$$

Let us consider a typical system with the following paramters

$$\begin{aligned} \rho_A &= 0.6 \text{ kg m}^{-3} \\ v/C_S &= 0.5 \\ L/\ell_m &= 2 \\ \phi S_A &= 1.6 \times 10^8 \text{ W/m}^2 \\ \lambda &= 10^{-5} \text{ m} \\ (\gamma-1) &= 0.5 \\ \beta_g &= 1.7 \times 10^{-4} \\ C_S &= 360 \text{ m/sec} \\ b &= 7 \text{ cm} \\ \tau_o &= 10^{-5} \text{ sec} \end{aligned} \tag{105}$$

Under these conditions the maximum allowable density (pressure) is given by Eq. (103) as $(\rho_o/\rho_A)_{cr} = 0.38$.

It is interesting to note that Eq. (98) does not contain the flux explicitly and is thus independent of the level of pumping. We must be careful, however, to note that Eq. (98) holds only in Eq. (85) holds. This implies a condition on the flux exceeding some minimum amount. Also, Eq. (95) assumes the substitution of Eqs. (86) - (91) for Eqs. (70) - (75). If the latter are used, τ_o will enter the stability condition explicitly.

The linear instability, if it exists, will as we have seen, involve an exponentially growing acoustic wave. This wave need have only small amplitude to result in large flux variations. We may see this qualitatively from Eq. (82). The unstable modes will tend to be close to the (important) neutral modes since they have a small damping time compared to the gain-flux modes (i.e., $S_V << S_B$). Hence,

$$\frac{\partial \phi_{1i}}{\partial t} \sim (\tau_{1i})\, S_{BA} \approx C_S \left(\frac{\ell_m}{a}\right) \tau_{1i} \tag{106}$$

and

$$\frac{\phi_{1\ell}}{\phi_o} \approx \frac{a}{2L} \cdot \frac{1}{\ell\pi} \cdot \frac{C}{C_S} \left(2\ell_m g_{1\ell} + \alpha \frac{\rho_{1\ell}}{\rho_o} \right) \qquad (107)$$

and the amplification can be quite significant (in practice $\sim 10^3 - 10^4$).

Equation (98) suggests difficulties in trying to run a high-powered CO_2 EDL in a cw mode. A solution suggested by this analysis is to damp the acoustic mode further by means of an acoustic absorber: for example, an acoustic muffler on the cathode.

This has been tried and found to be successful.[2,3] In a subsequent paper we will investigate the effects of an acoustic absorber, as well as more realistic kinetics and compare our results with experiments undertaken at AERL.

---

2. Kellen, P.F., Mattson, A.C., Ahouse, D.R., and Yoder, M.J., Optical Engineering 18, 340 (1979).

3. Korff, D., Glickler, S.L., and Daugherty, J.D., "Acoustic Instability Model for High Power cw EDL Lasers,: 30th Annual Gaseous Electronics Conference, Palo Alto, Cal., Oct. 18-24, 1977.

SECTION III

ALIGNMENT SENSITIVITY

In the previous section we have ignored gain variations in the direction of flow. Such variations can lead to extreme alignment sensitivities, as we shall now show.

There are two effects involved. The first is the variation of output coupling with position of the optical axis on the feedback mirror. This is basically a diffraction effect(4) and is illustrated in Figure 6.

In Figure 6 N_{eq} is the system equivalent Fresnel number, defined by

$$N_{eq} = \frac{a^2}{2\lambda L} \frac{M - 1}{M} \tag{108}$$

where a is the collimating mirror diameter, M is the system magnification, and the other symbols have been explained above. ϵ is defined as the normalized position (one dimensional) of the optical axis on the feedback mirror (ϵ = + 1, 0, - 1 correspond to top, middle and bottom of the mirror, respectively).

The second effect is the variation of the system gain with position of the optical axis. This effect arises because of the variation of the gain with temperature for a particular value of J, the initial angular momentum of the radiating molecule. This variation arises through the partition function. In fact,

$$\text{gain} \sim \frac{2J + 1}{T} e^{-BJ(J + 1)/T} \tag{109}$$

where B is the vibrational constant for the transition and T is the temperature.

Our flux equation (for the variation of the total flux, not a Fourier component) is (x is the flow direction, and x = 0 is the optical axis)

$$\frac{\partial \phi_1}{\partial t} = c\phi_o \left(g_1 - \alpha_1 \frac{g_o b}{\rho_o} u_1\right) \tag{110}$$

---

4. Kellen, P. and Smith, M., Opt. Eng., 18, pp. 157-160 (March/April 1979).

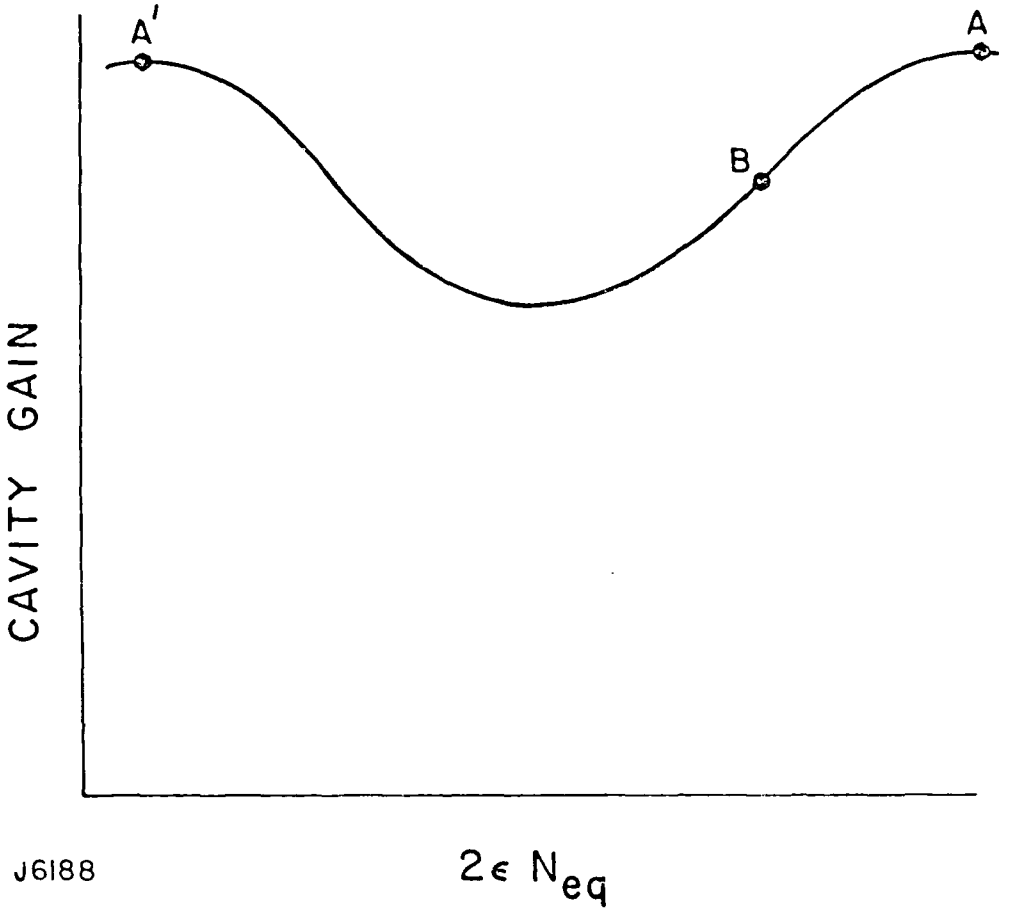

Figure 6. Variation of g_c with N_{eq}. The variation of 2 N_{eq} from crest to crest (A to A') is of the order of unity. At A or A', g_c is relatively insensitive to change in optical axis. At point B it is sensitive.

where μ_1, proportional to the tilt angle, is defined by

$$\mu_1 \equiv \frac{\partial}{\partial x} \rho_1 (x) \Big|_{x=0}$$

$$\alpha_1 \equiv \text{dimensionless coupling constant} \tag{111}$$

We shall derive α_1 below.

The gain equation along the optical axis (or the average system gain across the beam, which can be shown to the equivalent) satisfies the equation

$$\frac{\partial g_1}{\partial t} = -\frac{g}{\tau} - \frac{(g_o\phi_1 + g_1\phi_o)}{\tau\phi_s} + \frac{\partial g}{\partial \mu_1}\frac{d\mu_1}{dt} \tag{112}$$

In Eq. (112) the last term on the right-hand side represents the effect of the gain variation with optical axis position. We rewrite Eq. (112) in the form

$$\frac{\partial g_1}{\partial t} = -\frac{g}{\tau} - \frac{(g_o\phi_1 + g_1\phi_o)}{\tau\phi_s} + \frac{\alpha_2 b g_o}{\rho_o}\frac{\partial \mu_1}{\partial t} \tag{113}$$

where α_2 is a dimensionless constant whose value will be found below.

The heating equation takes the form

$$\partial_t (\partial_t^2 - C_s^2 \partial_x^2) \rho_1(x) = (\gamma - 1)\, \partial^2 f(x)\, (g_o\phi_1 + g_1\phi_o) \tag{114}$$

Where $f(x)$ denotes the variation in gain along the flow direction (g_o and g_1 are assumed to have the same spatial dependence). The equation for μ_1 ($\equiv \rho_1'(0)$) then becomes

$$\partial_t(\partial_t^2 - C_s^2 \partial_x^2) \rho_1'(x)\Big|_{x=0} = (\gamma - 1)\, \partial_x^3 f(x)\Big|_{x=0} (g_o\phi_1 + g_1\phi_o) \tag{115}$$

where the prime denotes derivatives with respect to x. Henceforth, we take

$$\left[\partial_x^2 \rho_1 (x)\Big|_{x=0}\right] \approx \frac{1}{b^2}\mu_1 \tag{116}$$

to simplify the analysis. If a standing wave exists in the flow channel (analogous to an open-ended organ pipe) then Eq. (116) follows naturally. In any event, it serves as a reasonable approximation. Similarly we take

$$(\gamma - 1)\ \partial_x^{\,3} f(x)\big|_{x=0} \equiv \frac{\alpha_3}{b^3}(\gamma - 1) \tag{117}$$

where α_3 is derived below.

Our three coupled equation for this case are given by

$$A \begin{pmatrix} \tilde{\phi}_1\ (s) \\ \tilde{g}_1\ (s) \\ \tilde{\mu}_1\ (s) \end{pmatrix} = 0 \tag{118}$$

where ($r \equiv 1 + \frac{\phi_o}{\phi_s}$ and v is the gas flow velocity)

$$\begin{bmatrix} A = s & -c\phi_o & cg_o\phi_o \frac{\alpha_1 b}{\rho_o} \\ \frac{g_o}{\tau\phi_s} & s + \frac{v}{b} + \frac{r}{\tau} & -\frac{bg_o}{\rho_o}\alpha_2 s \\ \frac{\alpha_3 g_o}{b^3}(\gamma - 1) & \frac{\alpha_3}{b^3}\phi_o(\gamma - 1) & -(s + \frac{v}{b})\left((s + \frac{v}{b})^2 + \frac{C_s^{\,2}}{b^2}\right) \end{bmatrix} \tag{119}$$

A Routh-Hurwitz stability criterion, using leading-order terms as in the previous chapter, leads to the stability requirement

$$(\gamma - 1)\ \alpha_1\alpha_3 \lesssim \frac{\phi_A}{\phi_s} \cdot \frac{2}{\tau_c} \cdot \frac{1}{C_s g_o} \tag{120}$$

where

$$\phi_A \equiv \rho_o C_s^{\,3} \text{ and } \tau_c = \frac{b}{v} \tag{121}$$

We shall now derive expressions for α_1 and α_3 (which, as we shall see, is $\sim \alpha_2$).

To determine α_1 we must relate changes in ε to changes in ρ' $(x = 0)$. We have

$$\frac{2\pi}{\lambda} \phi_{tilt} = \frac{2\pi}{\lambda} \beta_g \frac{1}{\rho_a} \frac{\partial \rho}{\partial x} \ell_M \tag{122}$$

where ℓ_M is the thickness of the optical medium and ϕ_{tilt} is the tilt of a ray due to refraction. The optical axis will then tilt by

$$\Delta\psi = \frac{2M}{M - 1} \theta_{tilt} \tag{123}$$

Furthermore,

$$\frac{d_1}{2} \Delta\varepsilon = R_1 \Delta\psi \tag{124}$$

where d_1, R_1 are the diameter and radius of curvature of the feedback mirror, respectively. Hence,

$$\Delta\varepsilon = \frac{2R_1}{d_1} \cdot \frac{2M}{M - 1} \cdot \beta_g \cdot \ell_M \cdot \frac{\Delta\rho'(0)}{\rho_a} \tag{125}$$

Now, let us denote the change in g_c when ε changes by $(1/N_{eq})$ as ηg_o. Then,

$$\begin{aligned} \Delta g &= \frac{\Delta g}{\Delta \varepsilon} \Delta\varepsilon \\ &= (\eta g_o) N_{eq} \Delta\varepsilon \\ &= (\eta g_o) N_{eq} \cdot \frac{2R_1}{d_1} \cdot \ell_M \cdot \frac{2M}{M - 1} \cdot \frac{\beta_g}{\rho_a} \cdot \Delta\rho'(0) \\ &\equiv \frac{\alpha_1 g_o b}{\rho_o} \Delta\rho'(0) \end{aligned} \tag{126}$$

Therefore,

$$\alpha_1 = \eta N_{eq} \frac{4M}{M - 1} \frac{R_1}{b} \frac{\ell_M}{d_1} \beta_g \frac{\rho_o}{\rho_a} \tag{127}$$

For a typical case

$$\eta \approx 0.1, \quad N_{eq} = 10, \quad M = 2, \quad \frac{R_1}{b} = \frac{20}{0.1} = 200$$

$$\frac{\rho_o}{\rho_a} = 0.1, \quad \beta_g = 2 \times 10^{-4}, \quad \frac{\ell_M}{d_1} = \frac{1 \text{ m}}{2 \text{ cm}} = 50$$

so that

$$\alpha_1 \approx \alpha$$

We note, furthermore that α_1 will be much less than its calculated value if the system is aligned at, e.g., points A or A' in Figure 6. (The calculation in Eqs. (126) and (127) is for point B in that figure.)

We may schematically denote the variation of system gain with optical axis by the diagram in Figure 7.

An analysis identical to that above leads to

$$\alpha_2 = \eta' N_{eq} \frac{4M}{M-1} \frac{R_1}{b} \frac{\ell_M}{d_1} \beta_g \frac{\rho_o}{\rho_a} \tag{128}$$

Now, α_2 arises from the temperature variation of the gain as given in Eq. (109).

Taking

$$J = 18,\ T_{inlet} = 173°K,\ T_{opt.\ axis} = 380°$$

we obtain

$$\alpha_2 \approx 0.5$$

for a typical case.

Since α_2, α_3 are both dimensionless constants due to the same effect we take them to be equal. We then obtain the following stability boundary.

$$\eta\,\eta'\,(N_{eq})^2 \left[\frac{4MR_1\ell_M}{(M-1)bd_1}\right]^2 \beta_g^2 \left(\frac{\rho_o}{\rho_a}\right)^2 \lesssim \frac{2\rho_o C_s^3}{\phi_s} \cdot \frac{1}{C_s g_o} \cdot \frac{1}{\tau_c} \tag{129}$$

For a numerical example, take

$M = 2$	$R_1 = 20$ m	$b = 10$ cm
$\eta = 0.1$	$\eta' = 0.05$	$\ell_M = 1$ m
$\rho_o/\rho_a = 0.1$	$d_1 = 2$ cm	$\beta_g = 2 \times 10^{-4}$
$g_o = 0.5\ m^{-1}$	$C_s = 300$ m/sec	$\tau_c = 10^{-3}$ sec
$\rho_o C_s^3/\phi_o \simeq 20$	$N_{eq} = 1$	

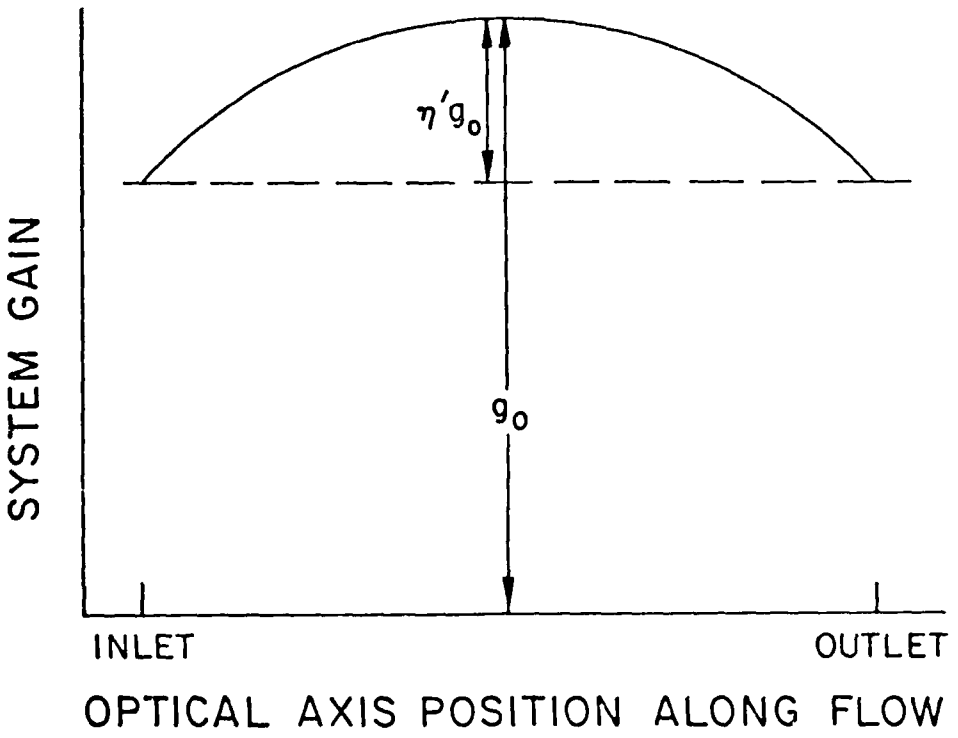

Figure 7. Schematic Picture of System Gain Variation with Optical Axis Position

In such a case, we have

$$\frac{32}{25} > \frac{2}{3} \text{ (unstable)}$$

An instability in this system would result in large wanderings or the pointing angle and possibly to line jumping if the optical axis moved sufficiently far so that the gain were greater for a different J number.

Even in the absence of an instability, of course, the matrix A determines the system response to external perturbations. In particular, if we have mirror vibrations (q_c perturbation) the coupling ensures that we would obtain a response at the acoustic frequencies. Such a response would not obtain in standard treatments.

Finally, we stress that if the system is aligned at a stable point (A or A' in Figure 6) no instability obtains. η_1 (or η) is negligable and Eq. (129) is automatically satisfied.

SECTION IV

MODE MEDIUM INTERACTIONS: DIFFERENTIAL FORMULATION

A. INTRODUCTION

The analysis in this section will deal mainly with an attempt to recast the instability discussed in Section II in terms of more conventional medium instabilities such as are found in plasma physics. Some of these, such as the free electron laser, harmonic generation, and optical modulation by sound waves are beneficial. Others, like thermal blooming, self-focusing and mode-medium interaction (MMI) are deleterious.

The analysis in the previous two sections emphasized the Huygens-Fresnel-Kirchhoff integral solution to the wave equation. In this section, instead, the differential equations will be analyzed and comparison with the other derivation will be made along the way. The differential formulation has the advantage that it can be easily extended into the nonlinear regime, in which the amplitude of the perturbation has built up to a large value. It also has the advantage that it demonstrates how the instability discussed in Section II (hereafter referred to as MMI-1) is related to more conventional instabilities. To do this, Maxwell's equations including a time-varying conductivity (to account for cavity and medium losses) and a time-varying dielectric function will be used. It will be seen that MMI-1 results when the conductivity is modulated and when all the electromagnetic waves have the same unperturbed frequency. This is a form of nonresonant amplitude modulation and instability, which is different from the conventional method of amplitude modulation in which resonant coupling of electromagnetic modes which are separated by the modulation frequency occurs. On the other hand, Brillouin scattering, which is primarily a phase modulation, results when the dielectric function is modulated. The coupling is strongest when the electromagnetic modes are separated by the modulation frequency. This is the mechanism that will be studied in this section. The equations of motion for the electromagnetic and acoustic waves are derived. The secular determinant is solved. It is shown to have unstable roots in the limit in which the ratio of cavity flux to the saturation flux is small, so that gain-flux oscillations can be neglected. Finally, the nonlinear regime is briefly examined.

B. MODE-MEDIUM INTERACTIONS

Our starting point will be Maxwell's equations with the appropriate boundary conditions (cavity losses) and medium gain

and losses. Since the laser is in an unstable-resonator configuration, the boundary conditions are rather complicated (see Appendix D). Thus to simplify matters, we will lump all the losses in a phenomenological conductivity function. The medium gain will be computed semiclassically from the imaginary part of the susceptibility. A simple model of this is discussed in Appendix E.

Thus, the governing equations are, in mks units,

$$\nabla \cdot D = 0 \tag{130}$$

$$\nabla \cdot B = 0 \tag{131}$$

$$\nabla \times E = -\frac{\partial B}{\partial t} \tag{132}$$

$$\nabla \times H = J + \frac{\partial D}{\partial t} \tag{133}$$

where $D = \varepsilon E$, $J = \sigma E$, ε contains the effects of dielectric polarization and σ contains both the medium losses and the cavity loss. From Eqs. (130) - (133) the following wave equation can be derived for transverse electromagnetic waves:

$$\nabla^2 E - \mu_0 \frac{\partial^2 D}{\partial t^2} = \mu_0 \frac{\partial J}{\partial t} \tag{134}$$

(μ_0 is the free-space permeability). Assume that

$$\varepsilon = \varepsilon^{(0)}(r) + \varepsilon^{(1)}(r,t) \tag{135}$$

$$\sigma = \sigma^{(0)}(r) + \sigma^{(1)}(r,t) \tag{136}$$

The entire scattering calculation can actually be done in terms of σ or ε. The only reason for keeping both is to stick to the convention which associates the gain of the system with the imaginary part of ε and the losses with the real part of ε. Similarly, scattering is associated with the real part of ε and not the imaginary part of ε even though formally (with the proper interpretation) it can be calculated in terms of either function. In what follows we maintain the convention. Substituting Eqs. (135) - (137) into Eq. (134) leads to,

$$\nabla^2 E - \mu_0 \varepsilon^{(0)}(r) \frac{\partial^2 E}{\partial t^2} - \mu_0 \sigma^{(0)} \frac{\partial E}{\partial t} = \mu_0 \frac{\partial^2}{\partial t^2} \varepsilon^{(1)}(r,t) E - \mu_0 \frac{\partial}{\partial t} \sigma^{(1)}(r,t) E \tag{137}$$

This equation will now be solved in a perturbative fashion.[5] However rather than expanding in normal modes, we will use the multiple-time-scale expansion of secular equations.[6] Expanding $E = E^0 + E^{(1)} + E^{(2)}$, realizing that $E^{(0)} = 0$ since there is no steady-state space-charge field, leads to

$$\nabla^2 E^{(1)} - \mu_0 \varepsilon^{(0)} \frac{\partial^2 E^{(1)}}{\partial t^2} - \mu_0 \sigma^{(0)} \frac{\partial E^{(1)}}{\partial t} = 0 \qquad (138)$$

$$\nabla^2 E^{(2)} - \mu_0 \varepsilon^{(0)} \frac{\partial^2 E^{(2)}}{\partial t^2} - \mu_0 \sigma^{(0)} \frac{\partial E^{(2)}}{\partial t} = \mu_0 \frac{\partial^2}{\partial t^2} \varepsilon^{(1)} E^{(1)} - \mu_0 \frac{\partial}{\partial t} \sigma^{(1)} E^{(1)} \qquad (139)$$

If $\varepsilon^{(1)}$ and $\sigma^{(1)}$ in turn depend on the electric fields, then third and higher-order equations will result. Equation (138) describes the equilibrium eigenmodes of a loaded resonator including all the losses. This equation for the unstable-resonator geometry is discussed in Appendix D and in more detail in another part of this report. The normal modes of $E^{(2)}$ are the same as those for $E^{(1)}$ (since the left-hand sides of the equations are identical). However, since $E^{(2)}$ is driven by products of first-order quantities it is conceivable that the left-hand side is driven at a natural frequency. If this should happen to be the case then our perturbation expansion will break down. The reason is that $E^{(2)}$ contains a secular response which will make $E^{(2)} > E^{(1)}$. To get around this problem those components of the right-hand side of $E^{(2)}$ are incorporated into the equation for $E^{(1)}$, which is now allowed to have a slowly varying amplitude. First the eigenmodes of Eq. (138) have to be found. Towards this end let,

$$E^{(1)}(r,t) = E_k^{(1)} e^{-i\omega_k t + ikz} + c\cdot c \qquad (140)$$

where c·c stands for complex conjugate and $E_k^{(1)}$ satisfies,

---

5. A. Yariv, Quantum Electronics, John Wiley & Sons, NY (1967)

6. N. Krylov, N.N. Bogoliubov, Intro. to Nonlinear Mechanics, Princeton U. Press, Princeton, NJ (1947)

$$\left(\nabla_T^2 + 2ik\frac{\partial}{\partial z} + k_0^2\right)E_k^{(1)}(r) = 0 \qquad (141)$$

where

$$k_0^2 = \frac{\omega_k^2}{c^2}\left\{1 - \frac{k^2c^2}{\omega_k^2} - \alpha_{R0}N_0 + i\frac{g^{(0)}}{k} - i\frac{g_c^{(0)}}{k}\right\} \qquad (142)$$

$g^{(0)}$, $g_c^{(0)}$ are the equilibrium gain and loss terms. The loss includes medium and output-coupling losses; it is related to $\sigma^{(0)}$ by, $g_c^{(0)} = \mu_0\sigma^{(0)}(r)\omega_k/k$. The relationship between the dielectric function and the medium susceptibility is given in Appendix E. The dipole moment per molecule, given by $p = (\alpha E + c.c)$, results in a macroscopic polarization $P = N_0 p$. Finally, since $D^{(1)} = \varepsilon^{(0)}E^{(1)} = \varepsilon_0 E^{(1)} + P$, we find that in our simple semi-classical picture $\varepsilon^{(0)} = \varepsilon_0(1 + \alpha_{R0}N_0 - ig^{(0)}/k)$. The equation for the equilibrium gain is given by

$$\nabla \cdot g^{(0)}V^{(0)} = -\frac{g^0}{\tau} + \frac{g^{(0)}I^{(0)}}{I\phi_s} + P \qquad (143)$$

where $V^{(0)}$ is the equilibrium flow velocity of the gas, τ is the collisional deactivation time of the upper state and P is the pumping rate. The solution to Eqs. (142) and (143) constitutes the equilibrium eigenmodes of the resonator, since the resonator boundary is included in $\sigma^{(0)}$. The details are given in Appendix D. Any perturbation in the equilibrium fields can be expanded in the complete orthonormal set of eigenfunctions (which are assumed to exist). However, since a secular response is anticipated, the Fourier coefficients will be assumed to be time dependent and the appropriate set of equations describing the time evolution of the coefficients will now be derived. That is, let

$$E(r,t) = \sum_k u_k(t)E_k^{(1)}(r)e^{-i\omega_k t + ikz} \qquad (144)$$

and substitute this into Eq. (137), keeping in mind that $u_k(t)$ is slowly varying and $E_k^{(1)}$ satisfies Eq. (141). The perturbation expansion in Eqs. (138) and (139) thus is redone to take into account anticipated secularity in the response of $E^{(2)}$. Assume also that

$$\varepsilon^{(1)}(r,t) = \sum_k a_k(t)\varepsilon_k^{(1)}(r)e^{-i\omega_k t + ikz} \qquad (145)$$

$$\sigma^{(1)}(r,t) = \sum_k b_k(t)\sigma_k^{(1)}(r)e^{-i\omega_k t+ikz} \tag{146}$$

where $E_k^{(1)}(r)$ and $\sigma_k^{(1)}(r)$ are the appropriate spatial, dielectric and loss-modulation eigenfunctions to be determined self-consistently. Note that in Eqs. (144) - (146) k is a summation index; there is no implication that the k's are the same in these equations. Substituting Eqs. (144) - (146) into Eq. (137) yields,

$$\sum_k e^{-i\omega_k t+ikz} E_k^{(1)}(r)\frac{2i\omega_k}{c^2}\frac{\partial u_k}{\partial t}$$

$$= \mu_0\frac{\partial^2}{\partial t^2}\sum_{k'} a_{k'}\varepsilon_{k'}^{(1)}e^{-i\omega_{k'}t+ik'z}\sum_{k"} u_{k"}E_{k"}^{(1)}e^{-i\omega_{k"}t+ik"z}$$

$$- \mu_0\frac{\partial}{\partial t}\sum_{k'} b_{k'}\sigma_{k'}^{(1)}e^{-i\omega_{k'}t+ik'z}\sum_{k"} u_{k"}E_{k"}^{(1)}e^{-i\omega_{k"}t+ik"z} \tag{147}$$

Note that the secularity-producing terms lead to slow variations in the mode amplitudes as expected. To pick out a particular eigenmode on the left, multiply the left and right sides by the complex conjugate of the left and integrate over the resonator volume and time:

$$\frac{\partial u_k}{\partial t} = +\frac{ic^2}{2\omega_k}\sum_{k',k"}\int dVdt\ \exp[i(\omega_k-\omega_{k'}-\omega_{k"})t-i(k-k'-k")z]$$

$$\times\ (\omega_{k'}+\omega_{k"})^2\mu_0 a_{k'}u_{k"}E_k^{(1)*}E_{k"}^{(1)}\varepsilon_{k'}^{(1)}$$

$$+\frac{c^2}{2\omega_k}\sum_{k',k"}\int dVdt\ \exp[i(\omega_k-\omega_{k'}-\omega_{k"})t-i(k-k'-k")z]$$

$$\times\ (\omega_{k'}+\omega_{k"})\mu_0 b_{k'}u_{k"}E_k^{(1)*}E_{k"}^{(1)}\sigma_{k'}^{(1)} \tag{148}$$

where the eigenmodes are normalized such that $\int d^2r E_k^{(1)*}E_k^{(1)} = 1$.

There are several possible cases of interest:

(i) Consider first the case in which there is no dielectric modulation ($\varepsilon_{k'}^{(1)}(r) \equiv 0$).

Taking the limit that $\omega_{k'}$ (the slow modulation of the gain and loss term) compared to optical frequencies is negligible requires that $\omega_k = \omega_{k''}$. That is, the two electromagnetic waves have the same natural (unperturbed) frequency of oscillation. One way this could happen would be if $k'' = k$, i.e., the lasing mode is "coupled" to itself by loss modulation arising from the acoustic wave. Alternatively, the two modes may be distinct, although degenerate in frequency; this case is treated in detail in Section II. In the self-coupling case we obtain

$$\frac{\partial u_k}{\partial t} = c^2 \mu_0 (b_{k'} e^{-i\omega_{k'} t}) u_{k''} \int d^2r \, E_k^{(1)*} \sigma_{k'}^{(1)} E_{k''}^{(1)} \qquad (149)$$

with a similar equation for $u_{k''}$. Making the following identification

$$\alpha_R \delta\rho\phi_0 = c^2 \mu_0 b_k e^{-i\omega_{k'} t} u_{k''} \int d^2r \, E_k^{(1)*}(r) \sigma_{k'}^{(1)}(r) E_{k''}(r)$$

results in the equation used in MMI-1 with $\delta\rho$ being the density perturbation by the acoustic wave. The gain term can be obtained from the polarization term as is done in Appendix D. The above identification of $\sigma_{k'}^{(1)}$ with density fluctuations is not unreasonable since the cavity and medium losses for simple systems can be related to the quality factor of the system which in turn depends on the index of refraction. Besides the case $\omega_k = \omega_{k''}$ it is also possible to consider the resonant triplet $\omega_k = \omega_{k''} + \omega_{k'}$, $k = k' + k''$ where now the two electromagnetic modes are separated by the acoustic frequency. The only difference is that now the $e^{-i\omega_{k'} t}$ term in Eq. (149) is replaced by unity. The right-hand side is again related to the density fluctuation. This is the case of conventional amplitude modulation by a resonant triplet.

(ii) Consider now separately the case of no cavity and medium loss variation ($\sigma_{k'} = 0$) but now include a dielectric modulation $\varepsilon_{k'} \neq 0$. To proceed further we develop a simple model for $\sigma_{k''}$. The specific modulation of the medium that is to be studied is that due to an acoustic wave.

---

7. M. Born, E. Wolf, Principles of Optics, Pergamon Press, NY (1959)

From microscopic considerations (see Appendix E) it follows that the dipole moment of a molecule is given by $p = (\alpha E_{eff} + c.c)$ where α is a frequency-dependent proportionality constant and $E_{eff} = E$ for a gas. The macroscopic polarization[8] of the medium is then given by (for N molecules/cubic centimeter)

$$\mathbb{P} = Np \tag{150}$$

with the dipole moment given by $p = (\alpha E + c.c)$. Note that α, N both depend upon the intensity of the field. Since the secular part of the response comes from products of first-order quantities, using $D_{sec} = \varepsilon^{(1)}E^{(1)} = \varepsilon_0(\alpha_{0R}N_k^{(1)} - i\frac{g_k^{(1)}}{k})E_k^{(1)} + c.c$ leads to

$$\frac{\partial u_k}{\partial t} = i\frac{\omega_k}{2}u_{k"}\alpha_{0R}\int d^2r N_k^{(1)}(t,r)E_k^{(1)*}E_{k"}^{(1)}$$
$$+ cu_{k"}\int d^2r g_k^{(1)}(t,r)E_k^{*(1)}E_{k"}^{(1)} \tag{151}$$

where it was assumed that the fast acoustic exponential variation has been extracted via the requirement that

$$\omega = \omega_{k'} + \omega_{k"} \tag{152}$$

$$k = k' + k" \tag{153}$$

and the fast transverse variation in $N_k^{(1)}$ and $g_k^{(1)}$ is taken care of by the electric field variations which have different transverse mode structure

$$k_\perp' = k_\perp' + k_\perp" \tag{154}$$

where $k_\perp'$ is fixed by the acoustic-resonator geometry. In the plane wave case the spatial integrals can actually be done and lead to

$$\frac{\partial u_k}{\partial t} = i\frac{\omega_k}{2}\beta_g\frac{\rho_{k'}^{(1)}}{\rho_a}u_{k"} + \frac{c}{2}g_{k'}^{(1)}u_{k"} \tag{155}$$

---

8. A. Yariv, Introduction to Optical Electronics, Holt, Rinehart, Winston, NY (1971)

$$\frac{\partial u_{k''}}{\partial t} = \frac{i}{2}\omega_{k''}\beta_g\frac{\rho_{k'}^{(1)*}}{\rho_a}u_{k''} + \frac{c}{2}g_{k'}^{(1)*}u_k \qquad (156)$$

$\beta_g = \alpha_{0R}\rho_a/m$ is the Gladstone-Dale coefficient, ρ_a is the atmospheric density and * denotes complex conjugate quantities. Equations for $g_{k'}^{(1)}$, $N_{k'}^{(1)}$ will be derived in the next section.

The only term which can drive the gain equation resonantly [that is, so that Eqs. (152) - (154) are satisfied] is the flux term. Thus, the secular part of the gain equation is

$$\frac{\partial g_{k'}^{(1)}}{\partial t} = -\gamma_g g_{k'}^{(1)} - g_0\frac{(r-1)}{\tau}\frac{u_k u_{k''}^*}{\phi_0} \qquad (157)$$

where $r = 1 + \phi_0/\phi_s$ and $\phi_0 = c\varepsilon_0 u_k^2/2$ and $\gamma_g = 1/\tau + V_0/b$ (where V_0 is the flow velocity and b, the anode-cathode distance) is the total damping of the gain term including convection and deactivation of the upper level.

The equations describing the medium are the continuity, momentum and heat-transport equations,

$$\frac{\partial\rho}{\partial t} + \nabla\cdot\rho V = 0 \qquad (158)$$

$$\frac{\partial V}{\partial t} + V\cdot\nabla V = -\frac{\nabla P}{\rho} \qquad (159)$$

$$\frac{\partial P}{\partial t} + V\cdot\nabla P = \frac{\gamma P}{\rho}\left(\frac{\partial\rho}{\partial t} + V\cdot\nabla\rho\right) + (\gamma-1)\frac{dQ}{dt} \qquad (160)$$

where ρ, V, P, dQ/dt are the mass density, fluid velocity, pressure and heat deposition rate; γ is the ratio of specific heats.

Linearizing Eqs. (158) - (160) would produce the standard acoustic-wave equation. However, since the heat deposition term can have components at the acoustic frequency, this leads to a secular response in the acoustic equation. This secularity is once again taken care of by letting the amplitudes be slowly varying. The linearized acoustic-wave equation (for the mass density) is given by

$$\left(\frac{\partial}{\partial t} + V_0\frac{\partial}{\partial x}\right)\left(\frac{\partial^2}{\partial t^2} + V_0\frac{\partial^2}{\partial x^2} - C_A^2\frac{\partial^2}{\partial y^2} + 2V_0\frac{\partial^2}{\partial t\,\partial x}\right)\rho^{(1)} = (\gamma-1)\nabla^2 p \qquad (161)$$

where V_0 is the transverse flow velocity and $C_a^2 = \gamma RT$ is the acoustic velocity. The heating term has been included in anticipation of the secularity. The heating term is obtained for a CO_2 laser by conservation-of-energy arguments; it takes the following form:

$$P = \left(Cg^0 \frac{\nu_1}{\nu_0} u_k u_{k"}^* + \left(\phi_0 \frac{\nu_1}{\nu_0} + \phi_s \frac{\nu_3}{\nu_0} \right) g_{k'}^{(1)} \right) e^{-i\omega_{k'} t + ik_a' \cdot r} + c \cdot c \tag{162}$$

where ν_1/ν_0 is the ratio first excited state to ground state and c·c stands for complex conjugate. Since P does indeed vary at the acoustic frequency (note that use of Eqs. (152) - (154) was made) it will produce a secular response in Eq. (161). The slowly varying piece of the acoustic wave is produced by,

$$\frac{\partial \rho_{k'}^{(1)}}{\partial t} = - \gamma_a \rho_{k'}^{(1)} + \frac{(\gamma - 1)}{2C_a^2} P_{k'} \tag{163}$$

where γ_a is the convective damping of the acoustic waves, $P_{k'}$ is given by Eq. (162) and $\rho_{k'} = mN_{k'}$ where m is the mass.

The linear instability is obtained by assuming that one of the electromagnetic waves has large amplitude and hence decays into the second electromagnetic wave and the acoustic oscillations. Thus assuming the ϕ_0 = constant and using Eqs. (156), (157) and (163) leads to the determinantal equation for the instability. Assuming that $u_{k"} \sim e^{\delta t}$, $\rho_{k'} \sim e^{\delta^* t}$, $g_{k'} \sim e^{\delta^* t}$ leads to,

$$\begin{pmatrix} \delta & -c\frac{u_k}{2} & -i\omega_{k"}\frac{\sigma_{or}u_k}{2m} \\ cg_0\frac{(\gamma-1)}{\tau}\frac{u_k^*}{\phi_o} & \delta+\gamma_g & 0 \\ \frac{(1-\gamma)cg_0}{2C_a^2}\frac{\nu_1}{\nu_0}u_k^* & (1-\gamma)\frac{c}{2C_a^2}\left(\phi_0\frac{\nu_1}{\nu_0}+\phi_s\frac{\nu_3}{\nu_0}\right) & \delta+\gamma_a \end{pmatrix} \begin{pmatrix} u_{k"} \\ g_k^* \\ \rho_{k'} \end{pmatrix} = \begin{pmatrix} \\ 0 \\ \\ \end{pmatrix} \tag{164}$$

Setting the determinant of Eq. (164) equal to zero, leads to the polynomial equation for the instability. Defining

$$\alpha_1 = \frac{cg_0}{\tau}(r-1),\quad \alpha_2 = \frac{\omega_{k''}}{4}\frac{\beta_g}{\rho_a}\frac{(\gamma-1)}{c_a^2}cg_0\frac{\nu_1}{\nu_0}\left|\phi_0\right|^2$$

$$\beta = \frac{\omega_{k''}}{4}\frac{\beta_g}{\rho_a}\frac{g_0}{c}\frac{(r-1)}{\tau}\frac{\gamma-1}{c_a^2}\left(\phi_0\frac{\nu_1}{\nu_0} + \phi_s\frac{\nu_3}{\nu_0}\right)$$

where β_g = Gladstone-Dale constant and ρ_a is atmospheric density, we obtain

$$(\delta)(\delta+\gamma_g)(\delta+\gamma_a) + \alpha_1(\delta+\gamma_a) - i\alpha_2(\delta+\gamma_g) + i\beta = 0 \quad (165)$$

The acoustic damping is given by $\gamma_a = V_o/b$ where V_o is the transverse gas flow velocity and b is the anode-cathode distance. The damping in the gain equation is given by $\gamma_g = V_o/b + 1/\tau$ where τ contains all the collisional relaxation rates.

C. NONLINEAR SATURATION

If now, it is assumed that u_k does not stay constant but decreases significantly (as energy is transferred to the other waves), it is necessary to include an evolution equation for u_k. That is Eq. (155) must be included together with Eqs. (156), (157), and (163). Unlike the three-wave equations of plasma physics, which can be solved in terms of Jacobi elliptic functions, this set of equations can only be solved numerically. Some insight into these solutions can be obtained by examining the conserved quantities. Using Eqs. (155) - (157) and (163) leads to,

$$\frac{\partial}{\partial t}\left(\frac{\left|u_k\right|^2}{\omega_k} + \frac{\left|u_{k''}\right|^2}{\omega_{k''}}\right) = \frac{\omega_k + \omega_{k''}}{\omega_k\omega_{k''}}\left(cg_{k'}u_k^*u_{k''} + c.c\right) \quad (166)$$

This can further be reduced by using the equation for $g_{k'}$.

$$\frac{\partial}{\partial t}\left(\frac{\left|u_k\right|^2}{\omega_k} + \frac{\left|u_{k''}\right|^2}{\omega_{k''}} + \frac{\omega_k+\omega_{k''}}{\omega_k\omega_{k''}}c\left|g_{k'}\right|^2\right) = -\left(\frac{\omega_k+\omega_{k''}}{g_0\omega_k\omega_{k''}}\right)\left(\frac{r}{\tau}+\frac{V_o}{b}\right)\left(\frac{\phi_0^2\left|g_{k'}\right|^2}{r-1}\right) \quad (167)$$

The convective damping has been included simply by replacing $V_0\partial/\partial X$ in the acoustic equation by V_0/b where b is the anode-cathode spacing.

In order to understand Eq. (167) it is necessary to examine Figure 8. During the linear-lasing stage the second electromagnetic wave is negligible and the acoustic noise has not made a transition in the anode-cathode direction. Once the primary electromagnetic wave, u_k has been saturated and reaches steady state and the acoustic noise has had time to propagate across the anode-cathode separation, the linear regime of the instability sets in, whereby the primary electromagnetic wave feeds the secondary electromagnetic (em) wave $u_{k''}$ and the acoustic noise. Eventually the primary em wave is totally depleted. This results in the secondary em wave also dying out in one or two round trips in the resonator because of the output coupling. However Eq. (167) implies that the nonlinear process of supplying energy back to the primary wave will not take place because of the dissipative nature of the acoustic waves. The energy can be made to flow into the secondary em wave and the acoustic wave but will not flow back to the pump. Thus, once the pump is depleted the instability stops. The entire process begins again, however, because u_0 builds up due to the laser properties of the medium. The acoustic wave may remain into this region because of its relatively long decay time. This feature may lead to a degradation of beam quality of pulsed lasers, as well.

D. SUMMARY

The physical processes involved in the instability are illustrated in Figure 9.

Consider a large-amplitude wave at frequency ω_0 and wave number k_0. In the presence of a density fluctuation at frequency ω and wave number k, a second electromagnetic wave ($\omega_0 - \omega$, $k_0 - k$) is excited through the nonlinear polarization. This wave is a higher-order mode of the unstable resonator and hence could have a higher loss rate than the fundamental mode. Therefore, it may not be excited in the absence of the density fluctuation. The two electromagnetic waves in turn amplify the density fluctuation through the heating term. In addition they excite fluctuations in the equilibrium gain through the flux-saturation term. This completes the feedback "loop." Since the heat deposition is a dissipative process, this instability is nonconservative and turns itself off. The reason for this is that once all the energy from the primary wave (ω_0, k_0) has been deposited into the secondary electromagnetic wave and the acoustic wave, there is no way of returning the energy to the primary wave as would be the case of ordinary conservative nonlinear instabilities. Because of the additional loss of the secondary wave (higher-order mode) it, too,

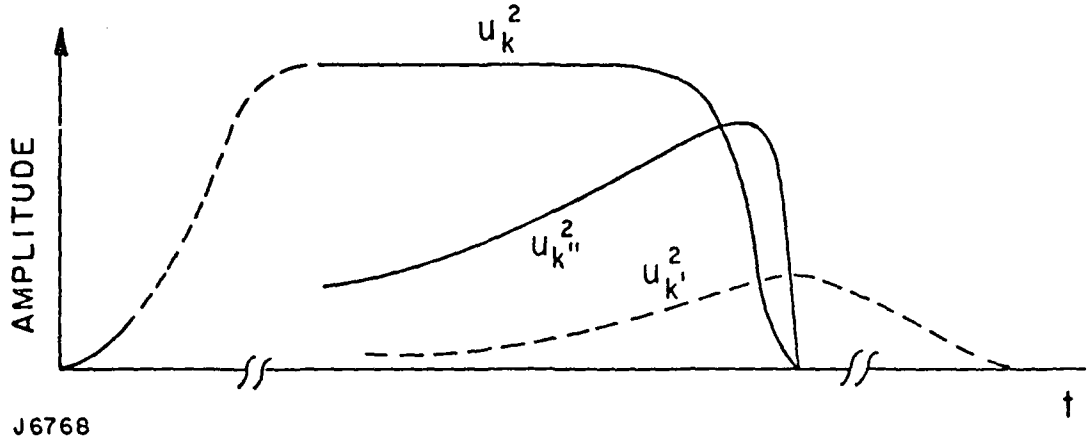

Figure 8. Nonlinear Saturation

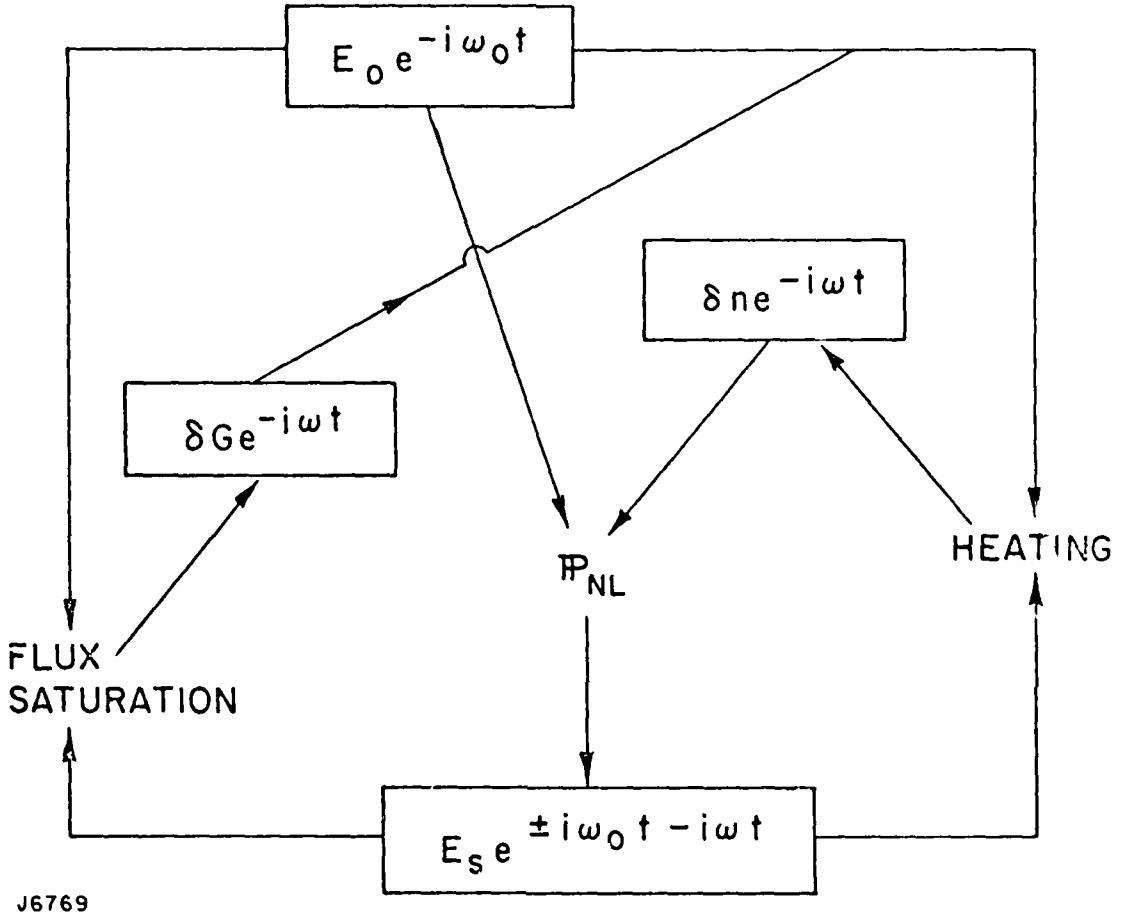

Figure 9. Physical Processes Involved in a Three-Wave Instability

leaks out once the primary wave has decayed. The whole process restarts because the primary wave is once again built up by the lasing medium. The acoustic waves may remain present throughout this phase because of their relatively long damping time constant.

The equations we have derived in our differential formulation reduce to those of Section II when the two electromagnetic modes are degenerate in frequency, as they must.

The process of dielectric modulation was studied and also shown to be unstable. This is a form of Brillouin scattering including the effects of gain-flux oscillations.

SECTION V

UNSTABLE RESONATORS WITH SATURABLE GAIN

A. INTRODUCTION

Unstable resonators have found widespread use in high-gain lasers. As early as 1965[9] it was recognized that these resonators are desirable for a number of reasons. These include:

1) The large mode volume that can be obtained.

2) The uniformity of illumination (and hence energy extraction) seen by the gain medium.

3) The relative freedom (compared to stable resonators) from undesired higher-order transverse modes.

In the realm of geometric optics, the operation of an unstable resonator such as the one shown in Figure 10 is obvious: The output is a plane wave. However, when diffractive effects are included, mode properties are not obvious and the calculation is complicated in the extreme. The understanding of unstable resonator properties that has evolved over the past 15 years has been derived from the gradual development of ever more sophisticated calculation techniques.[10-15] Prior to this report, the study of unstable resonators had advanced

---

9. Siegman, A.E., Proc. IEEE 53, p. 277 (1965).
10. Fox, A., and Li, T., Bell Syst. Tech. J. 40, pp. 453-488.
11. Streiffer, W., IEEE J. Quant. Elect. QE-4, pp. 229-230 (April 1968).
12. Bergstein, L., Appl. Opt. 7, p. 495 (1968).
13. Chen, L., and Felsen, L., IEEE J. Quant. Elect. QE-9, pp. 1102-1113 (November 1973).
14. Horwitz, P., J. Opt. Sci. Am. 63, pp. 1528-1543 (December 1973).
15. Moore, G., and McCarthy, R., J. Opt. Soc. Am. 67, pp. 228-241 (February 1977).

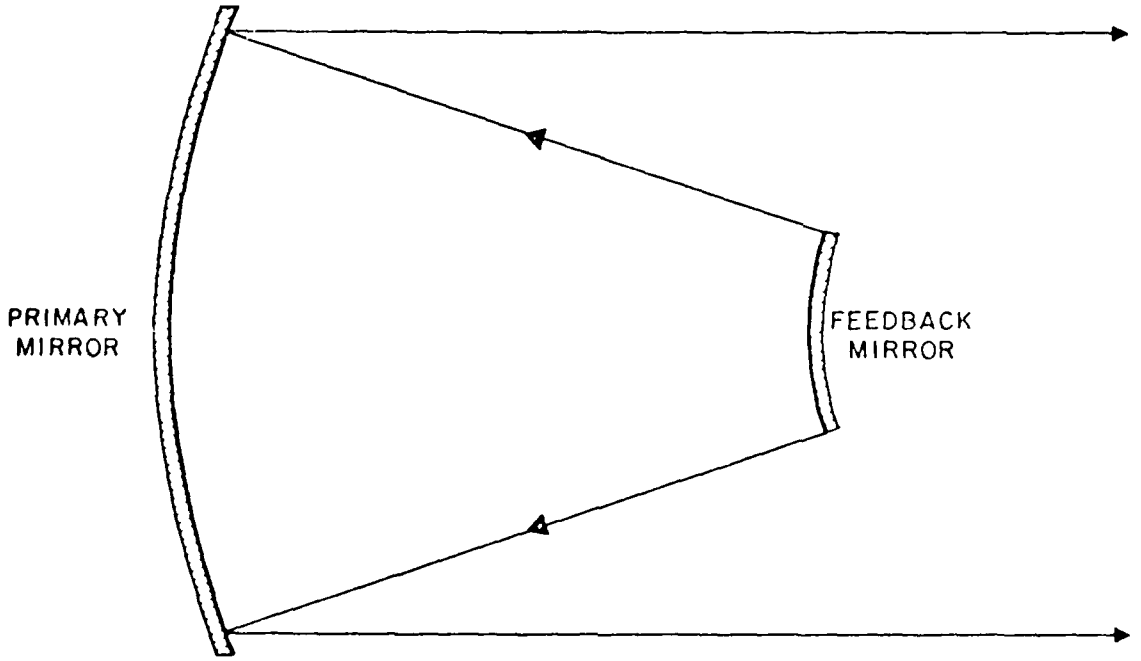

Figure 10. Telescopic Unstable Resonator, Showing Collimated Output Beam

to the point where the effects of diffraction and deterministic intra-cavity gain distributions were understood.(15) In this report we carry the level of understanding one step further, and include the self-consistency problem associated with gain saturation as found in actual lasers.

B. NOMENCLATURE AND STATEMENT OF PROBLEM

In this section, we express the coupled diffraction and saturated gain problem in terms of the one-dimensional strip confocal unstable resonator, as shown in Figure 11. Comparable analysis can be made using two-dimensional rectangular symmetry or circular symmetry resonators, but we wish to avoid these additional mathematical and computational complexities here. It should be noted that, for the case of empty (no gain) resonators, the diffractive properties differ only in detail among the several geometries.

In the absence of either a saturable or non-uniform gain, the optical properties of the strip resonator are described by the well-known integral equation(16)

$$\lambda f(x) = \left(\frac{2 i M^2}{M^2 - 1} F_{eff} \right)^{1/2} \int_{-1 + \varepsilon}^{+1 + \varepsilon} \exp \left[- i \pi \frac{2M^2}{M^2 - 1} F_{eff} \left(x' - \frac{x}{M} \right)^2 \right] \cdot f(x') \, dx' \tag{168}$$

In this equation

$f(x)$ = the complex optical amplitude in the plane of the feedback mirror

λ = the eigenvalue corresponding to $f(x)$

M = geometric magnification

F_{eff} = the so-called effective Fresnel number

$= (a^2/\lambda' L)[(M - 1)/2]$

λ' = wavelength of light (not to be confused with λ)

---

16. Weiner, M., Appl. Opt. 18, pp. 1829-1834 (June 1979). The basic resonator equation is described in numerous papers, but this work is the only one to express it explicitly in terms of the effective Fresnel number.

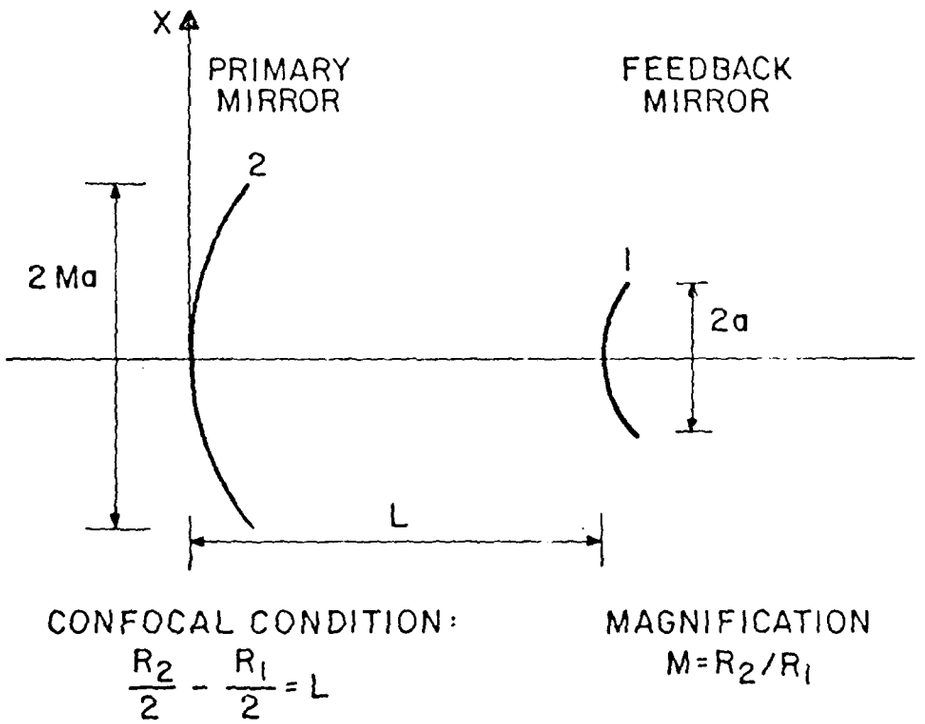

Figure 11. Nomenclature for Unstable Resonator

$2a$ = feedback mirror size

ϵ = the normalized optical axis offset or tilt. ϵ takes on values from 0 to 1.

Equation (168) is just a formulation of the requirement that the optical amplitude distribution reproduce itself, to within the constant λ, after making a round trip back and forth in the resonator. For example, in the limit $F_{eff} \to \infty$, diffraction effects vanish and Eq. (168) takes on the form

$$\lambda f(x) = f(x/M) \tag{169}$$

which has as a solution $f(x)$ = constant and $\lambda = 1$. This is readily identified with the geometric optics result of a plane wave scaled in size by a factor M every round trip, with the output coupling seen to be

$$L_c = 1 - (1/M) \tag{170}$$

which is just the fraction of the mode not blocked by the feedback mirror.

In many cases of practical interest, however (e.g., infrared lasers), a geometric description is not sufficient and diffraction effects must be included, even though the optical properties may be largely geometric in character. This corresponds to solutions of the integral equation for which

$$1 \lesssim F_{eff} \lesssim 100$$

$$1.5 \lesssim M \lesssim 4$$

For a given combination of M, F_{eff} and ϵ, there are several solutions, each with its eigenvalue and eigenfunction, corresponding to the several transverse modes of the resonator. With the eigenvalue equation defined as in Eq. (168), the (one-dimensional) output coupling $L_c(i)$ associated with each mode is given by

$$L_c(i) = 1 - \frac{|\lambda_i^2|}{M} \tag{171}$$

We may assess the effect of diffraction by monitoring output coupling, or equivalently, $|\lambda|$, as F_{eff} is varied.

Figure 3, from Ref. 13, shows such a curve for M = 2.9, ε = 0, and F_{eff} between 5 and 20. An overall periodicity in F_{eff} is apparent, as well as degenerate crossing points (e.g., $F_{eff} \cong 8.9$) where two modes share the same value of $|\lambda|$. In an actual laser, such points may cause undesirable mode hopping. A very similar pattern of diffraction-induced output coupling variation exists if F_{eff} is kept constant, but the position of the optical axis (ε) is varied.(17,18) Even if the modes are not actually degenerate, the magnitude of the output coupling ripple is important for assessing mode-medium interaction effects. This latter situation is perhaps the more likely in an operating device, as it can readily be induced by, say, a mirror vibration, or by a density perturbation, leading to MMI instabilities.

In any realistic high-efficiency laser the gain will always be saturated. The effect of the presence of gain saturation on theoretical curves such as depicted in Figure 12 has heretofore not been assessed, and provides the purpose for this study. In the main theoretical analysis, we consider only aligned resonators (ε = 0), but in Section E we show how tilted resonator behavior can be related to the aligned case.

C. METHODOLOGY

For the present analysis we have developed a new algorithm, combining a number of techniques which have not been used together before. The result is an iterative procedure which calculates not only the lowest loss mode, but also the higher-order resonator modes, simultaneously. Even for a highly saturated medium, convergence is obtained in five iterations or less, and there is no difficulty obtaining a solution in the presence of mode degeneracy.

We outline here the techniques which comprise the components of the algorithm. However, since the theoretical aspects of these are in places quite intricate, the reader is referred to the original references for complete details.

1. Initial Empty Resonator Calculation

For a given set of resonator parameters (M, F_{eff}, with ε assumed zero for the rest of the discussion), the empty resonator eigenvalues λ_i and corresponding mode distributions $f_i(x)$ are determined. The asymptotic theory of resonators is used.(14)

---

17. Perkins, J., and Cason, C., Appl. Phys. Lett. 31, pp. 198-200 (August 1977).

18. Kellen, P., and Smith, M., Opt. Eng. 18, pp. 157-160 (March/April 1979).

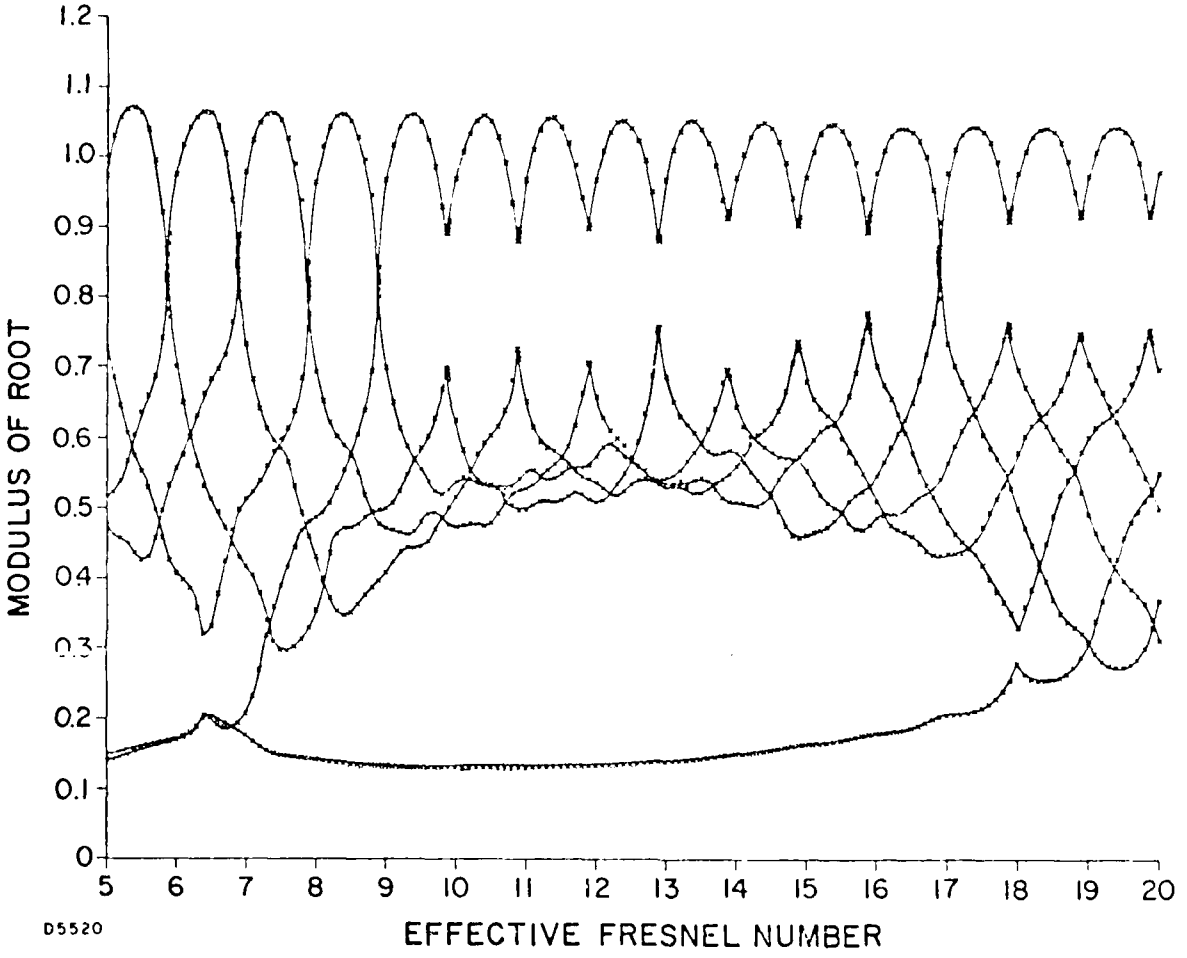

Figure 12. Modulus of Eigenvalues for Empty Unstable Resonator with M = 2.9 and F_{eff} from 5 to 20. Mode degeneracies occur where the curves cross.

This theory can be summarized, in fairly physical terms,[15] as follows. The amplitude function $f_i(x)$ is expanded as a series of slowly modulated cylinder waves, plus a core term $\hat{f}_i$ as follows:

$$f_i(x) = \sum_{n=1}^{N} \left\{ f_{n,i}(x) \frac{e^{ik\, r_n(x)}}{\sqrt{r_n(x)}} \pm f_{n,i}(-x) \frac{e^{ik\, r_n(-x)}}{\sqrt{r_n(-x)}} \right\} + \hat{f}_i(x) \tag{172}$$

The origins of the cylinder waves are successively further removed virtual images of the feedback mirror edges (Figure 13), corresponding to light that has made n trips around the resonator. Then r_n is the distance from the n^{th} virtual image to the observation point in the feedback mirror plane. In the Fresnel approximation, Eq. (172) becomes

$$f_i(x) = \sum_{n=1}^{N} \left(\frac{1}{w_n}\right)^{1/2} \cdot \left\{ \exp\left[\frac{\frac{1}{2} ik(x - x_n)^2}{w_n}\right] f_{n,i}(x) \pm \exp\left[\frac{\frac{1}{2} ik(x + x_n)^2}{w_n}\right] f_n(-x) \right\} + \hat{f}_i(x) \tag{173}$$

The origins of the cylinder waves are at the points

$$w_n = d(M^{2n} - 1) \tag{174a}$$

$$x_n = aM^n \tag{174b}$$

Use of Eq. (173) in Eq. (168) leads to a series of integrals which are solved by the method of stionary phase.[19] This is valid for $F_{eff} \gg 1$, but has been shown to give reasonable results for $F_{eff} \gtrsim 1$. When this is done, the modulation functions $f_{n,i}$ and the core term $\hat{f}_i$ are found to be expressible in terms of other resonator parameters. The final result is a complex polynomial in a parameter u:

19. Born, M., and Wolf, E., Principles of Optics, 5th Ed. (Pergamon, New York, 1975), pp. 752-754.

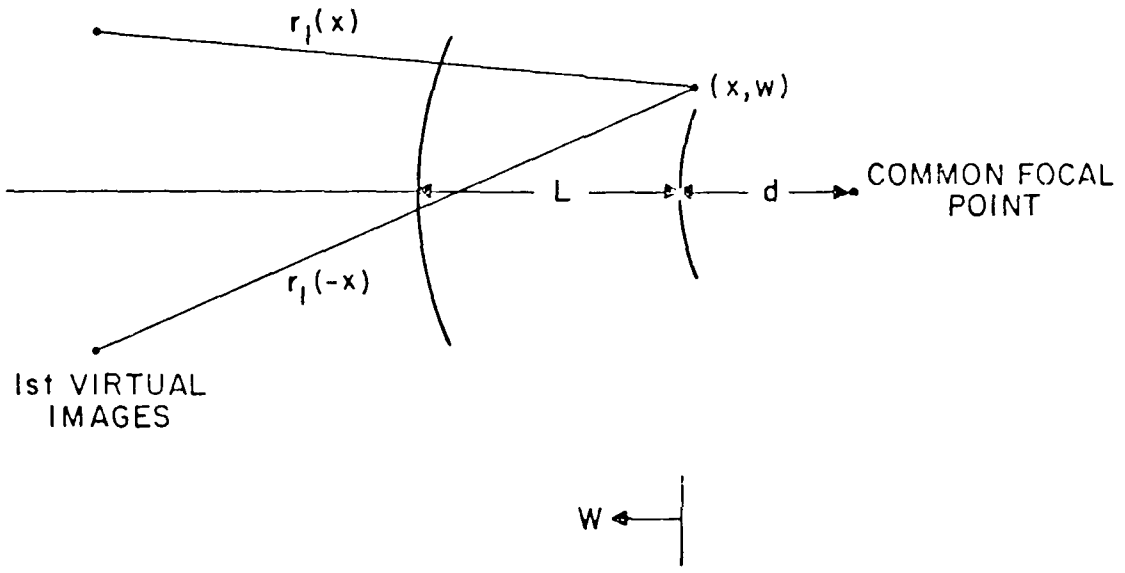

Figure 13. First Virtual Image of Feedback Mirror Edges. Coherent addition of contributions from numerous such virtual images gives rise to the complicated mode structure of the resonator.

$$1 = -\frac{1}{2\pi}\left(\frac{i}{2F_{eff}}\right)^{1/2}$$

$$\cdot\left\{\sum_{n=1}^{N+1}\left[\exp\left(2\pi i F_{eff}\beta_n\right)\beta_n^{-1/2} \pm \exp\left(2\pi i F_{eff}\beta_n^{-1}\right)\beta_n^{+1/2}\right]\mu^n\right.$$

$$\left.\cdot\left(\frac{1}{1-\mu} \text{ for symmetric modes when } n = N+1\right)\right\} \qquad (175)$$

The plus and minus signs denote symmetric and antisymmetric modes. Here

$$\beta_n = \frac{1 - M^{-n}}{1 + M^{-n}} \qquad (176)$$

and the original eigenvalue λ is found from

$$\lambda = \frac{1}{\mu^*} \qquad (177)$$

The lowest-loss mode corresponds to the larges value of $|\lambda|$. The corresponding eigenfunction is found from using

$$f_{n,i}(x) = \frac{(\mu M)^n(1 - M^{-2n})}{(1 - M^{-2})(a + M^{-n}x)} \qquad (178)$$

and

$$\hat{f}_i(x) = \frac{\mu^{N+1}}{1-\mu}\left[a(1 - M^{-2})\right]^{-1}$$

$$\cdot 2\,\frac{e^{2\pi i F_{eff}}}{\sqrt{d}} \qquad (179)$$

in Eq. (172). Since the expression for $\hat{f}_i$ has a factor $1 - \mu$ in the denominator, and since $|\lambda| = 1/|\mu| \sim 1$ for the lowest-loss mode, it dominates Eq. (172) for regions inside the shadow boundaries ($x = \pm Ma$) and represents the "geometric" part of the solution.

The number of virtual images, N, which are needed to fix the order of the polynomial, can be estimated in the following way.[20] Consider the confocal unstable resonator shown in Figure 14 with a spherical wavefront emanating from the common focal point. Radiation within the angle

$$\theta_1 = \frac{D/M}{f_2} \tag{180}$$

which makes one round trip through the cavity, will exit magnified to the whole mode size D. Similarly, radiation within the small core angle

$$\theta_n = \frac{D/M^n}{f_2} \tag{181}$$

which makes n round trips, is magnified M^n times, and also exits with the full mode size D. [This core region is where $\hat{f}_i(x)$ in Eq. (172) arises.] If we desire the cavity to be "diffraction limited" in the usual sense, the exiting radiation must have a cavity angular spread of

$$\theta_c = \frac{\lambda}{D} \tag{182}$$

By requiring the angular spread of the core region to match that of the whole cavity, i.e., $\theta_N = \theta_c$, we have

$$\frac{D}{M^N f_2} = \frac{\lambda}{D} \tag{183}$$

whence

$$N = \frac{\ln\ (8\ M\ F_{eff})}{\ln\ M} \tag{184}$$

In practice, it turns out to be useful to add two or three to N as calculated by Eq. (184), to guarantee that N will be large enough. A similar formula used by Horwitz[14] is

$$N = \frac{\ln\ (250\ F_{eff})}{\ln\ M} \tag{185}$$

---

20. Anan'ev, Y., Sov. J. Quant. Elect. 5, pp. 615-617 (1975).

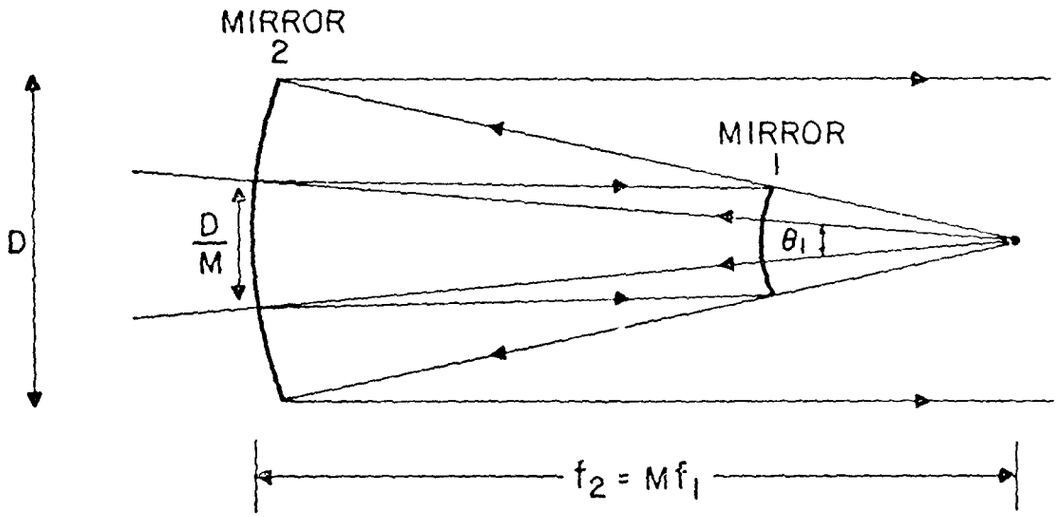

Figure 14. Angular Spread of the First Iteration. For radiation making only round trip of the cavity, the angular divergence θ_1 exceeds the output beam divergence λ/D.

2. Intensity Renormalization

The lowest-loss mode intensity distribution $I(x) = |f_o(x,d)|^2$, corresponding to λ_o, is normalized to the saturated intensity, I_s. To do this, we compute a geometric intensity, I_g, using the theory of geometric strip resonators with saturable gain.[21] We then require that the average intensity over the feedback mirror be the same with and without diffraction:

$$\frac{1}{a} \int_{-a}^{+a} I(x)\, dx = I_g \tag{186}$$

This is to a certain extent heuristic and is strictly true only in the limit $F_{eff} \to \infty$, but is a resonable requirement for the range of F_{eff}'s of interest.

In the geometric theory, we begin with an assumed field form in the cavity; namely, a modulated cylindrical wave emanating from the confocal point, and a modulated plane wave exiting the laser:

$$E = e^{ik(z + L + d)}\, f(z,r) - \frac{1}{\sqrt{\rho}}\, e^{ik\rho}\, g(r,\theta) \tag{187}$$

(Nomenclature is defined in Figure 15. The function $f(z,r)$ here is similar to but not the same as the f function of Section I.) The boundary conditions are that the amplitudes vanish on the mirrors:

$$f(0,r) = \frac{1}{(L + d)^{1/2}}\, g\left(L + d, \frac{r}{L + d}\right) \tag{188a}$$

and

$$f(d,r) = \frac{1}{d^{1/2}}\, g\left(d, \frac{r}{d}\right) e^{2ikL} \tag{188b}$$

By starting with the time-dependent wave equation

$$c^2 \nabla^2 E = \frac{\partial^2 E}{\partial t^2} - 2\, c\, G\, \frac{\partial E}{\partial t} \tag{189}$$

---

21. Moore, C., and McCarthy, R., J. Opt. Soc. Am. 67, pp. 221-227 (February 1977).

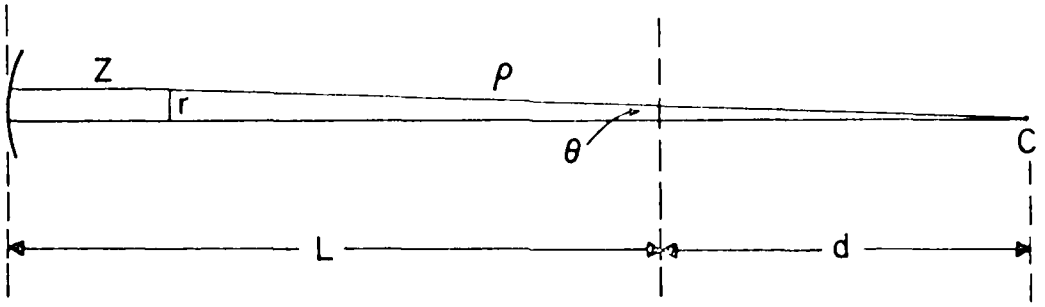

Figure 15. Nomenclature for Geometric Strip Resonator (after Ref. 21)

and neglecting all second-order derivatives, we obtain, using the assumed form for E, the rate equations

$$\frac{\partial f}{\partial z} = G\, f \tag{190a}$$

and

$$\frac{\partial g}{\partial \rho} = G\, g \tag{190b}$$

The gain function, G, is assumed to saturate according to the Rigrod relation[22,23]

$$G = \frac{G_o}{1 + I/I_s} \tag{191}$$

where I_s is the saturation intensity and I is obtained from

$$I = |f(z,r)|^2 + \frac{1}{\rho}\,|g(r,\theta)|^2 \tag{192}$$

The form of Eqs. (190) suggests defining

$$f(z,r) = f_g e^{H(z)} \tag{193}$$

Then, from the boundary conditions, Eq. (188), and noting that M = L + d/d, we have

$$H(0) = 0 \tag{194a}$$

$$H(L) = \frac{1}{4} \ln M \tag{194b}$$

Furthermore,

$$g(L + d - z) = (L + d)^{1/2}\, e^{-H(z)} f_o \tag{195}$$

---

22. Rigrod, W., J. Appl. Phys. 36, pp. 2487-2490 (August 1975).

23. This formula assumes no interference between forward and backward traveling waves. If such interference exists, the effect is to shift the overall value of intensity by a small amount. See G. Agrawal and M. Lax, J. Opt. Soc. Am. 69, pp. 1717-1719 (December 1979).

Using Eqs. (192, (193), and (195) in Eq. (191) yields

$$G = \frac{dH}{dz} = \frac{G_o}{1 + \left[e^{2H} + \left(\frac{L + d}{d + L - z}\right) e^{-2H}\right] f_g^2} \tag{196}$$

Determining a solution consists of finding a value of f_g such that the boundary conditions [Eq. (188)] are obtained when Eq. (196) is integrated. Then $I_q = \sqrt{M}\, f_q^2$ is used in Eq. (186) to normalize the diffractive result.

3. Propagation Through the Gain Region

The renormalized $f_o(x)$ is propagated through the gain region, using simultaneous forward and backward propagation.[24] This process is illustrated in Figure 16. Consider a point (x,w) in the region between mirrors. Here, w is a coordinate measured from right to left away from the feedback mirror.

The "forward" part of the propagation consists of the expanding protion of $f_o(x)$ reflected into the cavity by the feedback mirror, and thus propagates from right to left in the figure. In the absence of gain we have, from the scalar theory of diffraction, the complex amplitude at a point (x,w):

$$U_{ex}\ (x,w) = \int_{-a}^{+a} K(x,x_1)\ f_o(x_1)\ \exp\left[\frac{ik}{2d}\ x_1^2\right] dx_1 \tag{197}$$

The exponential term is the phase curvature resulting from the curved feedback mirror. In the Fresnel approximation K is the propagation function defined by

$$K(x,y) = \left[\frac{i}{\lambda L}\right]^{1/2} \exp\left[\frac{ik}{2L}\ (x - y)^2\right] \tag{198}$$

The "backward" portion is the entire extent of $f_o(x)$, prior to hitting the mirror, evolving backward in time. This propagation is effected using the complex-conjugate propagation function:

---

24. Louisell, W., et al., Appl. Opt. 18, pp. 2730-2731 (15 August)

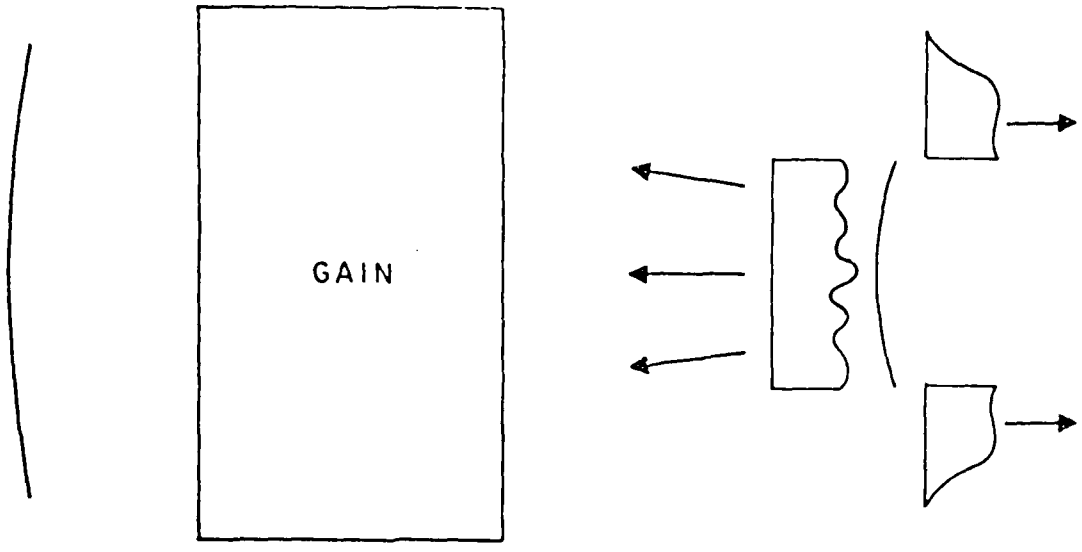

a) "Forward" Propagation

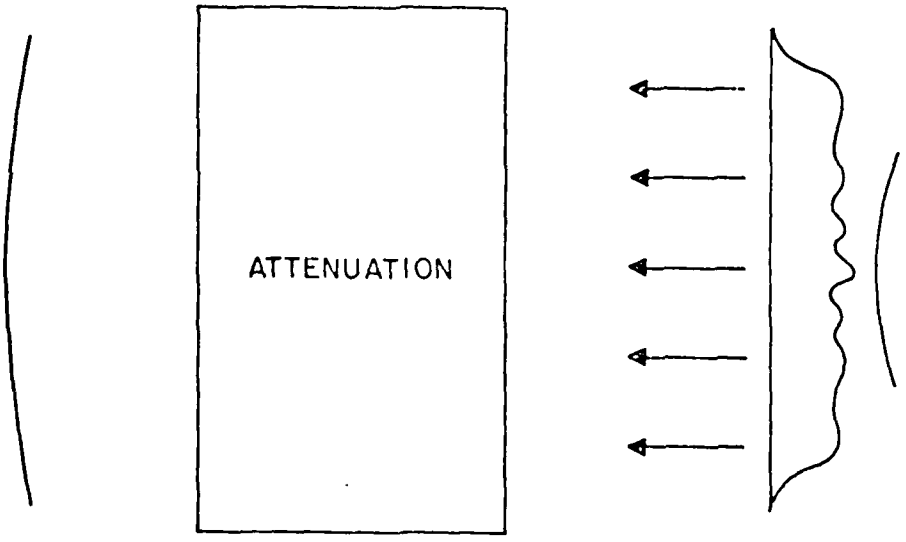

J6071

b) "Backward" Propagation

Figure 16. Simultaneous Forward and Backward Propagation

$$U_{BKW}(x,w) = \int_{-\infty}^{+\infty} K^*(x,x_1)\ f_o(x_1)\ dx, \qquad (199)$$

Thus it, too, propagates from right to left. In this way, both waves move into the gain region in the same spatial sense.

Locally, the saturated gain is computed using, again, the Rigrod formula:

$$G(x,w) = \frac{G_o}{1 + |U_{ex}(x,w)|^2 + |U_{BKW}(x,w)|^2} \qquad (200)$$

Of course, light reaching a particular (x,w') must have traversed gain in the region $w < w'$. To account for this, we insert in Eq. (198) a line integral term

$$G_{ex}(x,w,x_1) = \exp\left[\int G(\vec{\ell})\ d\vec{\ell}\right] \qquad (201)$$

where $\vec{\ell}$ is a vector connecting the observing point (x,w) with each point $(x_1,0)$ on the feedback mirror.

For the backward wave, gain becomes attenuation, so that

$$G_{BKW}(x,w,x_1) = \exp\left[-\int G(\vec{\ell})\ d\vec{\ell}\right] \qquad (202)$$

is used in Eq. (199). This scheme permits systematic calculation of G(x,w) in the direction of increasing w.

4. Modes in the Presence of Gain

The analysis of Moore & McCarthy[15] permits asymptotic calculation of unstable resonator modes [illegible] its function can be specified. In their work, G(x,w) was a postulated function, but this need not be so in general, and, as shown above, we calculate it from the mode pattern itself.

To include the effects of gain in the resonator analysis the eigenvalue polynomial [Eq. (175)] is modified to read

$$1 = -\frac{1}{2\pi}\left(\frac{i}{2F_{eff}}\right)^{1/2}\left\{\sum_{n=1}^{N+1}\Gamma_n'(a)\exp\left[\left(2\pi i F_{eff}\beta_n\right)\beta_n^{-1/2}\right.\right.$$

$$\left.\pm\Gamma_n'(-a)\exp\left(2\pi i F_{eff}\beta_n^{-1}\right)\beta_n^{+1/2}\right]\mu^n \qquad (203)$$

$$\left.\cdot\left(\frac{1}{1-\mu}\quad\text{for symmetric modes when } n = M+1\right)\right\}$$

The new functions, $\Gamma_n'(x)$, are integrated gain functions very similar to Eqs. (201) and (202), except that the path of integration forms n round trips through the cavity, starting at the mirror edge (x = a) and terminating at the point x. Specifically,

$$\Gamma_n'(x) = \exp\left\{\sum_{m=1}^{n}\left[\int_0^L G[X_1(w'),w']\,dw' + \int_0^L G[X_2(w'),w']\,dw'\right] - 2n\int_0^L G(0,w')dw'\right\} \qquad (204)$$

where the integration paths are along rays with coordinates

$$X_1(z') = \frac{M^{-n}}{1-M^{-2n}}\left\{\left[1+\frac{w'}{D}(M-1)\right]\left[M^{m-1}\right]\left[x-M^{-n}a\right] - \left[M^{m-1}\right]^{-1}\left[x-M^{n}a\right]\right\} \qquad (205a)$$

and

$$X_2(w') = \frac{M^{-n}}{1-M^{-2n}}\left\{M^{m}\left[x-M^{-n}a\right] - M^{-m}\left[1+\frac{w'}{D}(M-1)\right]\left[x-M^{n}a\right]\right\} \qquad (205b)$$

The physical significance of these rays is most apparent for $\Gamma'(\pm a)$; in this case, the rays must connect the virtual virtual images of the feedback mirror edges.

The amplitude function $f_i(x)$ is still specified by Eq. (172), save that now the component functions $f_{i,n}(x)$ and $f_i(x)$ are to be multiplied by $\Gamma_n'(x)$ and $\Gamma_N'(x)$, respectively.

In this analysis, we always assume that the lowest-loss mode determines the intensity in the gain region, so that I' functions have an implicit i = 0 subscript.

5. Iteration to Convergence

The updated f(x) amplitude distribution is propagated into the gain region as in step 3, and a new f(x) calculated as in step 4. This process is repeated until convergence is obtained, by which we mean that the change in the lowest-loss eigenvalue, λ_o, is less than some values

$$\Delta\lambda_o < \delta \qquad (206)$$

Since $\lambda_o \sim 1$, this is the same as having the fractional change into λ_o be less than δ.

For a G_oL of 5 (i.e., round trip unsaturated intensity gain is e^{10}), a convergence criterion of $\delta = 0.002$ requires $\lesssim 5$ iterations; for $\delta = 0.0005$, the number is eight to ten. There appear to be two reasons why convergence is rapid with this algorithm. First, the saturated gain calculation always begins with an $f_o(x)$ derived from an empty resonator calculation. Thus in a sense it treats gain as a perturbation. A second reason is that the integrated gain functions, I'(x), are fairly smooth, because they integrate out fine scale longitudinal (w-direction) gain ripple, and do not change by much between iterations.

It must be emphasized that the iterative algorithm presented in this paper is fundamentally different from the Fox-Li iteration[10] generally used to simulate lasers with saturable gain.[25] In the Fox-Li scheme, the resonator integral equation itself is iterated to convergence, starting with some assumed initial mode shape such as a plane wave or Gaussian. In such schemes, the only knowledge of the mode surviving from pass to pass is contained in the numerical array which specifies $f_o(x)$. The mathematical manipulation needed to propagate $f_o(x)$ around the cavity of necessity accumulates error, both from such sources as roundoff error, and from approximations used in the propagation scheme. The necessity for maintaining a highly accurate copy of f(x) implies high sampling frequency compared to typical structure scale sizes contained in f(x), with the result that computer storage requirements dictate a practical upper limit in Feff, usually around unity and certainly less than 10.

25. Szikias, E., and Siegman, A., Appl. Opt. 14, pp.1874-1889 (August 1975). The computer algorithm described in this paper is the archetype of a number of simulation codes in use today.

In contrast, the method presented here need only pass the eigenvalue λ_o from iteration to iteration. Furthermore, since the $\Gamma''(x)$ functions are sensitive only to the largest spatial variations in gain, a highly accurate propagation through the gain region is not essential.

D. RESULTS

The basic purpose of this calculation is to assess the effect of gain saturation on well-known diffractive mode properties. To this end, we consider the particularly illustrative case of a resonator with

$$M = 2.9$$

$$F_{eff} = 8.892,\ 9.390,\ \text{and}\ 9.863$$

Referring again to Figure 12 these F_{eff} values correspond to (in Horwitz's terminology) a so-called crossing point, a point of maximum mode separation, and a cusping point, respectively.

To choose appropriate small-signal gains, we consider the steady-state oscillation condition for a strip resonator in the geometric limit:

$$\frac{1}{M}\, e^{2\, G_o L/[1 + (I/I_s)]} = 1 \qquad (207)$$

or

$$G_o L = \frac{1}{2}\,[1 + (I/I_s)]\ \ln M \qquad (208)$$

We will consider the three regimes of interest:

$$I/I_s << 1$$

$$I/I_s \cong 1$$

$$I/I_s >> 1$$

A very low value of I/I_s is the same as the empty-resonator calculation and is calculated as a matter of course for any other case. As an example of the intermediate case we take $G_o L = \ln M = 1.065$, so that $I/I_s = 1$. For $I/I_s >> 1$, we have chosen $G_o L = 5.0$.

A comparison of the present method with other results is frustrated by the paucity of other results, and by the fact that, since other methods use Fox-Li iteration requiring low F_{eff}, no results are available at the conditions listed at the beginning of this section.

Nonetheless, we have calculated a case for comparison, with results obtained by Rensch and Chester.[26] In their work, a Fox-Li strip resonator calculation was modified to include a saturable gain sheet positioned right at the primary mirror: the amplitude wave as propagated to the primary mirror, amplified and saturated using the Rigrod formula (with local intensity doubled to account for incoming and outgoing waves) and propagated back to the feedback mirror. The resonator parameters are:

$$M = 2.5$$

$$F_{eff} = 0.64$$

$$G_o L = 4.583$$

For this value of F_{eff} the asymptotic method is below its regime of proven validity. Also, Rensch and Chester do not provide eigenvalues but only intensity distributions. Thus a comparison of their results with ours must of necessity be somewhat speculative.

Figure 17 compares bare resonator intensity patterns, and gives a clue as to how the asymptotic method breaks down at very low F_{eff}: the fine scale detail is lost, though the gross shape is basically the same. The situation with gain is comparable (Figure 18). It will be noted that there is a slight difference in the location of the side maxima. In our calculation, they occur at slightly higher values of x/a. We suspect that this is due to an imprecision on Rensch and Chester's part in calculating the effective Fresnel number, since with discrete integration schemes there is always an uncertainty in just where the feedback mirror ends.

For the principal calculations, the gain was confined to a region from z = 0.25 L to z = 0.75 L, since in many high power devices (where unstable resonators find the greatest use) the mirrors are somewhat removed from the lasing medium. However, this is not essential to the algorithm, and the gain can be placed arbitrarily between the mirrors.

---

26. Rensch, D., and Chester, A., Appl. Opt. 12, pp. 997-1013 (May 1973).

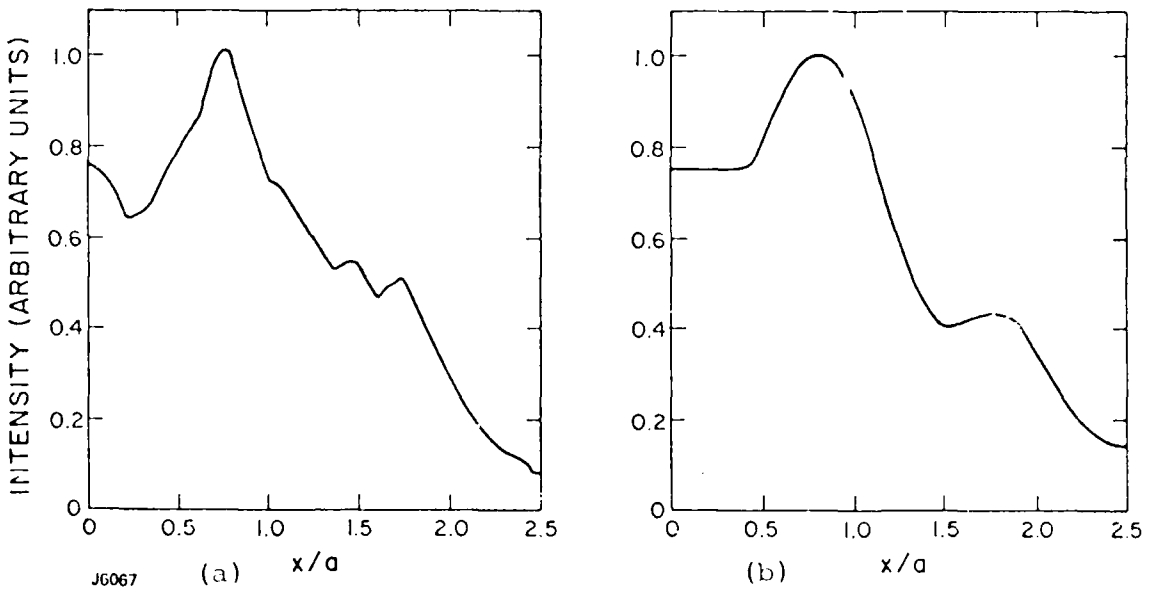

Figure 17. Empty Resonator Modes as Calculated (a) by Rensch and Chester and (b) by Our Analysis. Here M = 2.5 and F_{eff} = 0.64. Even though method (b) is used here outside its range of validity, the agreement with an exact calculation is quite good.

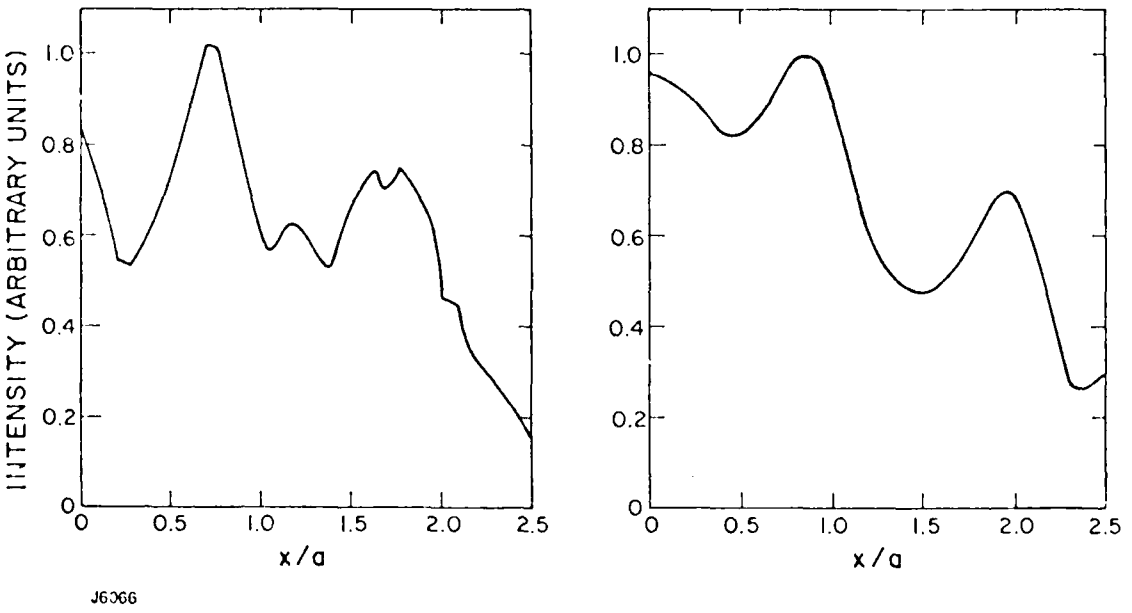

Figure 18. Same Calculation as Figure 8 Except Saturable Gain with $G_oL = 4.583$ Near the Primary Mirror

Results for $F_{eff} = 8.892$ and $G_oL = 1.065$ are shown in Figures 19 through 24. Figures 19 and 20 show intensity and phase for the first pass, i.e., before any gain saturation, but after renormalization. The units of intensity are such that $I_s = 1$. The results after 5 passes appear in Figures 21 through 23. The first depicts $\Gamma'_n(x)$ for various n. As n increases, the curves approach a limiting form. As one would expect, the $\Gamma'_n(x)$ have maxima and minima inversely related to those seen in the intensity plot. Inspection of the bare and saturated intensity profiles shows that the fine scale diffraction features are very nearly the same in both cases, save that the overall envelope of the intensity is made more uniform. We note that it would be hard to claim that the diffractive component of the pattern is exactly suppressed by gain saturation. Figure 15 depicts the saturated gain in the resonator. The optical axis coordinate is in percentage of w/L; i.e., 0 is the feedback mirror location and 100 the primary mirror. The gain scale is in units of gain per optical axis increment. Thus the unsaturated gain is seen to be $1.065/50 \sim 0.02$.

Figures 25 through 28 are for $F_{eff} = 8.892$ but with G_oL increased to 5.0. The most noticeable effect of the increased gain is that the very small amount of "stray light" well beyond the geometric mode size becomes significantly amplified. Since real devices often have scraper apertures specifically to exclude such radiation, its appearance in the present calculation is probably not important. One can also discern that the range of intensity excursions from a mean value has been still further flattened. Interestingly enough, the phase profiles are nearly identical among the three cases.

Figures 29 through 38 depict results for $F_{eff} = 9.39$, and those for $F_{eff} = 9.863$ are shown in Figures 39 through 48. It will be seen that the same qualitative observations can be made for these cases as well.

The preceding plots do not hint at the dramatic effect of gain saturation on eigenvalue, and hence, output coupling. In Figure 49 a portion of the empty cavity plot of Figure 12 is reproduced for F_{eff} between 8.5 and 10.5, along with results from the present calculations. It will be seen that the mode degeneracy at $F_{eff} = 8.892$ is lifted, even for the lesser value of $G_oL = 1.065$ corresponding to $I/I_s = 1$. Calculations at closely spaced intervals near $F_{eff} = 8.892$ have verified that the degeneracy is truly lifted, and not just moved to a nearby Fresnel number. It is also evident that even at the cusping point the ripple in mode separation is reduced, though, surprisingly, there is not as much difference between the $G_oL = 1.065$ and $G_oL = 5.0$ cases as there is between these and the empty-resonator case.

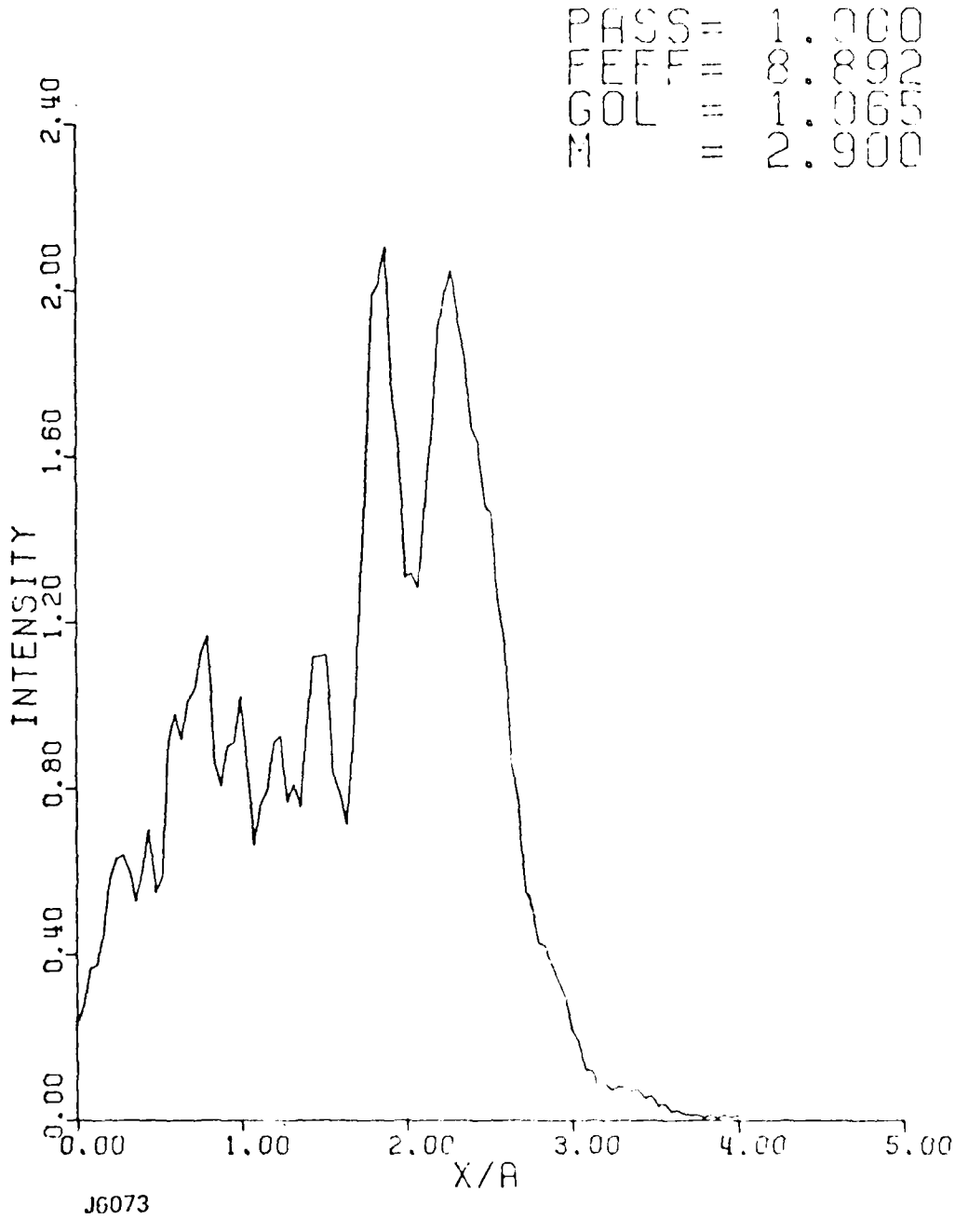

Figure 19. Intensity Profile for Empty Resonator. $F_{eff} = 8.89$.

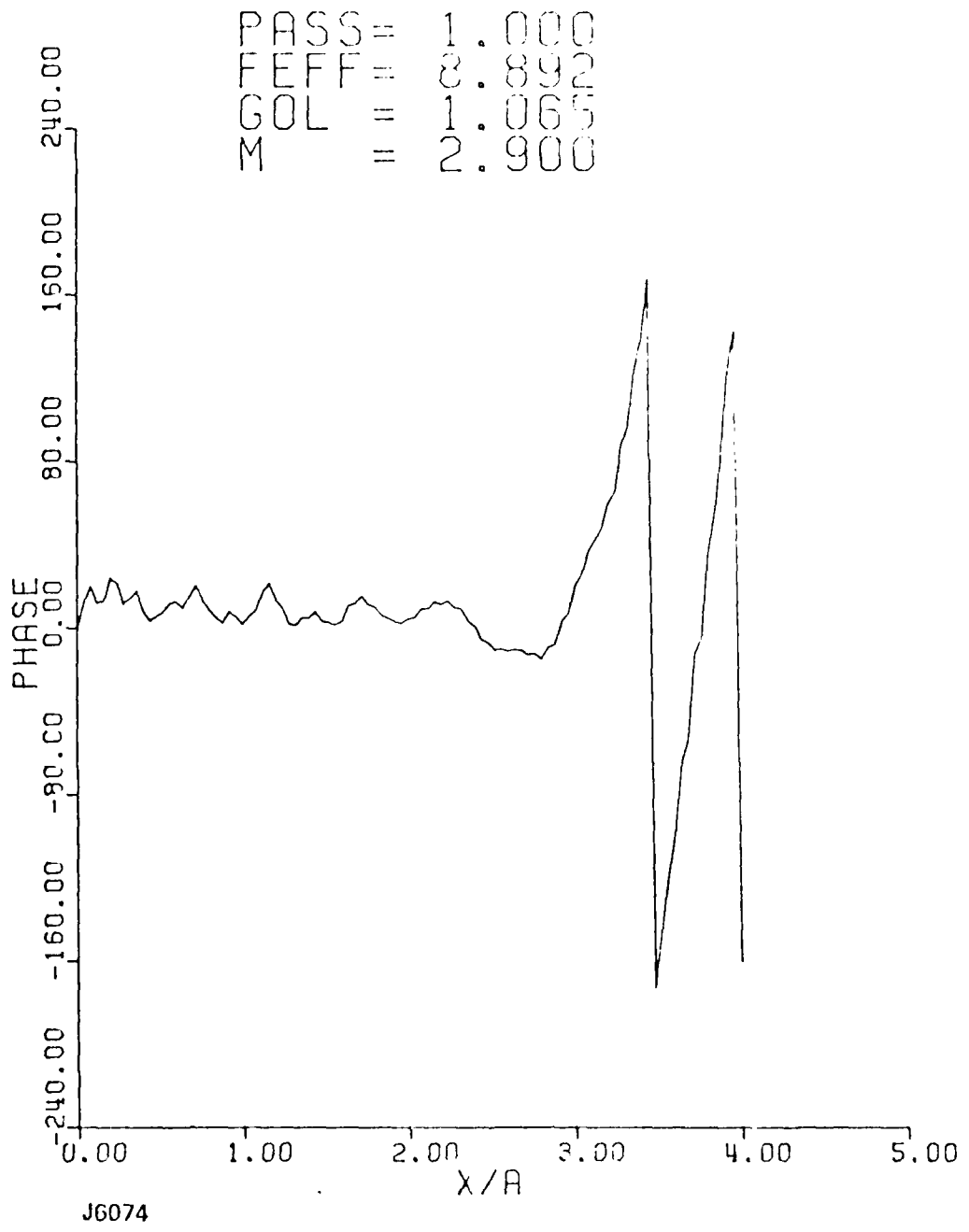

Figure 20. Phase Profile for Empty Resonator. F_{eff} 8.893.

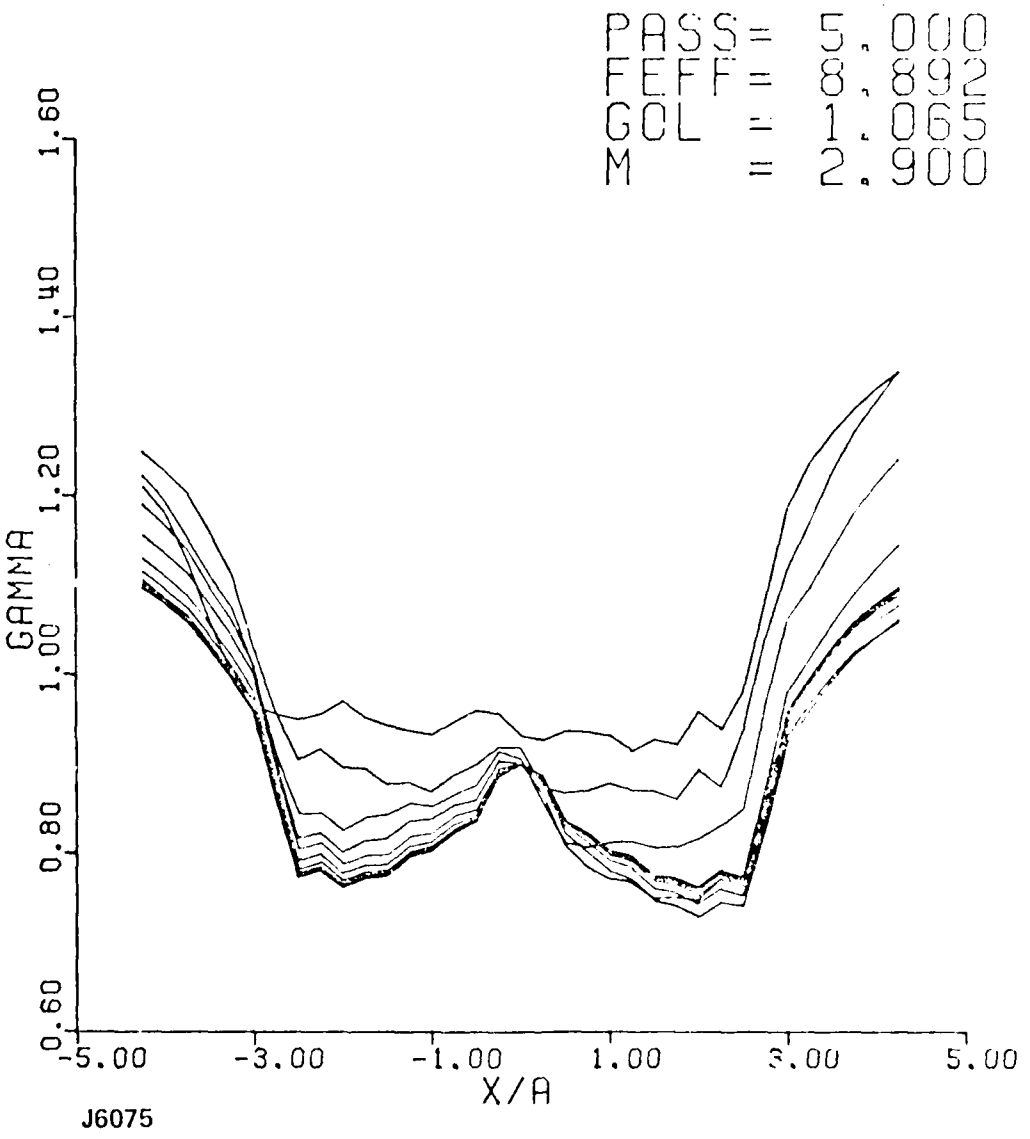

Figure 21. $\Gamma_n'(x)$ Profile for $G_{oL} = 1.065$. $F_{eff} = 8.892$.

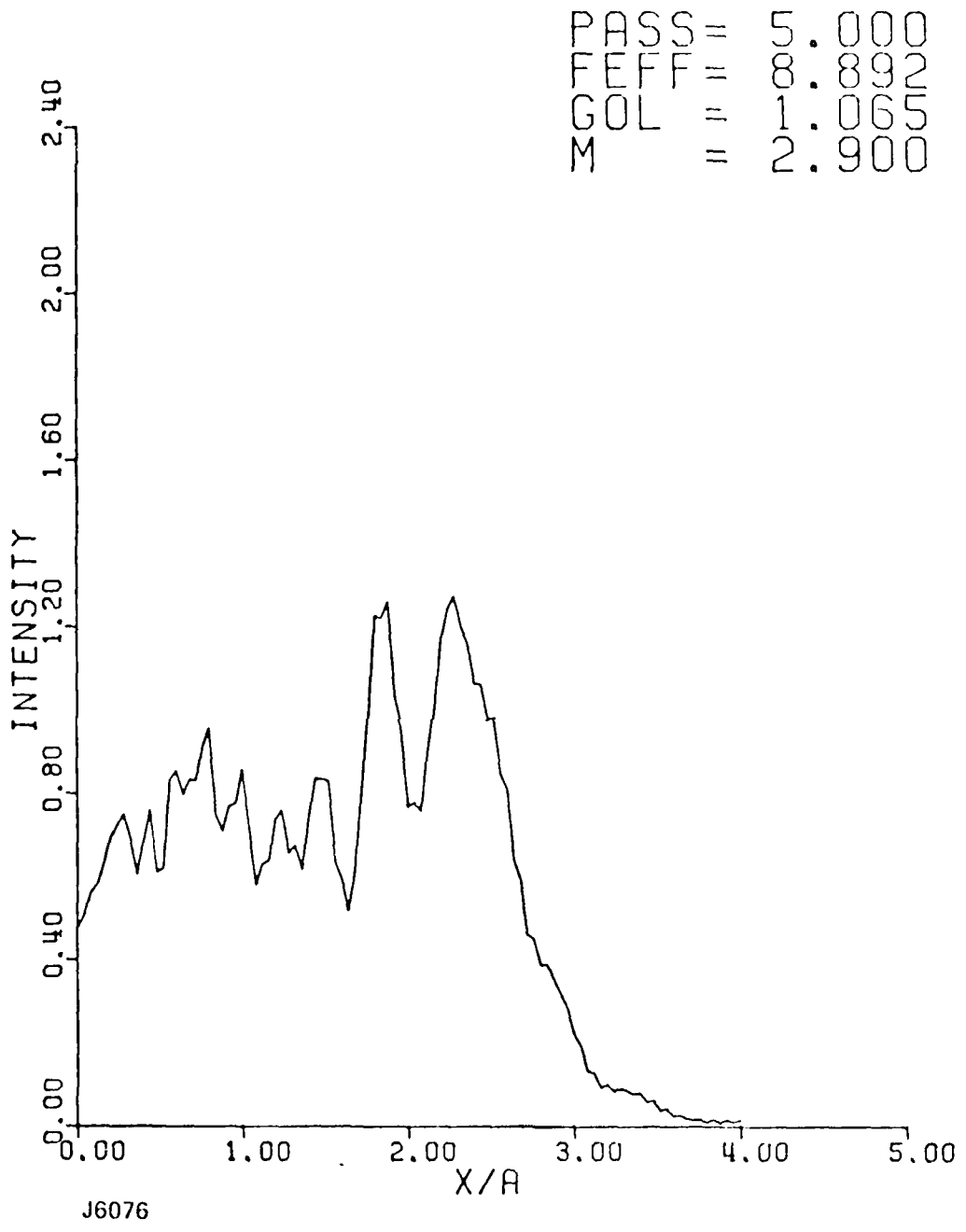

Figure 22. Intensity Profile for G_0L = 1.065. F_{eff} = 8.892. The result here is very similar in detail to the empty resonator case (Figure 19) but the envelope of the distribution is flatter.

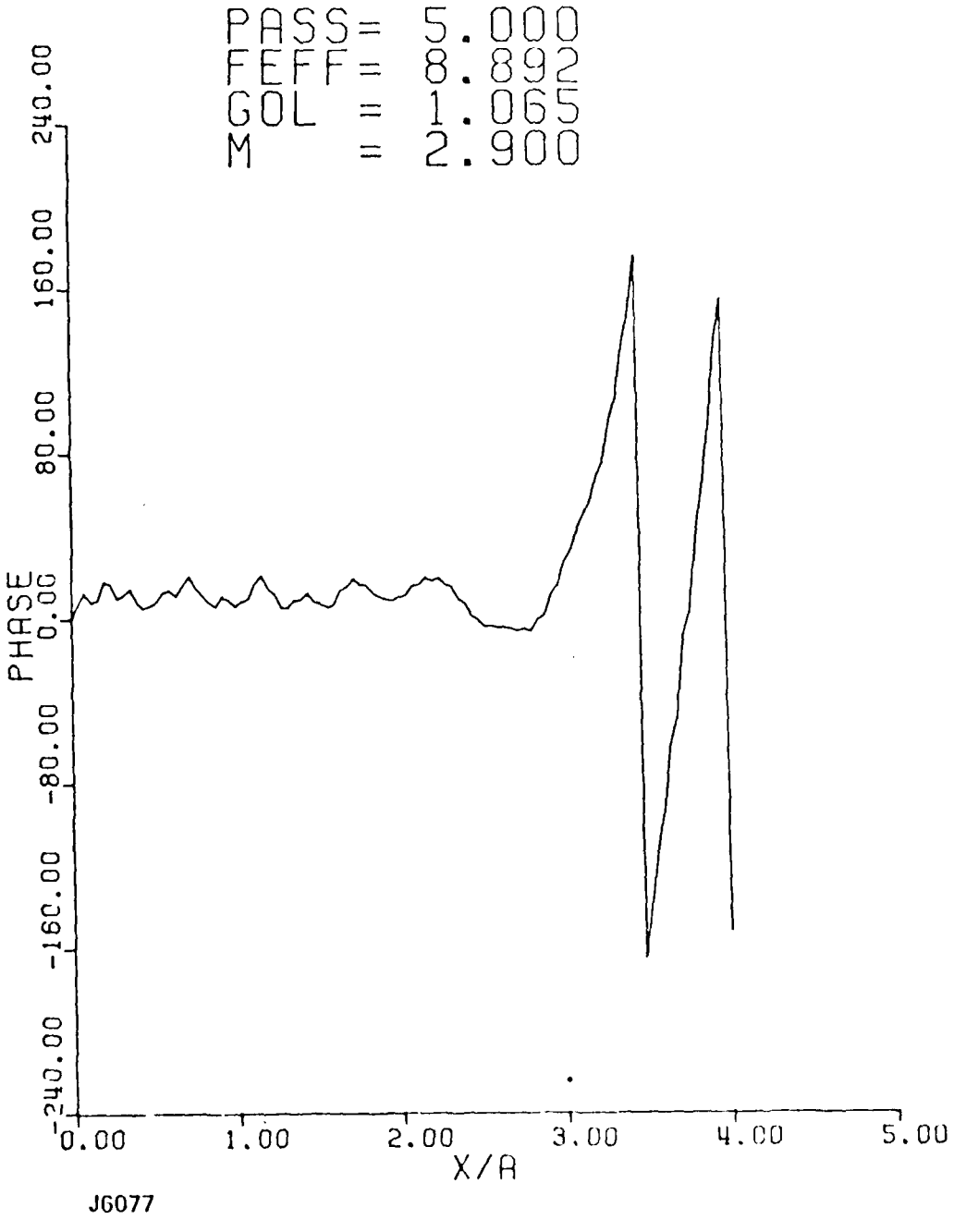

Figure 23. Phase Profile for G_0L = 1.065. F_{eff} = 8.892. This resembles the empty-resonator result even more than the intensity profile.

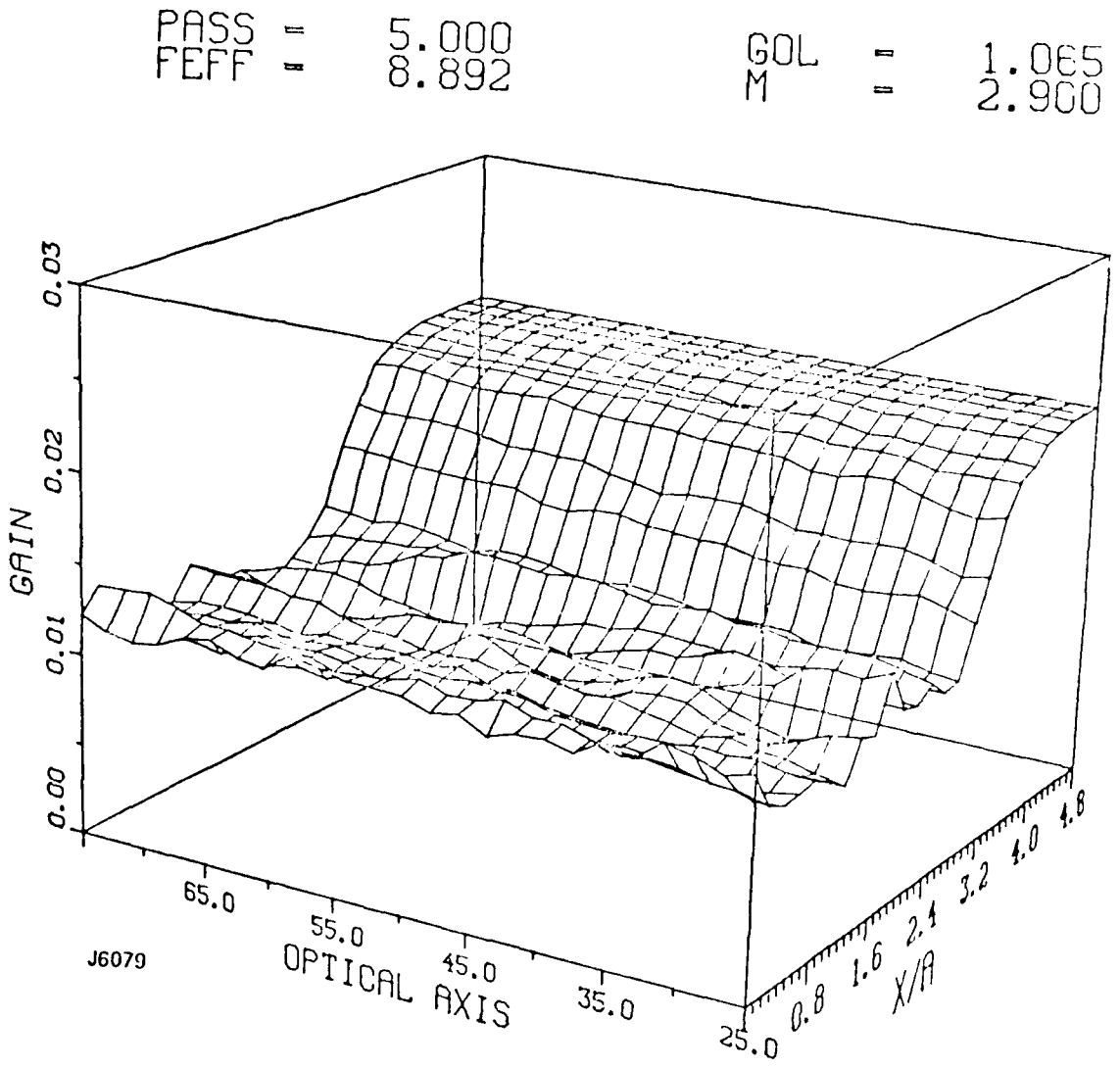

Figure 24. Saturated Gain Profile for G_0L = 1.065, F_{eff} = 8.892. The structure is caused by the local diffraction ripple of the right- and left-going beams.

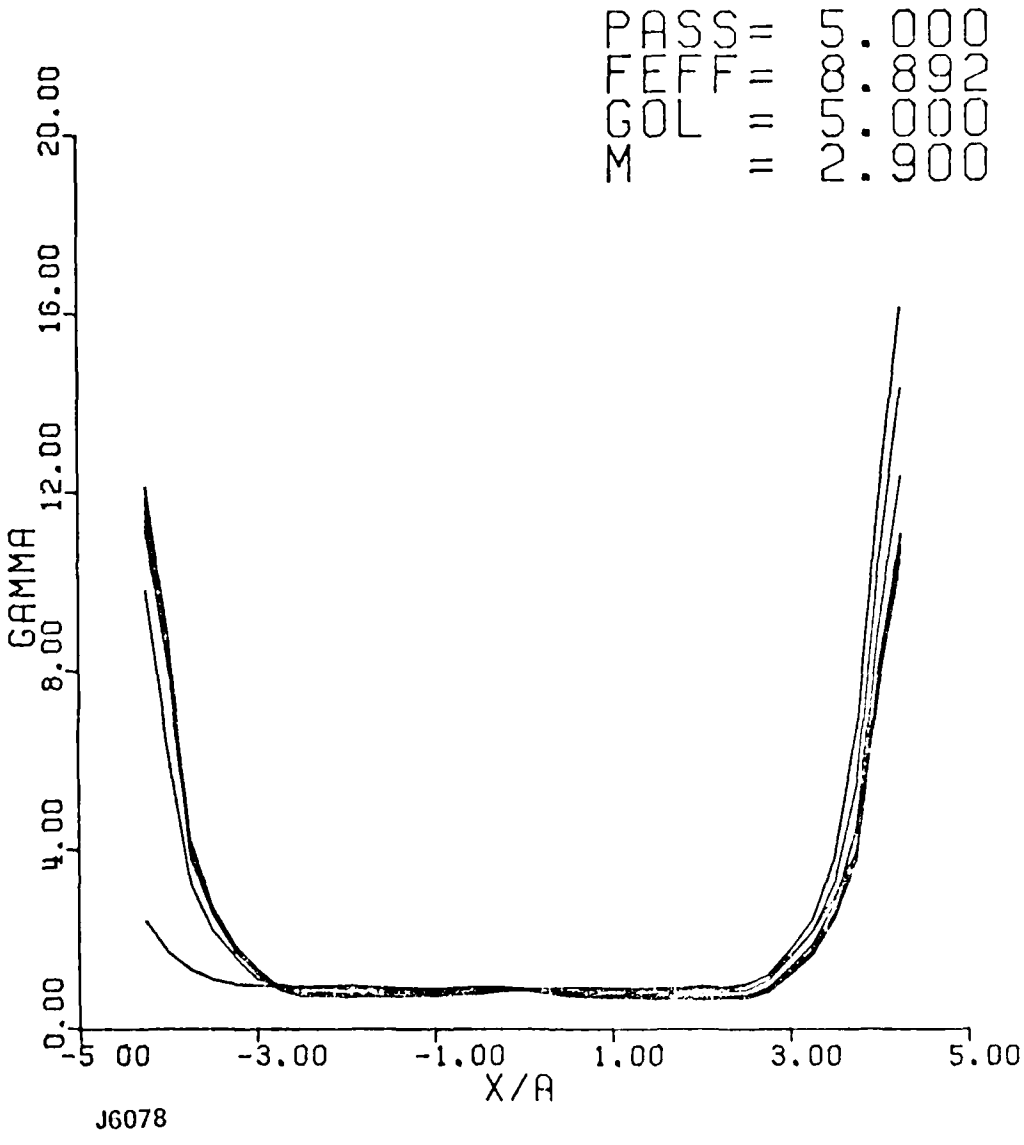

Figure 25. $F_n'(x)$ Profile for G_0L = 5.0. F_{eff} = 8.892. Compared to Figure 21, this curves shows the much higher gain in the geometric shadow region.

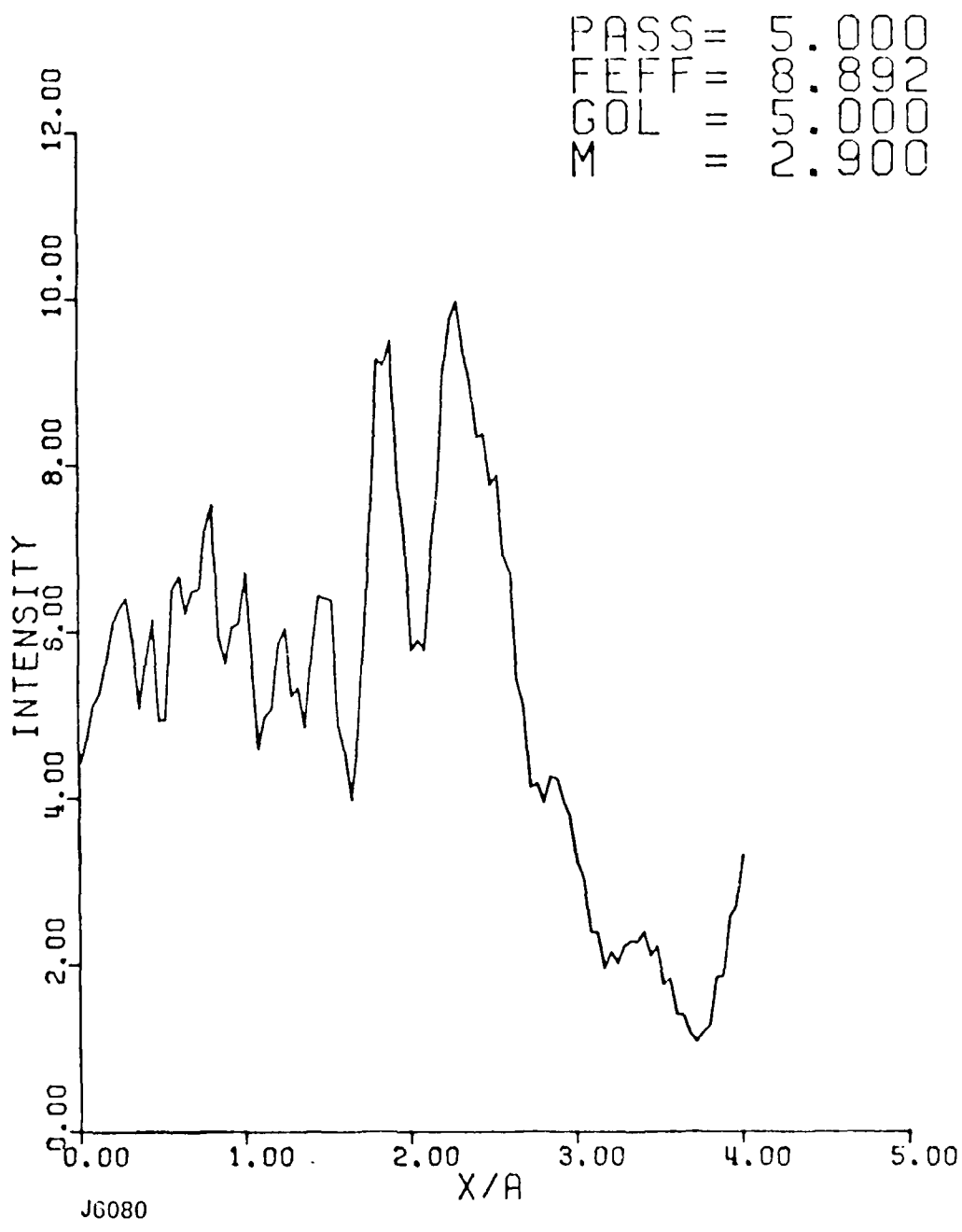

Figure 26. Intensity Profile for G_0L = 5.0. F_{eff} = 8.892. The upturn beyond X/A ~ 3.7 is considered the (enormous) unsaturated gain acting on stray light.

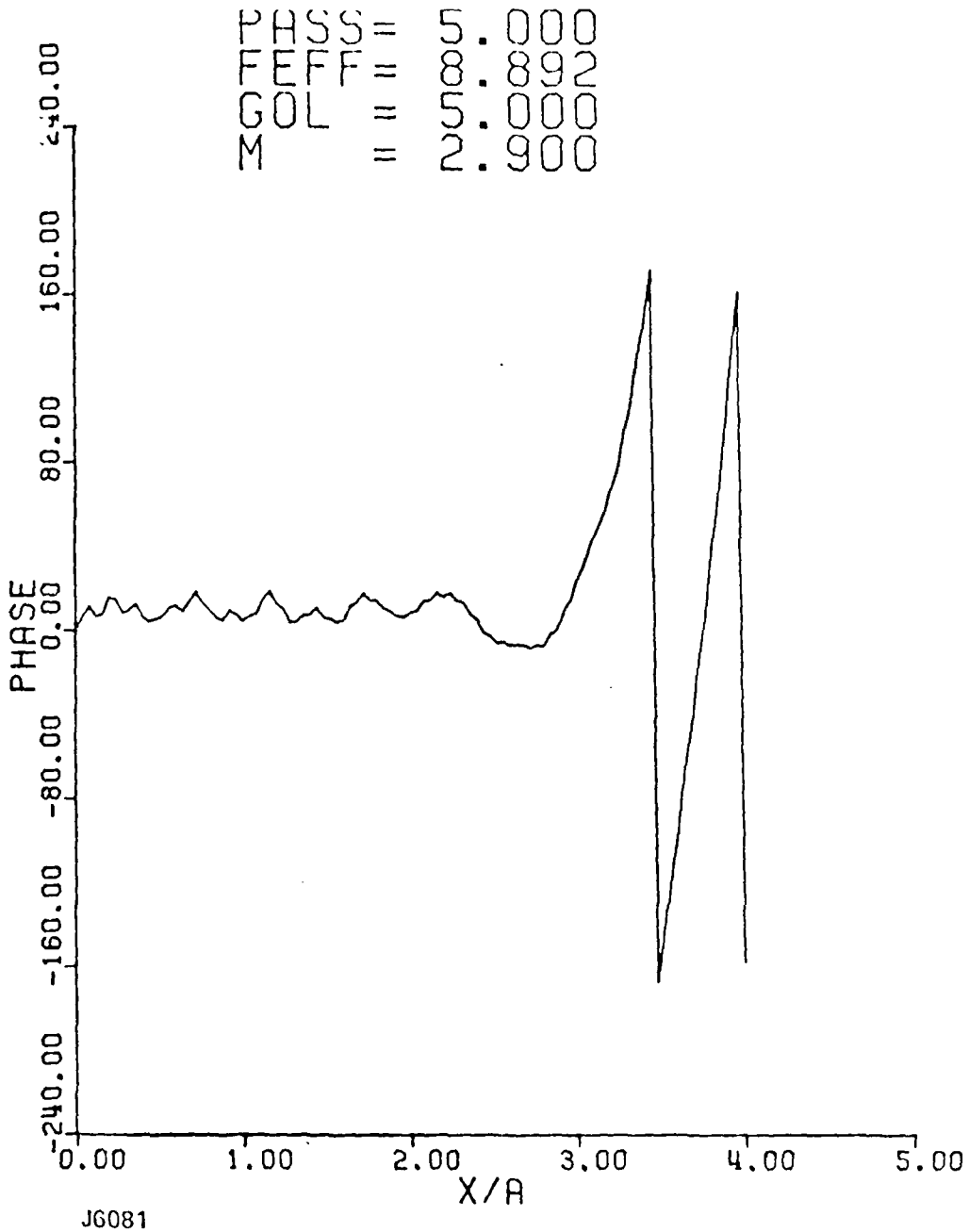

Figure 27. Phase Profile for G_0L = 5.0, F_{eff} = 8.892. In spite of the strong gain peaks, this curve is very similar to the empty resonator case (Figure 23).

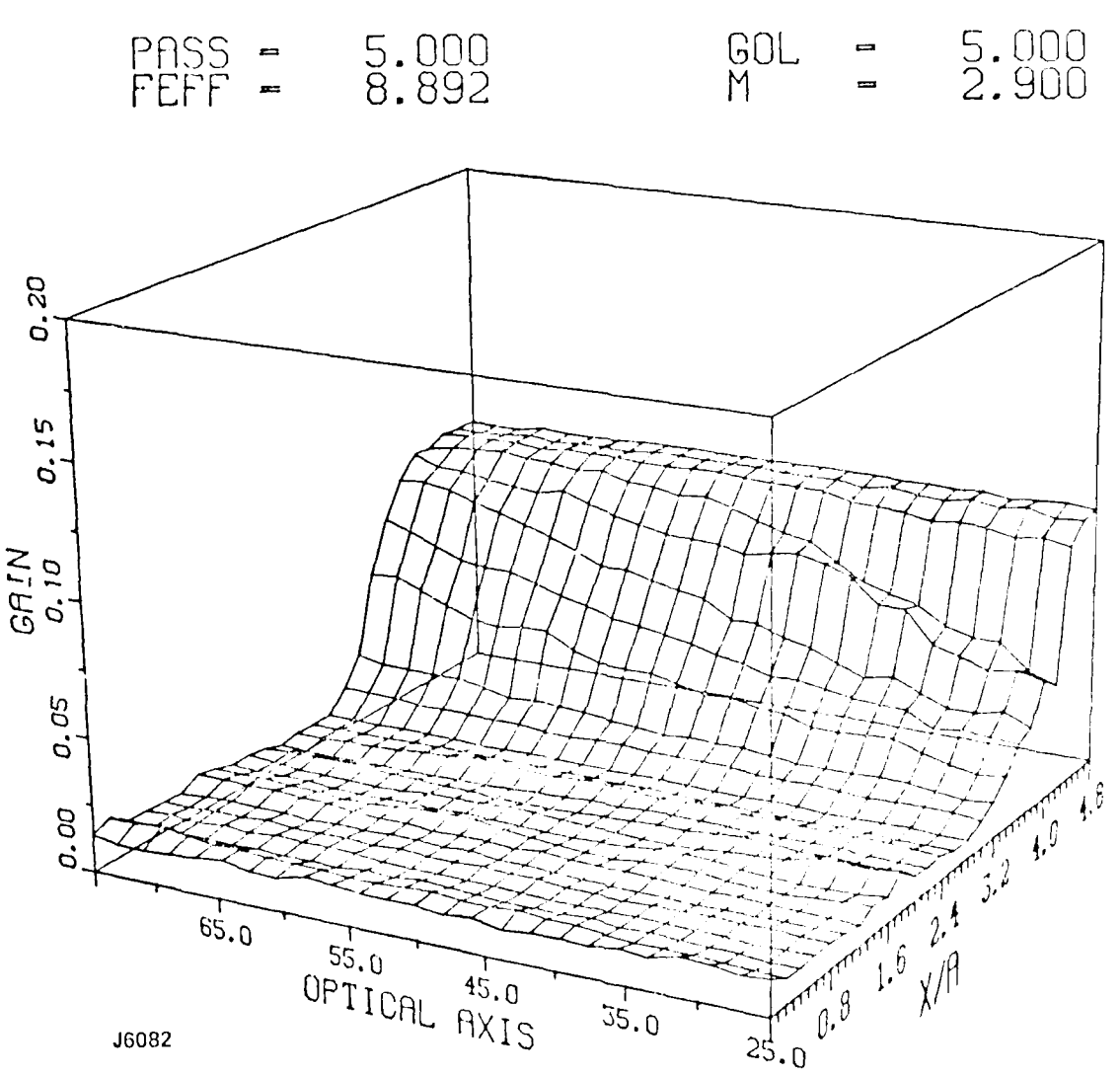

Figure 28. Saturated Gain Profile for G_L = 5.0, F_eff = 8.892. The scale required to show the small signal gain at large X/A makes the structure of the saturated gain for small X/A.

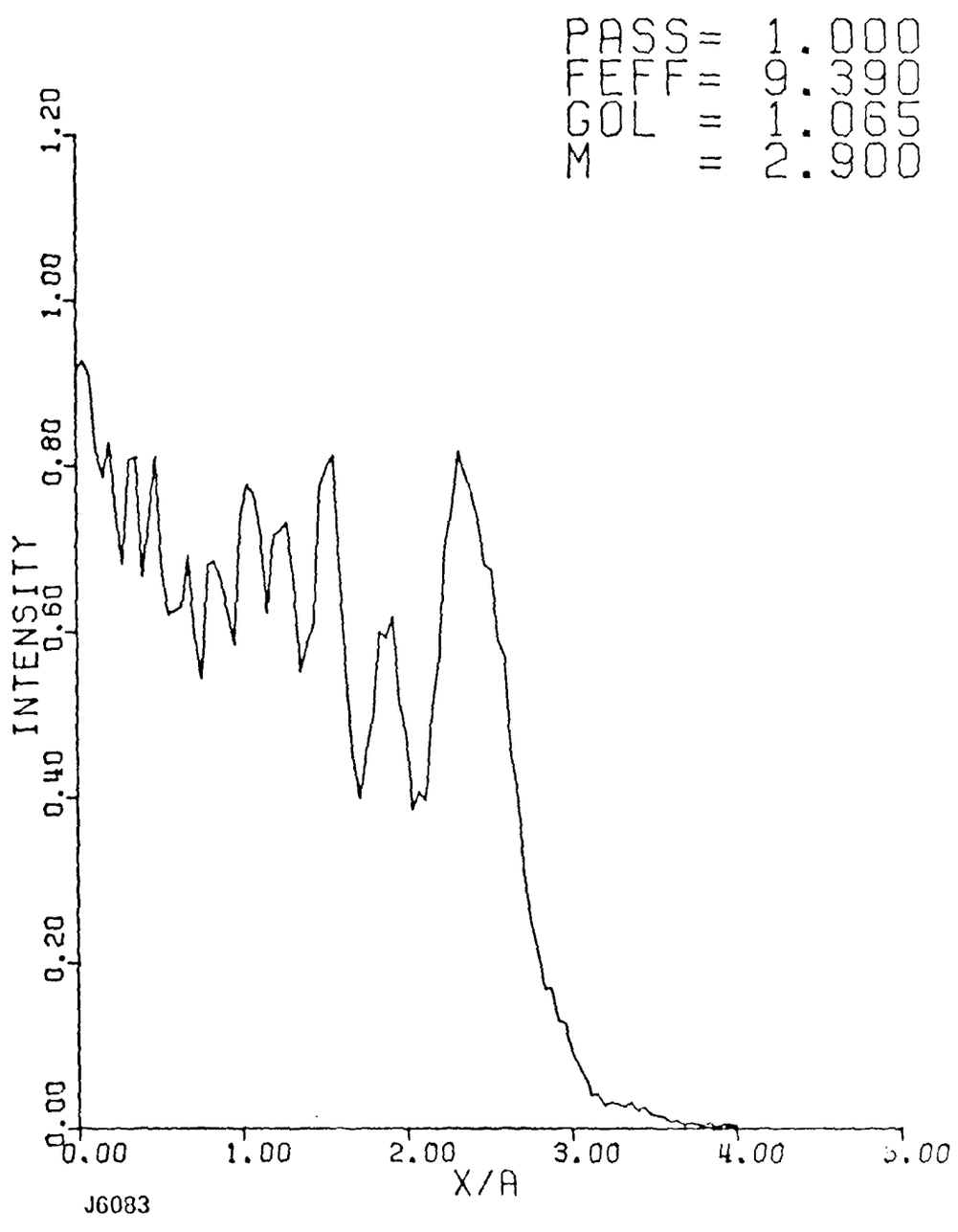

Figure 29. Intensity Profile for Empty Resonator, F_{eff} = 9.39.

AD-A100 905 AVCO EVERETT RESEARCH LAB INC EVERETT MA F/G 20/5
MODE MEDIUM INTERACTION. A THEORETICAL STUDY.(U)
SEP 80 A BALLANTYNE, C DUZY F49620-79-C-0195
UNCLASSIFIED AFOSR-TR-81-0519 NL

2 OF 2
AD A 100905

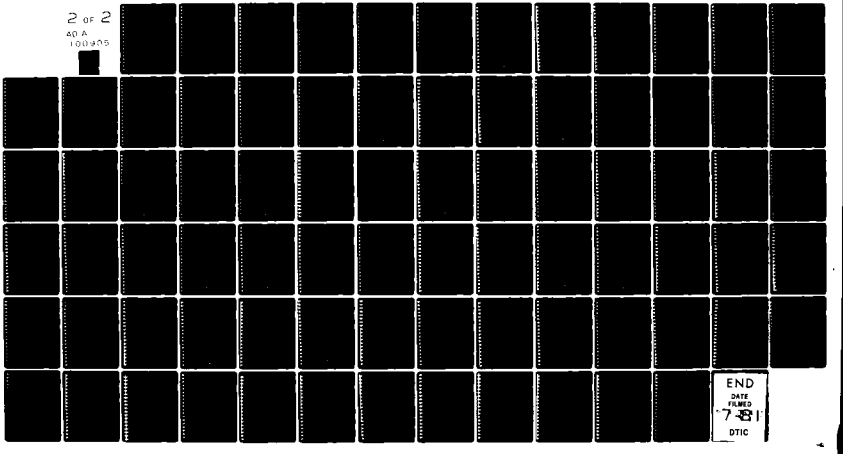

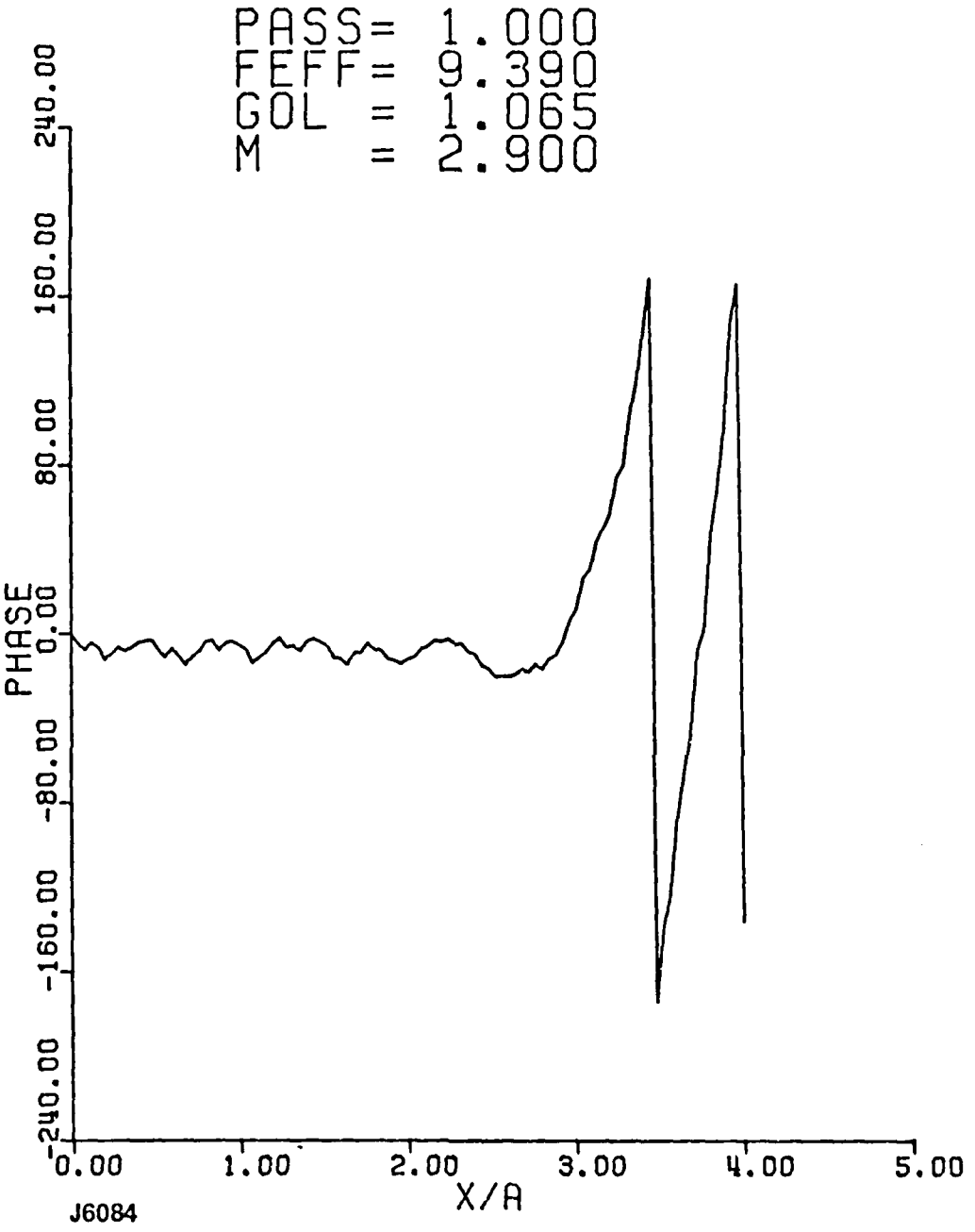

Figure 30. Phase Profile for Empty Resonator. F_{eff} = 9.39.

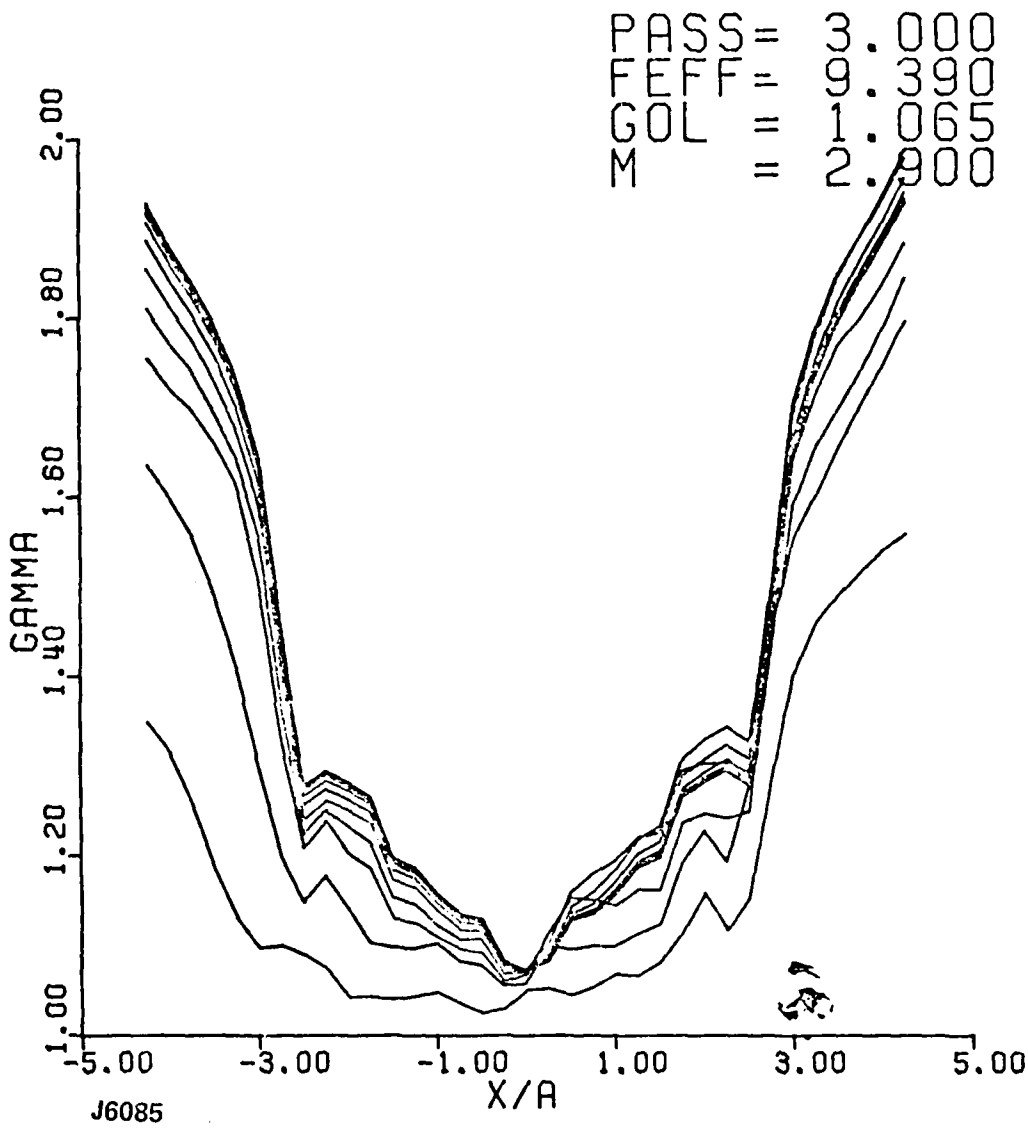

Figure 31. $\Gamma_n'(x)$ Profile for G_oL = 1.065. F_{eff} = 9.39.

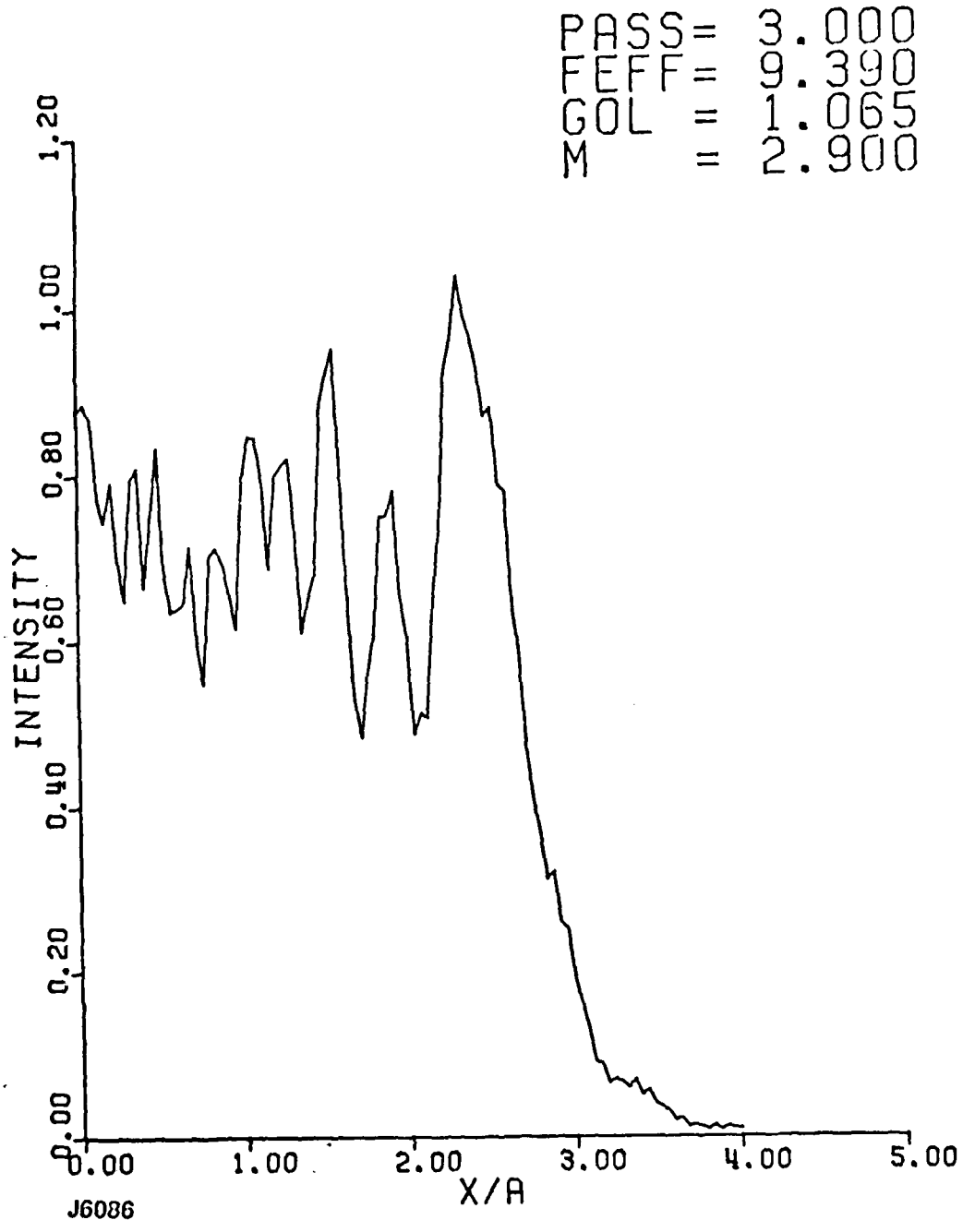

Figure 32. Intensity Profile for $G_oL = 1.065$. $F_{eff} = 9.39$.

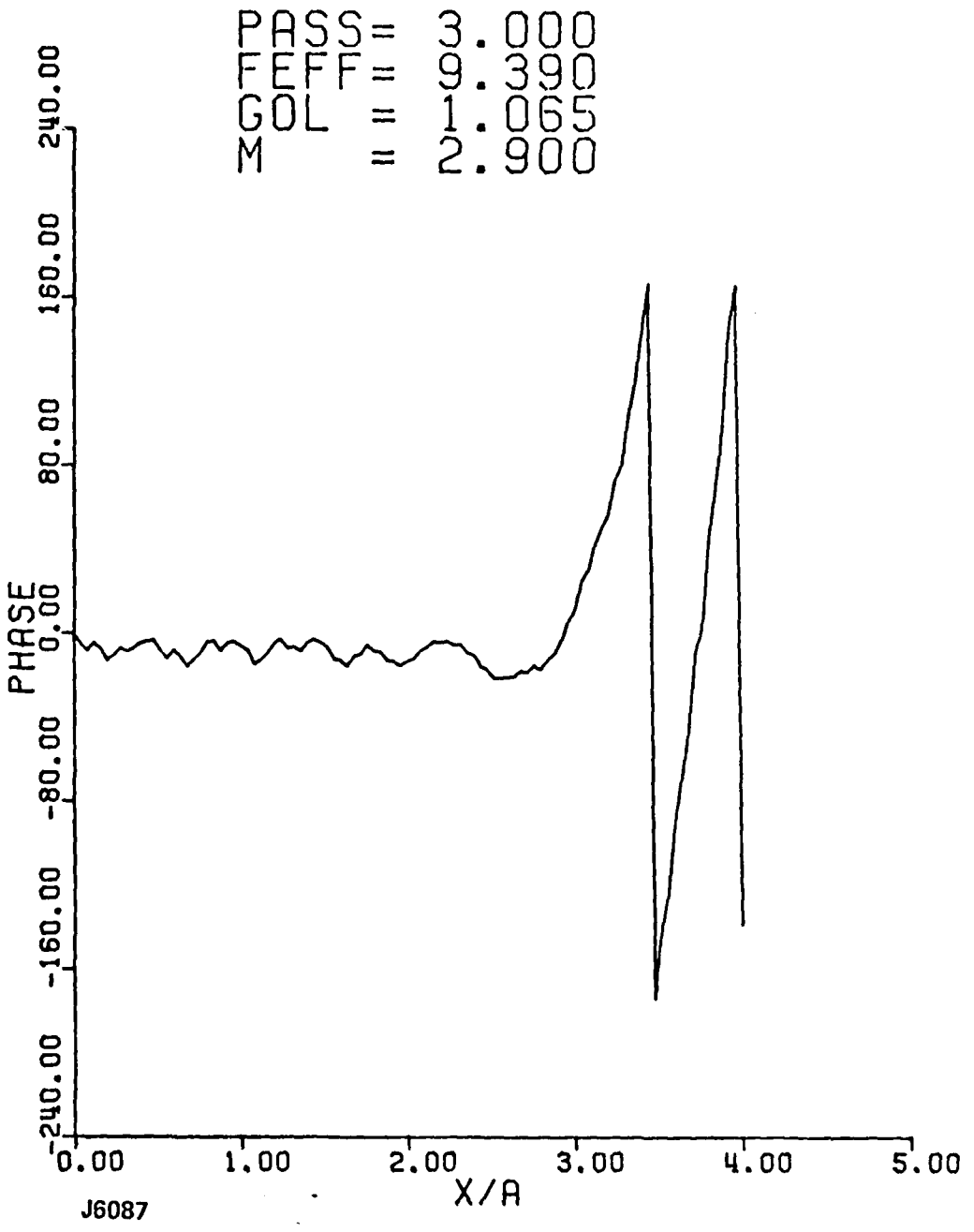

Figure 33. Phase Profile for G_oL = 1.065. F_{eff} = 9.39.

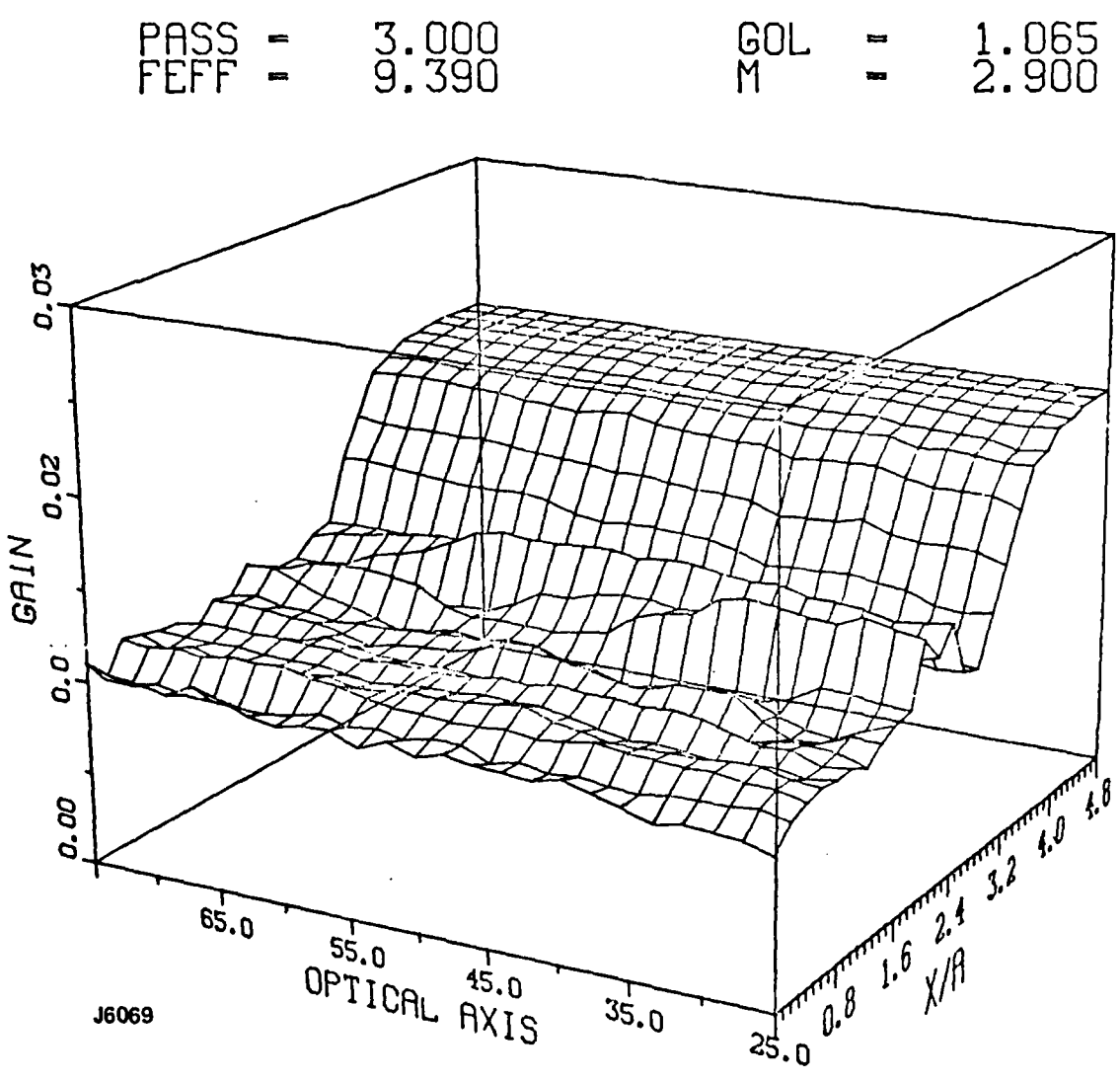

Figure 34. Saturated Gain Profile for G_oL = 1.065. F_{eff} = 9.39.

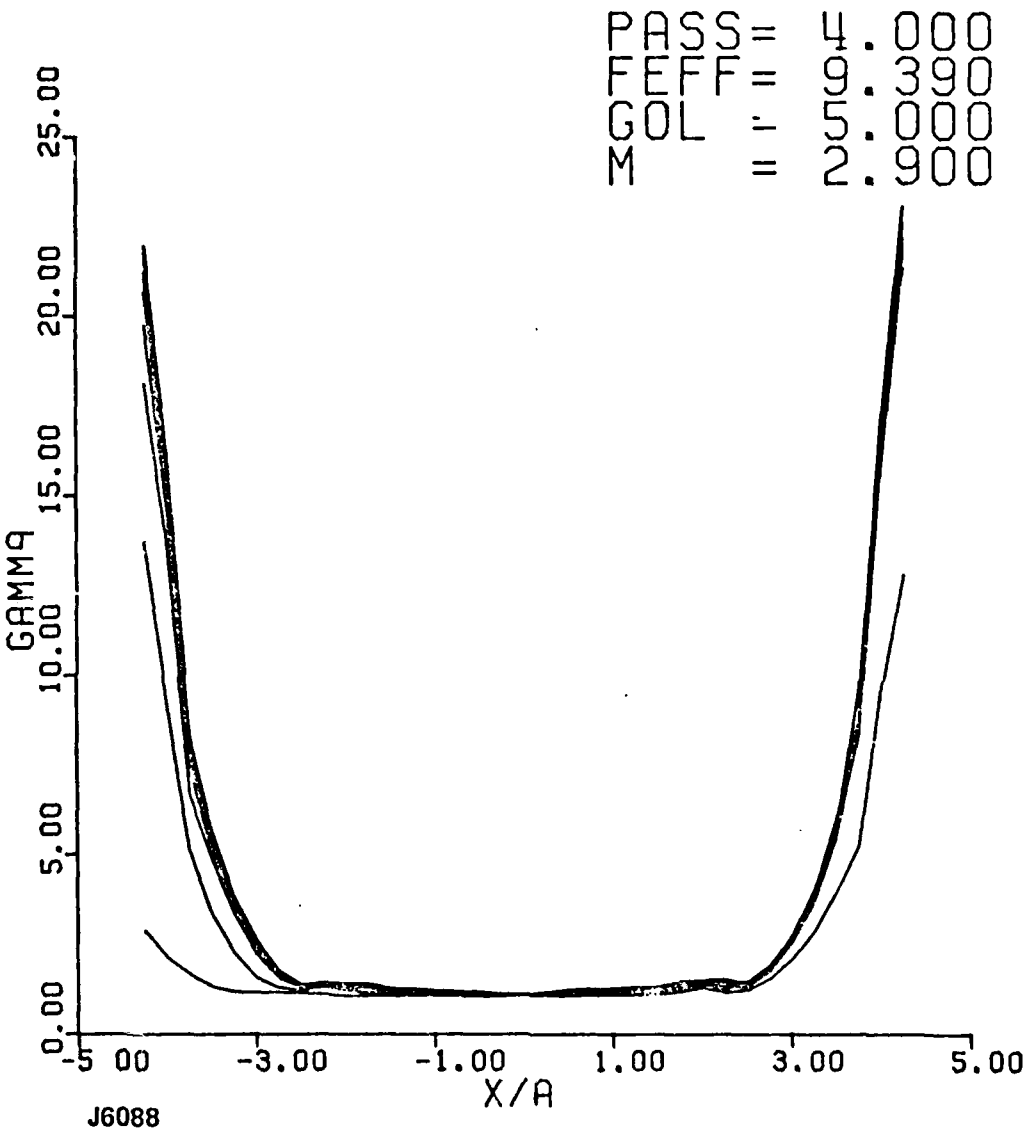

Figure 35. $\Gamma_n'(x)$ Profile for $G_oL = 5.0$. $F_{eff} = 9.39$.

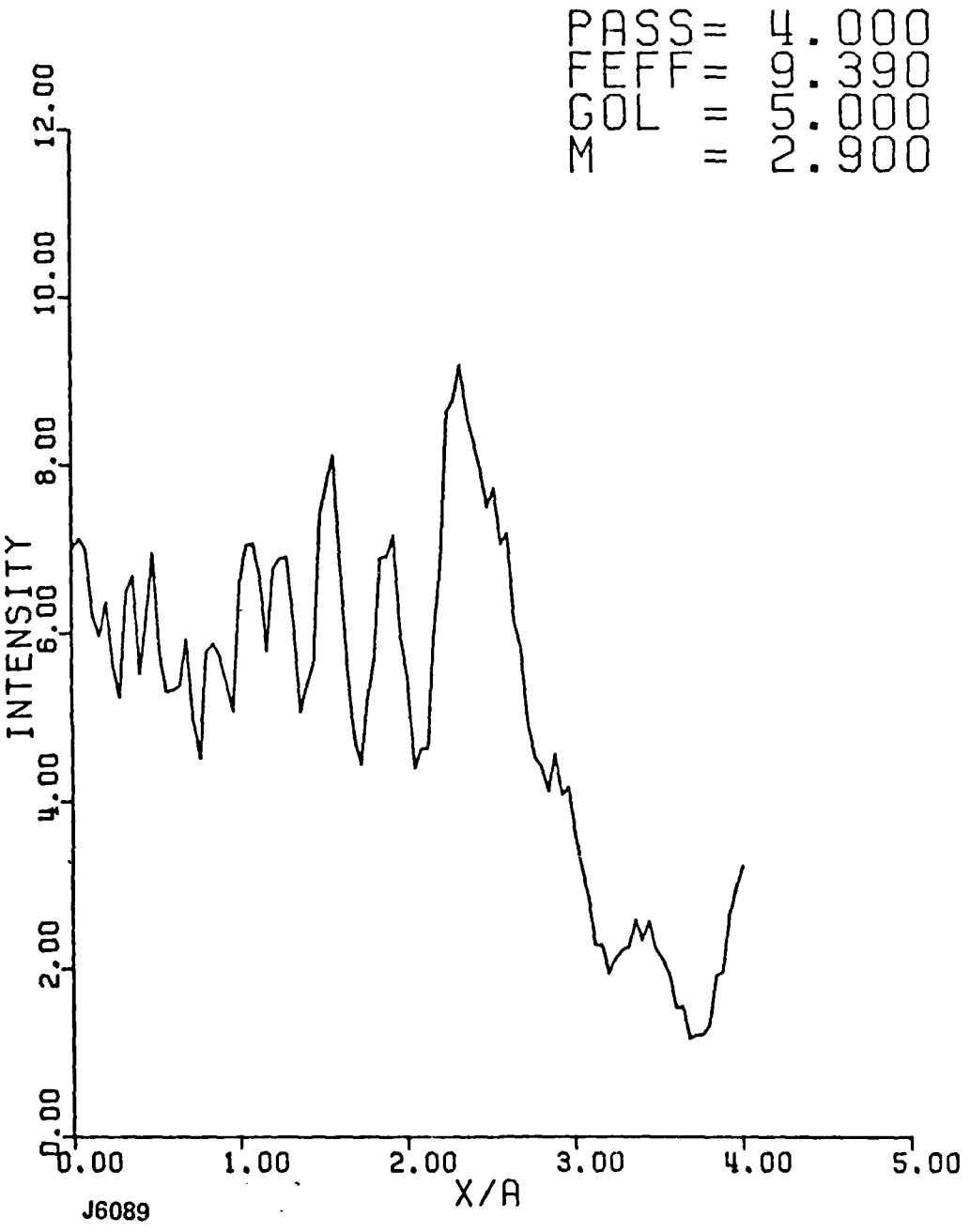

Figure 36 Intensity Profile for G_oL = 5.0. F_{eff} = 9.39.

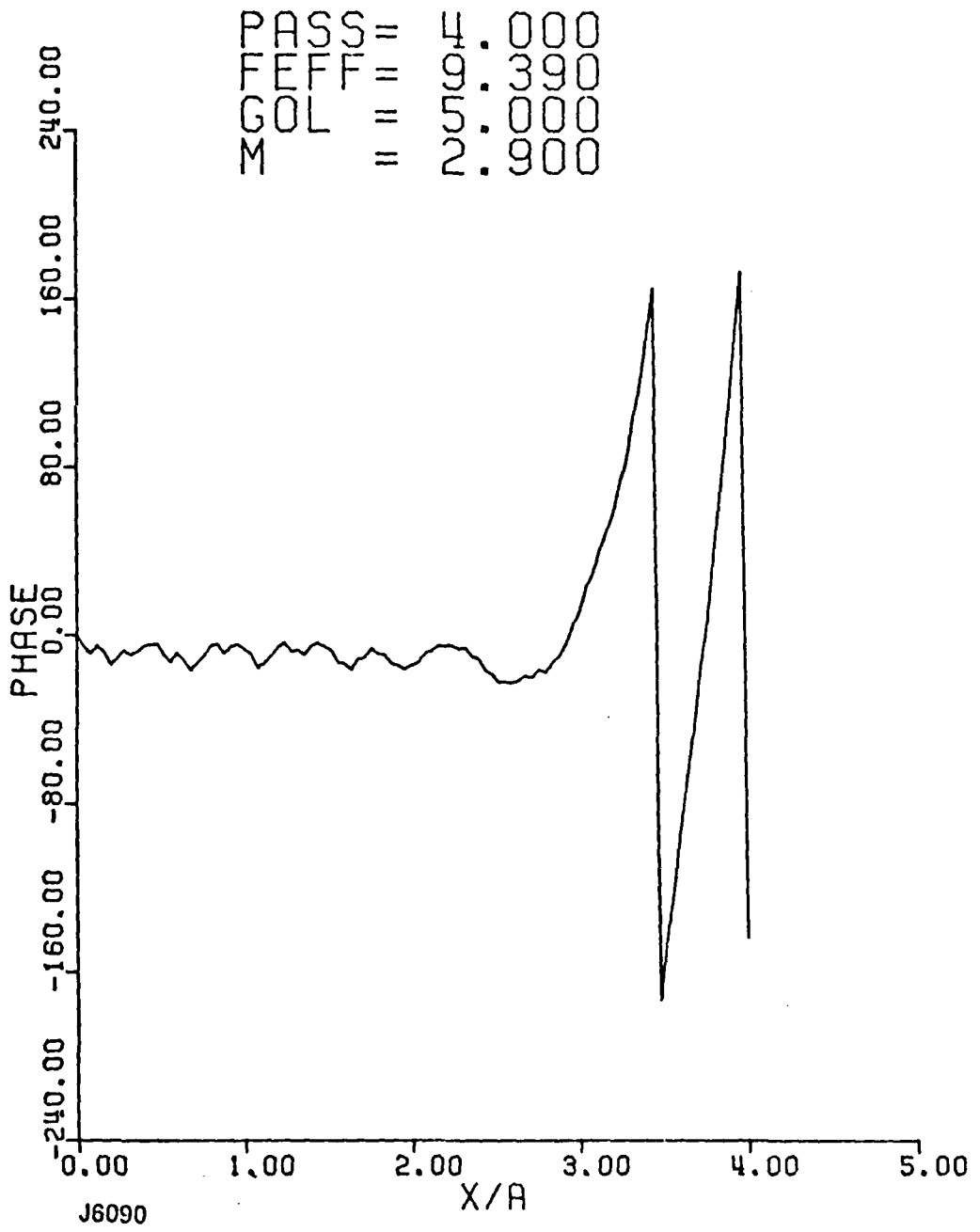

Figure 37. Phase Profile for $G_oL = 5.0$. $F_{eff} = 9.39$.

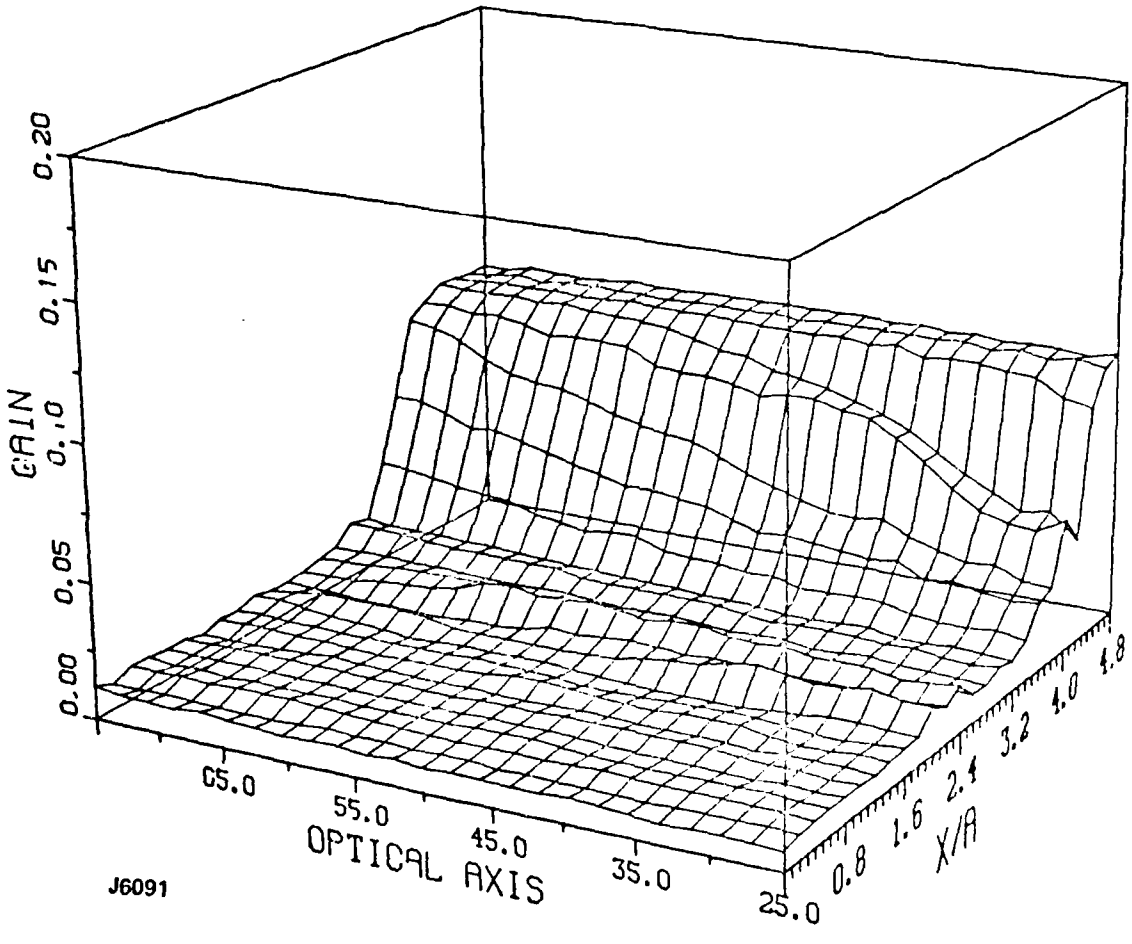

Figure 38. Saturated Gain Profile for $G_oL = 5.0$. $F_{eff} = 9.39$.

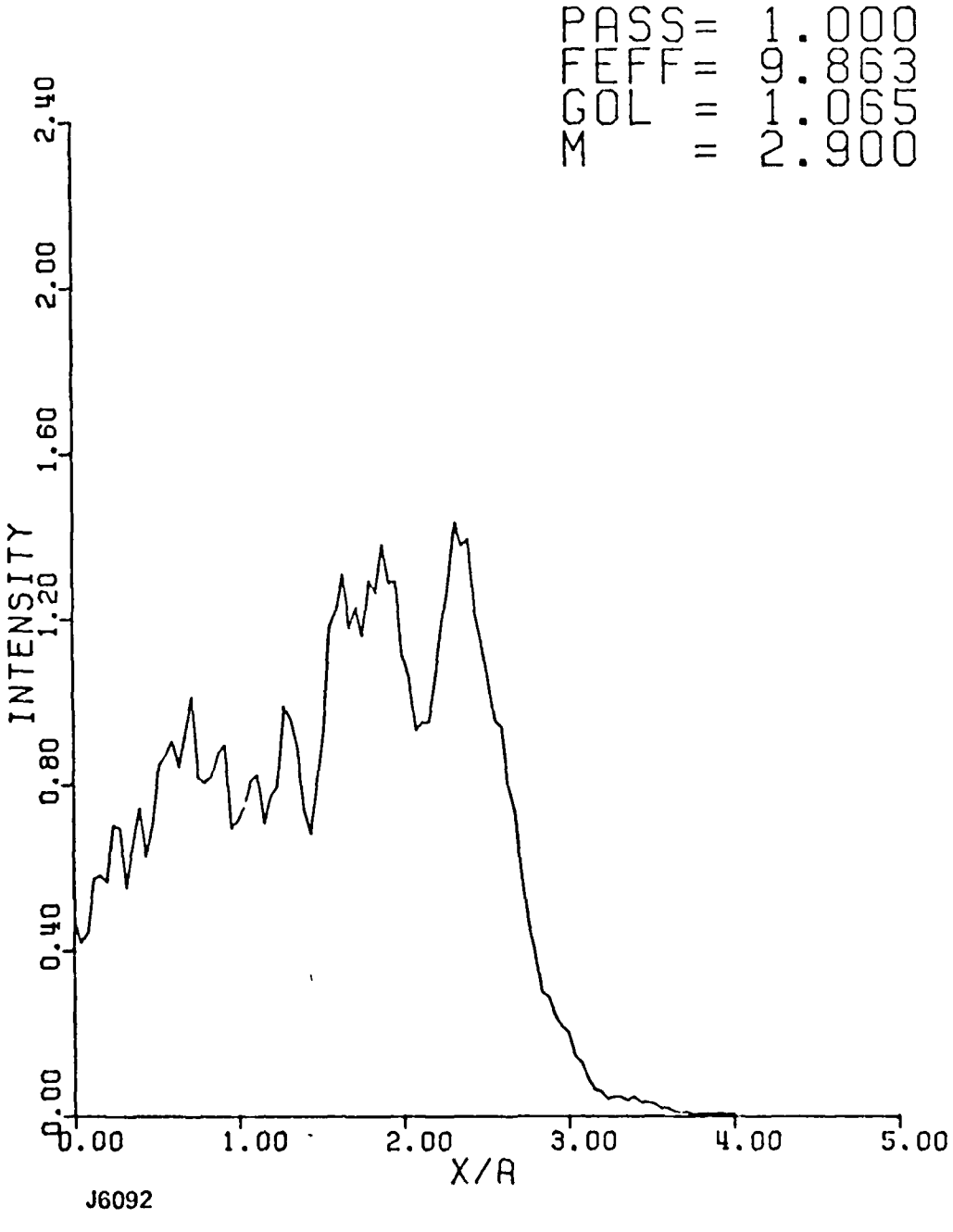

Figure 39. Intensity Profile for Empty Resonator. F_{eff} = 9.863.

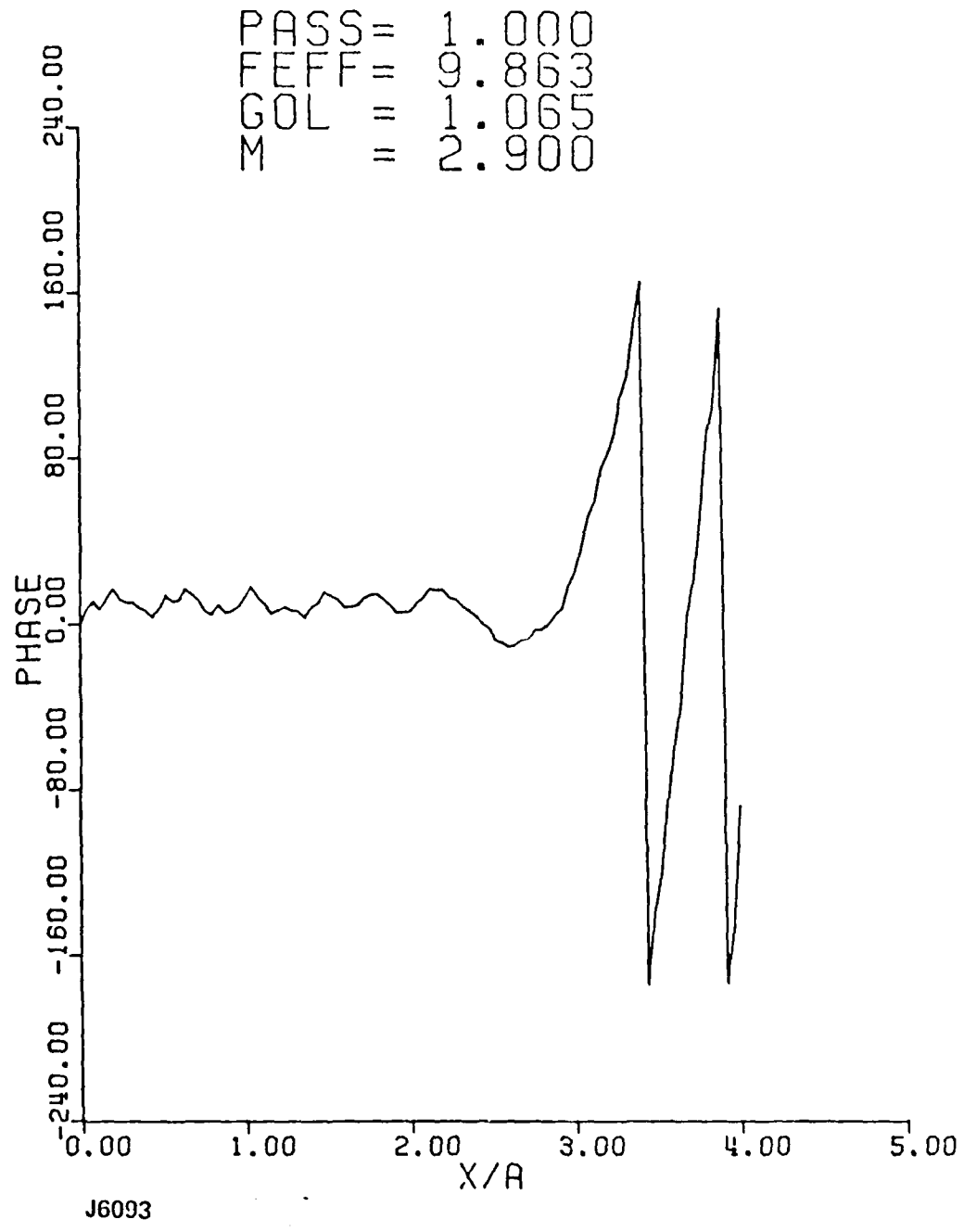

Figure 40. Phase Profile for Empty Resonator. F_{eff} = 9.863.

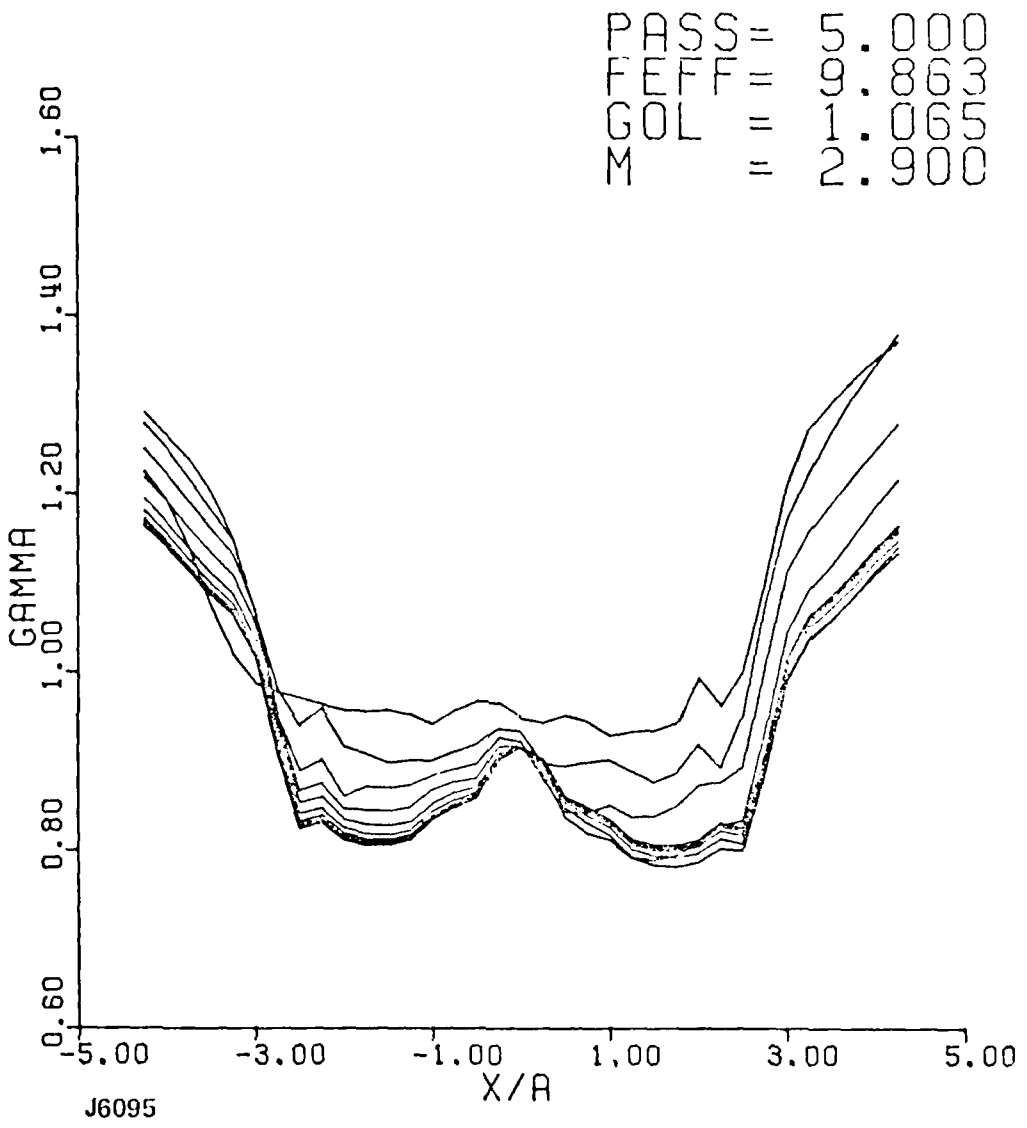

Figure 41. $\Gamma'_n(x)$ Profile for $G_oL = 1.065$. $F_{eff} = 9.863$.

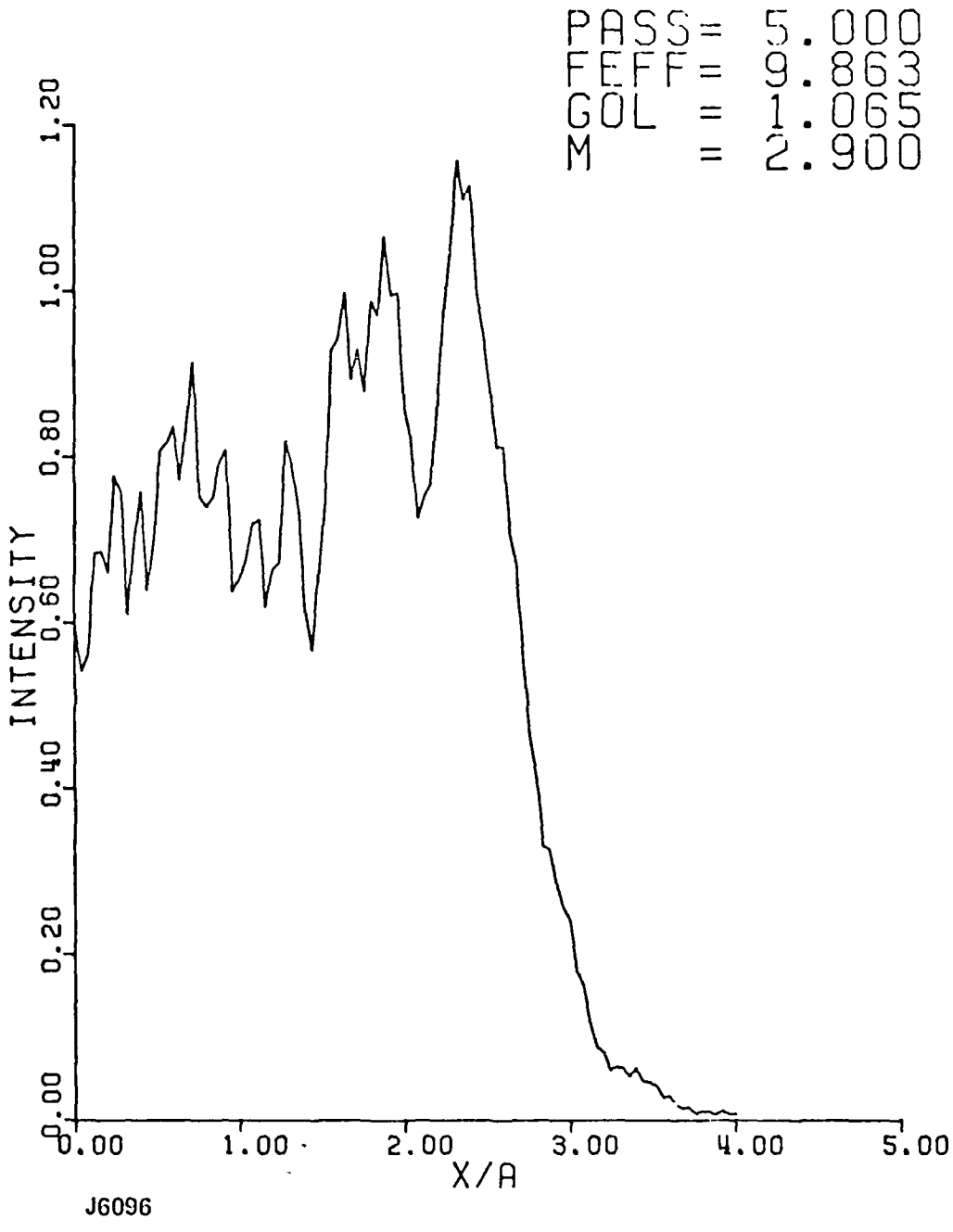

Figure 42. Intensity Profile for G_oL = 1.065. F_{eff} = 9.863.

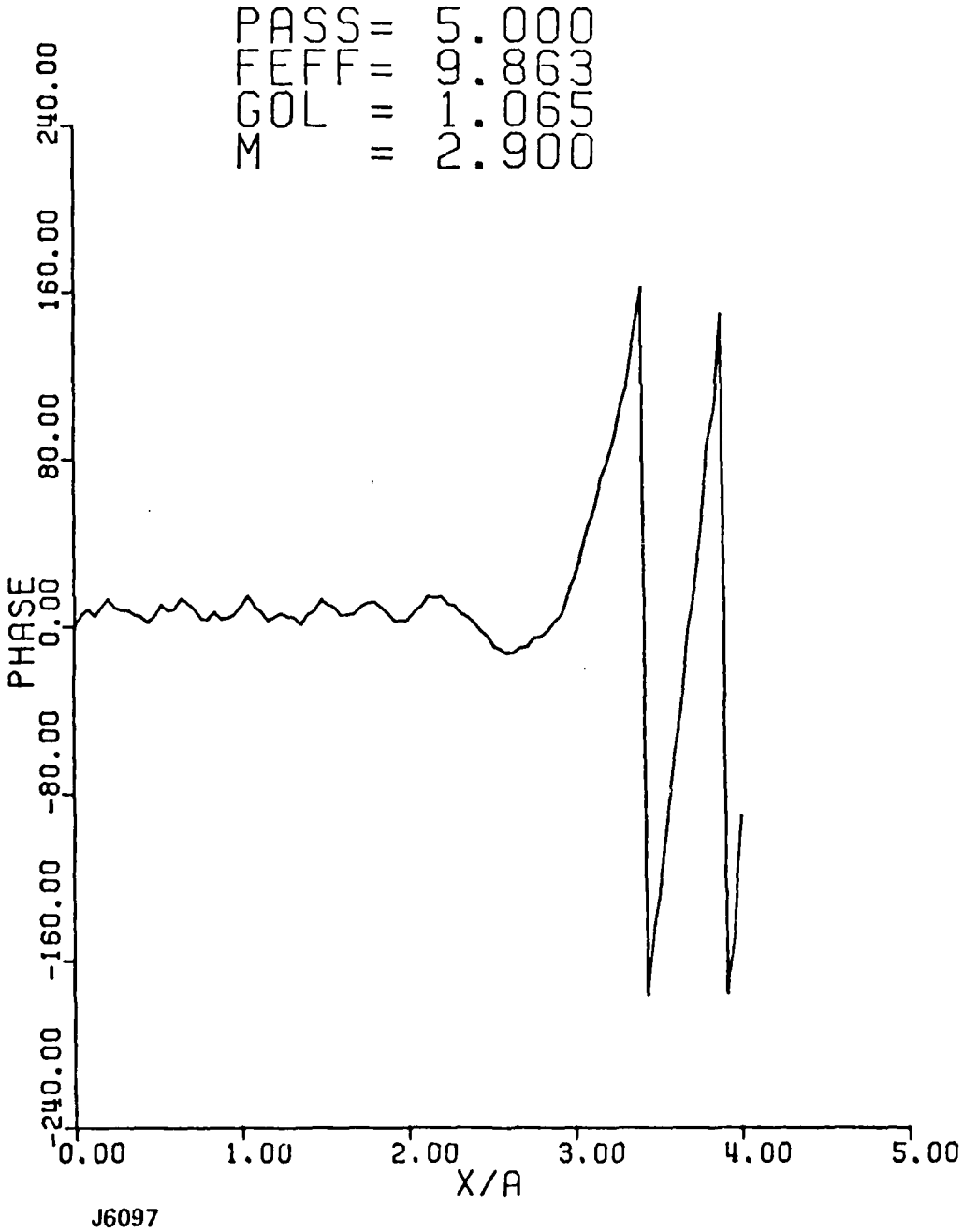

Figure 43. Phase Profile for $G_oL = 1.065$. $F_{eff} = 9.863$.

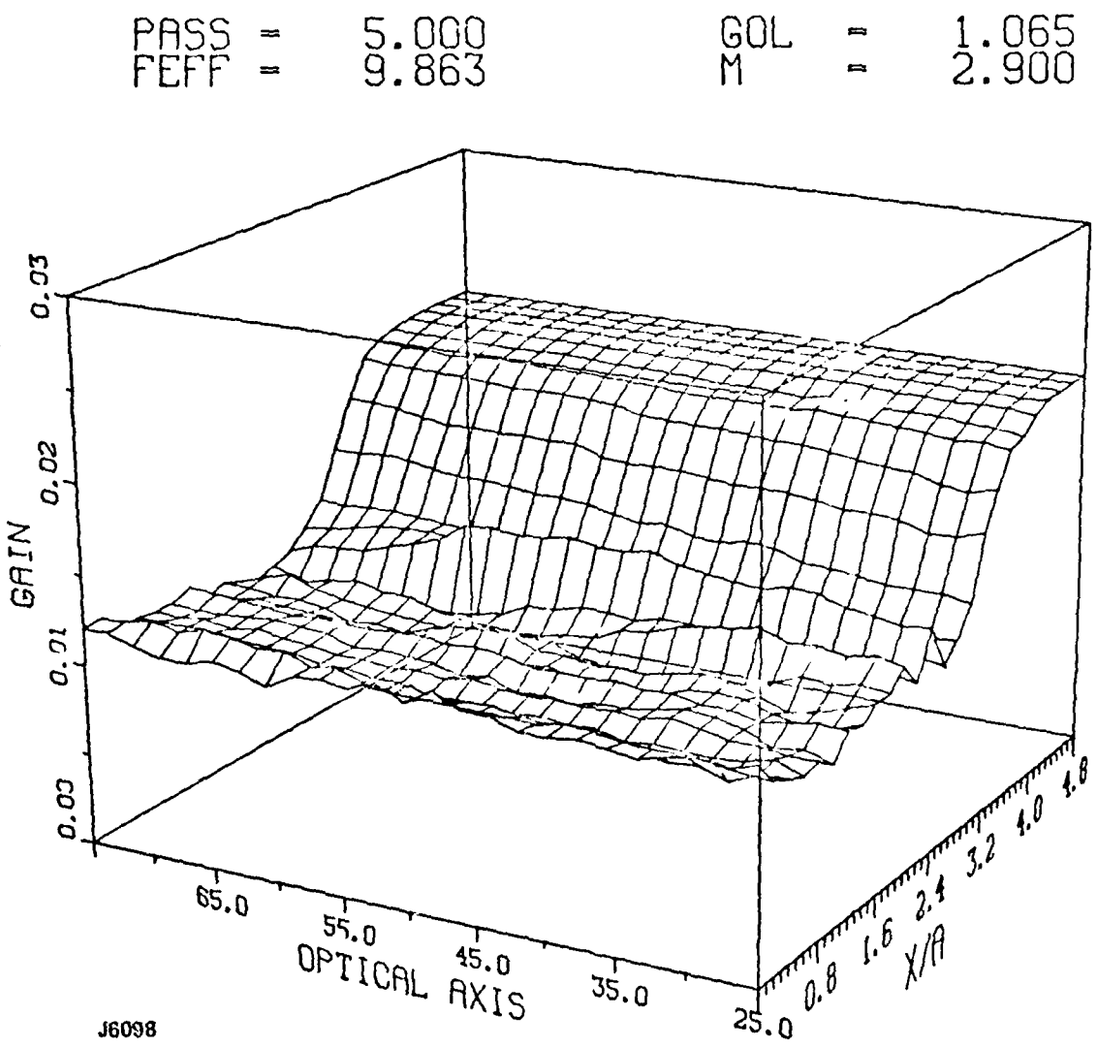

Figure 44. Saturated Gain Profile for G_oL = 1.065. F_{eff} = 9.863.

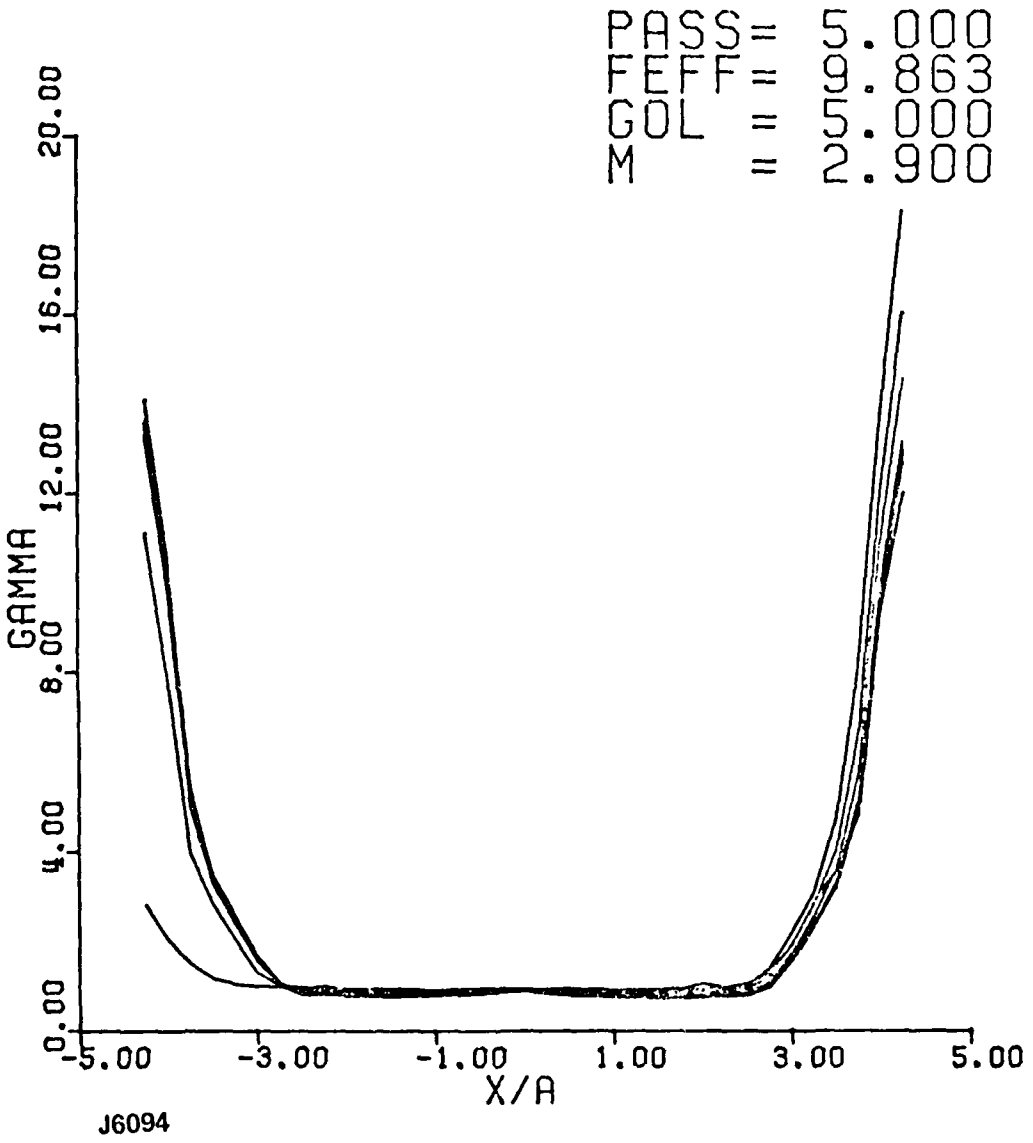

Figure 45. $\Gamma'_n(x)$ Profile for $G_oL = 5.0$. $F_{eff} = 9.863$.

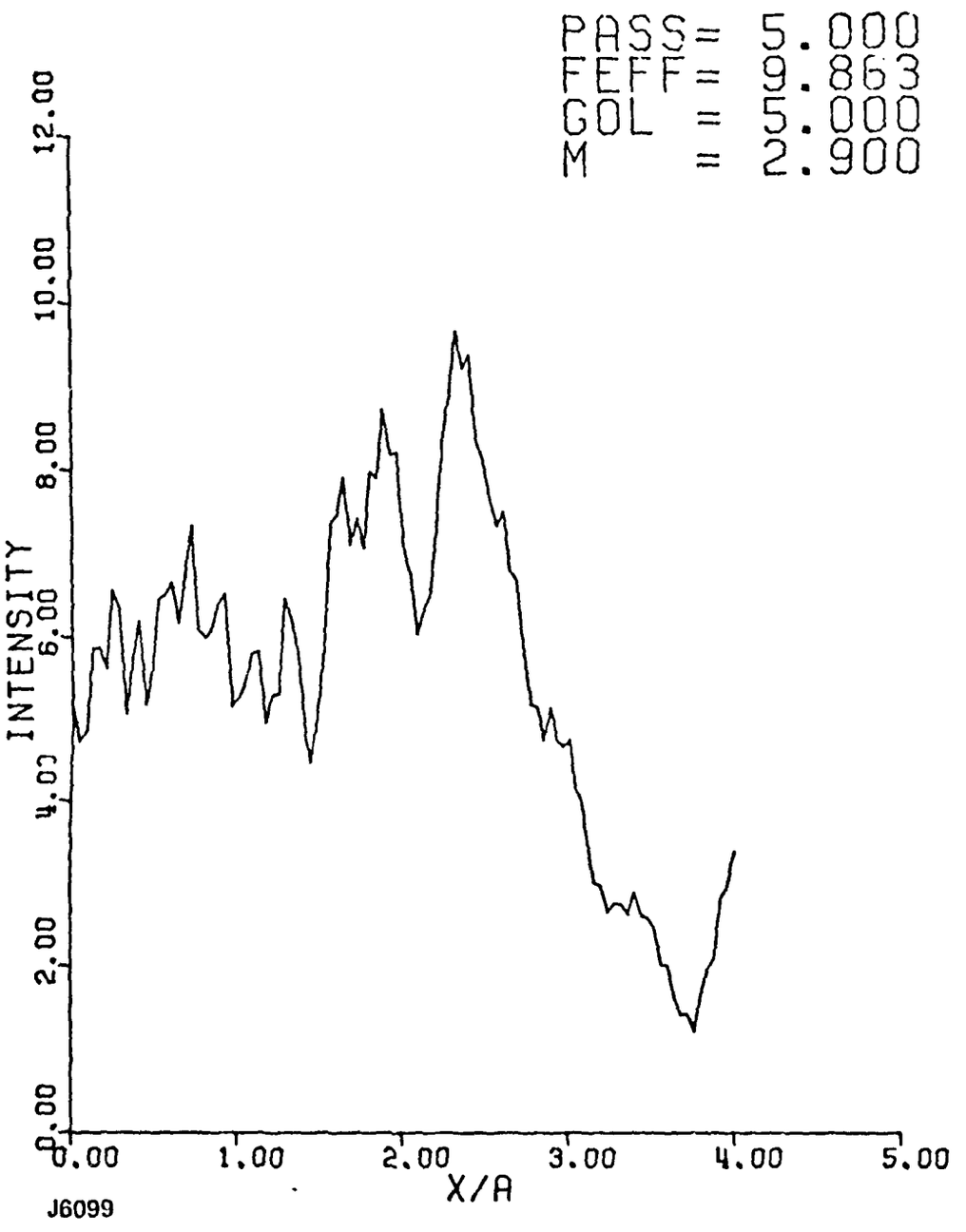

Figure 46. Intensity Profile for $G_oL = 5.0$. $F_{eff} = 9.863$.

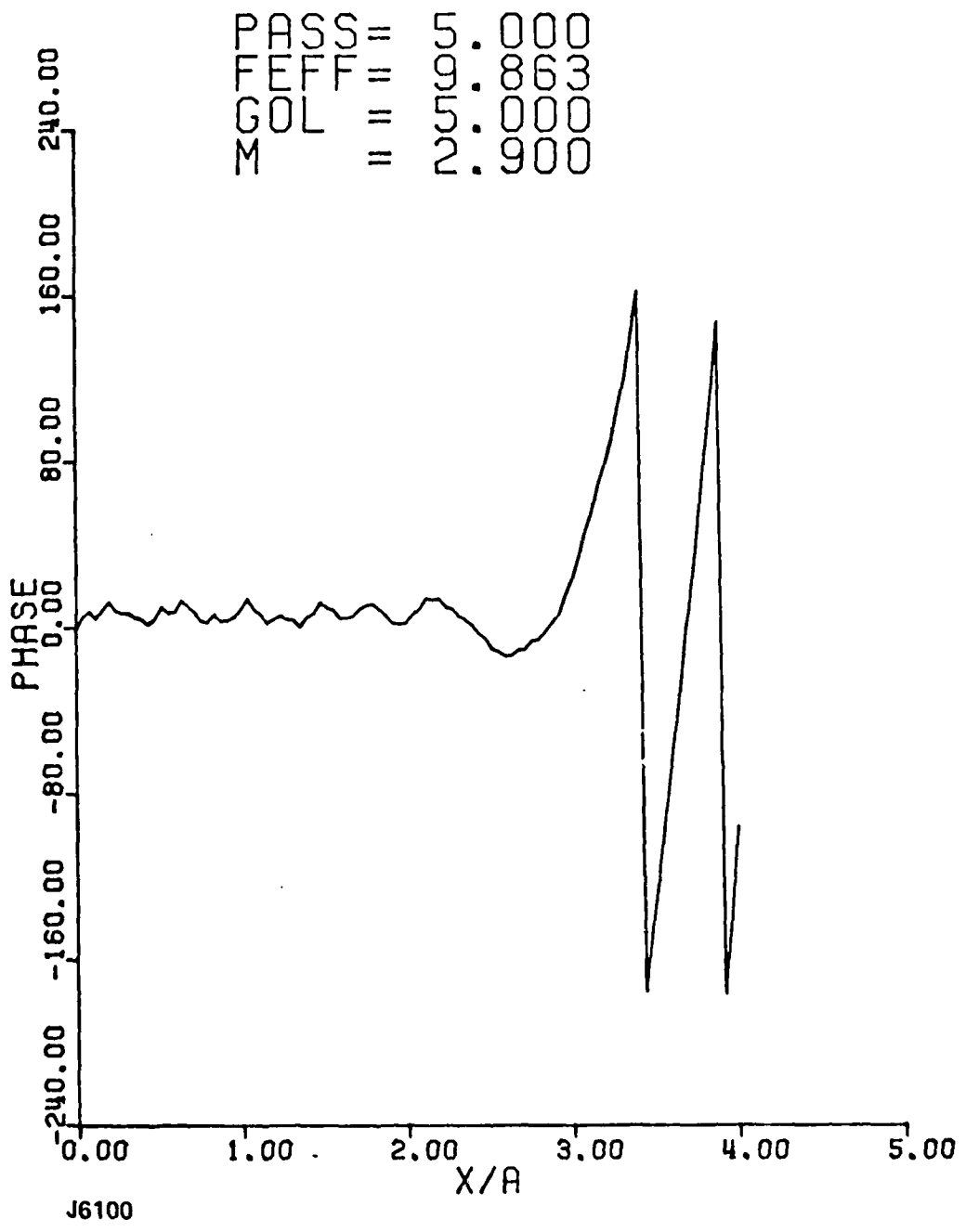

Figure 47. Phase Profile for $G_oL = 5.0$. $F_{eff} = 9.863$.

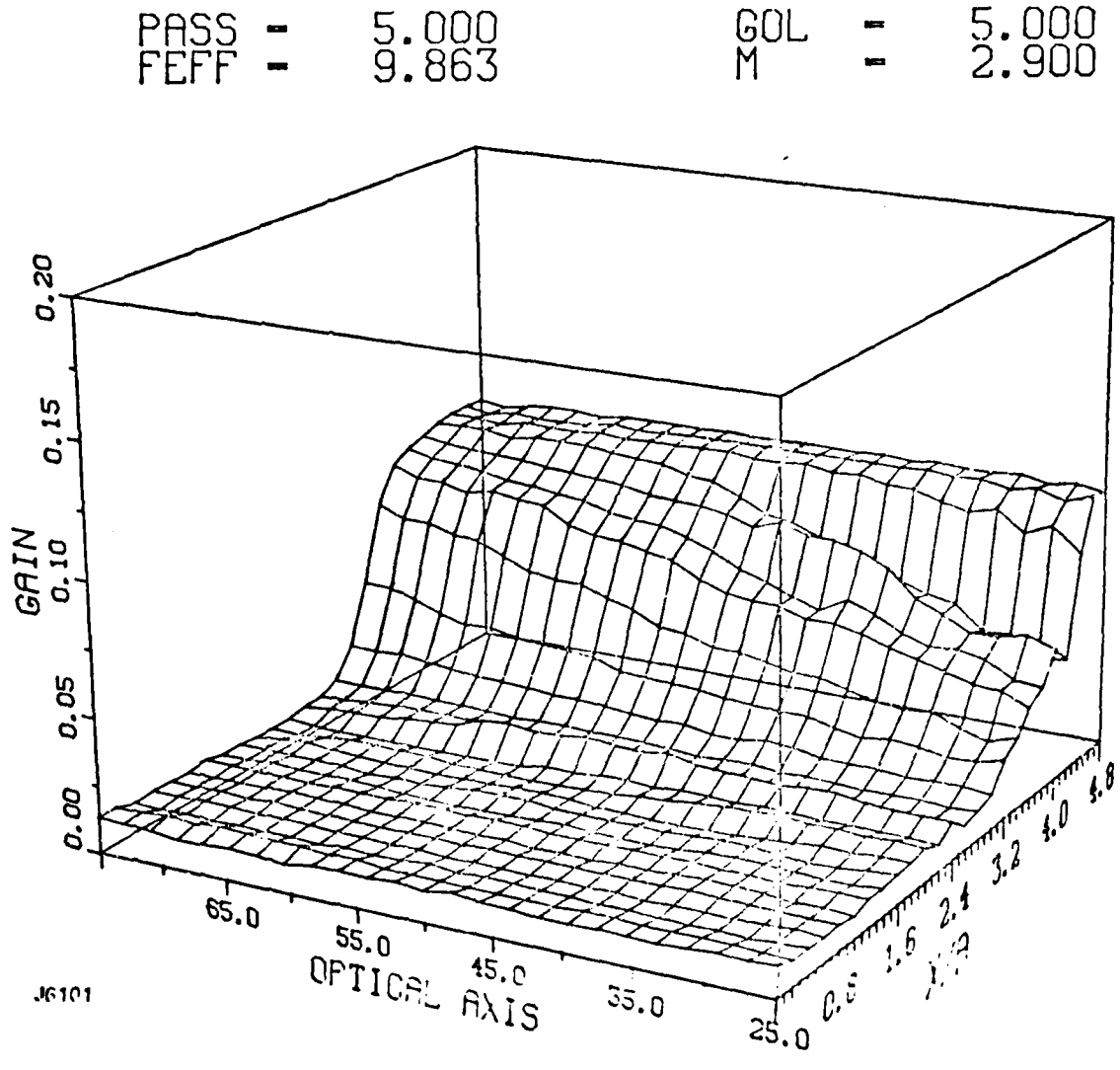

Figure 48. Saturated Gain Profile for G_oL = 5.0. F_{eff} = 9.863.

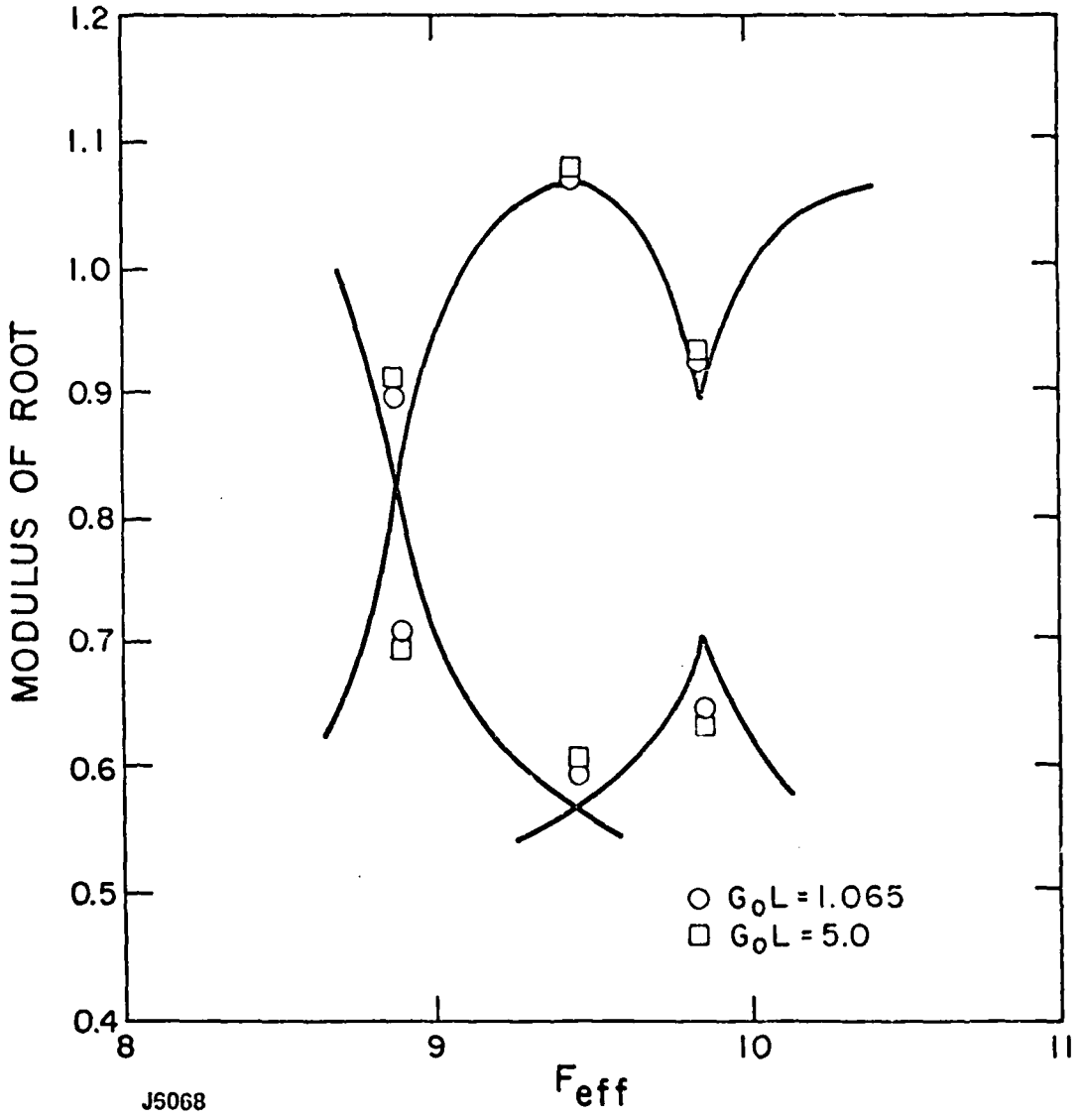

Figure 49. Effect of Saturable Gain on Mode Degeneracy. The solid curve is a portion of Figure 12, representing an "empty" resonator in the absence of gain saturation.

In a qualitative sense, saturable gain seems to produce an effect not unlike that of mirrors with rounded edges[27] or tapered reflectivity,[28] which reduce the influence of diffraction on mode properties. This is in spite of the fact that, as we have seen, the intensity profiles themselves are not really smoothed on a fine scale.

Horwitz has pointed out that empty resonator mode degeneracy occurs for F_{eff}'s less that some critical value, with that critical F_{eff} increasing quite rapidly as M approaches 1. In other words, the propensity for mode degeneracy is emphasized for low F_{eff} and low M. We hypothesize that for each value of F_{eff} and M corresponding to a mode degeneracy, there is also a critical G_oL which will lift that degeneracy. Though we have not explored this thesis exhaustively, we have performed a number of further calculations using $G_oL = 2$. For M = 2.9 there turn out to be no degeneracies for $F_{eff} > 2$. When M is reduced to 2.0, degenerate mode behavior is suppressed for $F_{eff} > 13$. For the empty resonator case, the corresponding critical F_{eff}'s are 17 and 43, respectively.

This result is of considerable importance for device design, as it frees F_{eff} in many cases of interest from being constrained to half-integer values, and, by inference, permits a more relaxed view of resonator alignment tolerances.

In light of the present results, one is tempted to speculate how the mode structure of circular mirror resonators would be affected by gain saturation. For such resonators, it has been shown that, in the absence of gain, the in-phase diffractive contribution from the mirror perimeter leads to strong mode degeneracy, persisting well into what might be thought of as the regime of geometric optics.[29] It is certainly not intuitive whether gain saturation could be expected to lift such a strong degeneracy. Clearly this is an area which warrants further study.

E. IMPLICATIONS FOR MMI

In an empty resonator, the peak-to-peak excursions in the value of the λ_o eigenvalue are, in the region where mode degeneracy exists, about equal to the geometric optics limit symmetric mode separation. (See Figure 12 or the figures of Refs. 14 and 16.) Since as $F_{eff} \to \infty$, $\lambda_o \to 1$ and $\lambda_1 \to \sim 1/M^{.25}$. This amounts to a fractional variation in the output coupling of

---

27. Santana, C., and Felsen, L., Appl. Opt. 17, pp. 2239-2243 (15 July 1978).

28. McAllister, G., et al., IEEE J. Quant. Elect. QE-10, pp. 346-355 (March 1974).

29. Butts, R., and Avizonis, P., J. Opt. Soc. Am. 68, pp. 1072-1078 (August 1978).

$$\frac{\Delta L_c}{L_c} \simeq \frac{\lambda_0^2 - \lambda_1^2}{M - 1} \simeq \frac{2\,\Delta\lambda}{M - 1} \tag{209}$$

which, for $M = 2.9$ is about 25%.[30] If saturable gain effects are included, on the other hand this variation is clearly cut at least in half, depending on the value of $G_o L$.

Even though these results are derived for varying F_{eff} with $\varepsilon = 0$, we now present an argument that they apply equally well to the varying-ε case, with F_{eff} constant, because the diffractive processes involved are essentially the same.[31] Consider the tilted resonator shown in Figure 50, with $\varepsilon = \varepsilon_o \neq 0$. We want to consider two effective Fresnel numbers, derived from the portion of the resonator on either side of the optical axis:

$$F_{eff}^{(1)} = F_{eff}^{(0)} (1 + \varepsilon)^2 \tag{210a}$$

$$F_{eff}^{(2)} = F_{eff}^{(0)} (1 - \varepsilon)^2 \tag{210b}$$

If ε is small compared to unity, then

$$F_{eff}^{(1)} \simeq F_{eff}^{(0)} (1 + 2\varepsilon) \tag{211a}$$

$$F_{eff}^{(2)} \simeq F_{eff}^{(0)} (1 - 2\varepsilon) \tag{211b}$$

Thus as ε increases from zero, the two half-resonator Fresnel numbers move in opposite directions away from $F_{eff}^{(0)}$. In particular, the output couplings associated with each half-resonator follow the usual periodic curves, as indicated in Figure 51, so that when $2\,\varepsilon\,F_{eff}^{(0)}$ is an integer, $F_{eff}^{(1)}$ and $F_{eff}^{(2)}$ are each an integer away from $F_{eff}^{(0)}$.

---

30. The observation that the next-to-lowest-loss eigenvalue has a geometric optics asymptote of $\sim M^{0.25}$ has not been noted previously, but is apparent from a close examination of the $|\lambda|$ vs F_{eff} plots.

31. A more rigorous exposition of the contributing diffractive effects of the two edges can be found in C. Santana and L. Felsen, Appl. Opt. 17, pp. 2352-2357 (1 August 1978). Curiously enough, that paper considers a fixed nonzero tilt (ε) with varying F_{eff}, but does not take up the complementary case, although the formalism for doing so is present.

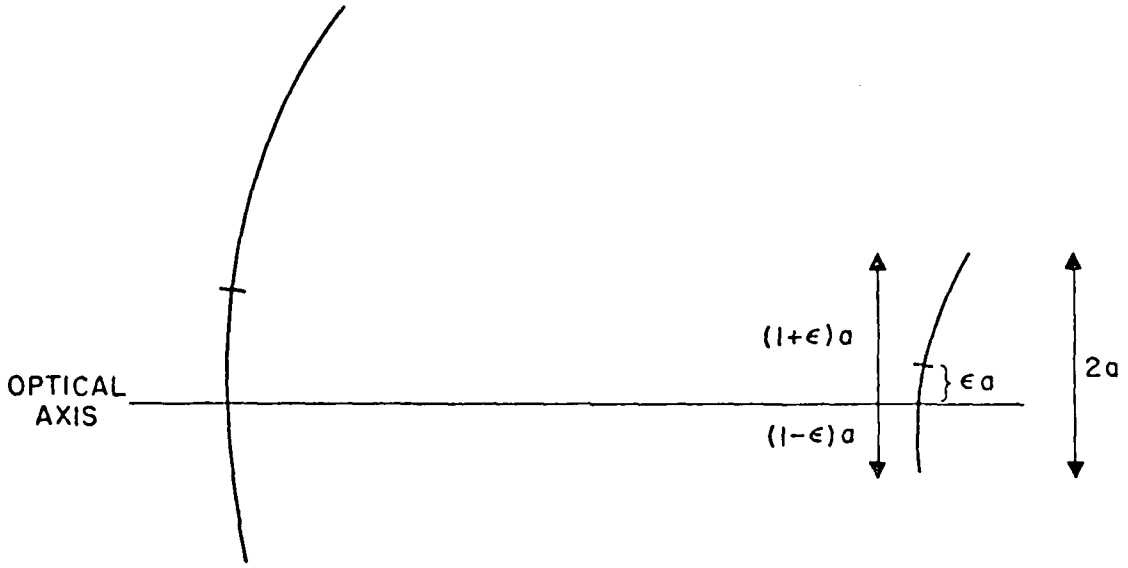

J6119

Figure 50. Tilted Resonator Nomenclature. The tick marks are the centers of the mirrors, denoting the optical axis when the resonator is untilted.

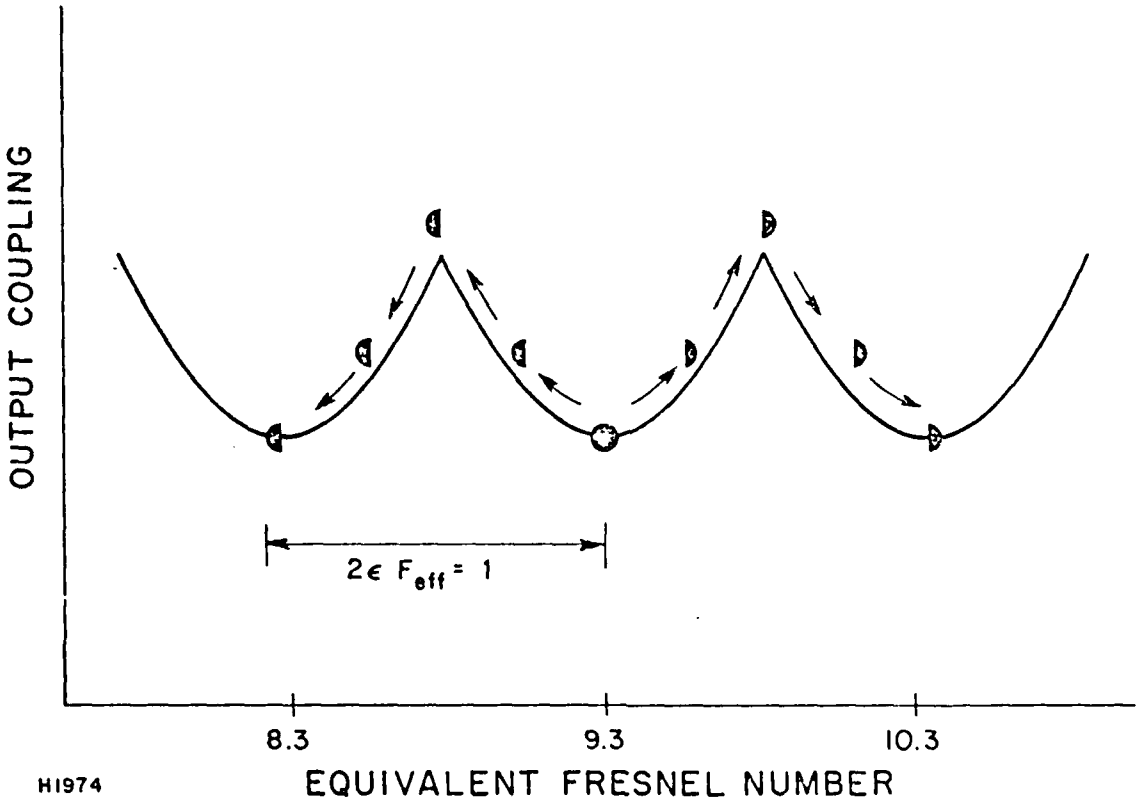

Figure 51. Output Coupling Variation in Tilted Resonators as Derived from Two Half Resonators. Each portion of the resonator to either side of the optical axis moves along the output coupling curve.

As justification for this argument, Figure 52 shows an empty-resonator calculation of $|\lambda|$ vs tilt in units of $2\varepsilon F_{eff}^{(0)}$, for $F_{eff}^{(0)} = 9.378$ and $M = 2.9$. The validity of this way of looking at tilted resonators can also be discerned from an examination of the mode patterns themselves. In Figure 53 we compare an exact calculation of $F_{eff}^{(0)} = 9.3$, $M = 1.9$, $2\varepsilon F_{eff} = 1$ with a composite formed by the left half of a mode pattern for $F_{eff}^{(0)} = 8.3$, $M = 1.9$, $\varepsilon = 0$ juxtaposed with the right half of a mode pattern for $F_{eff}^{(0)} = 10.3$, $M = 1.9$, $\varepsilon = 0$. The resemblance is quite closed indeed.

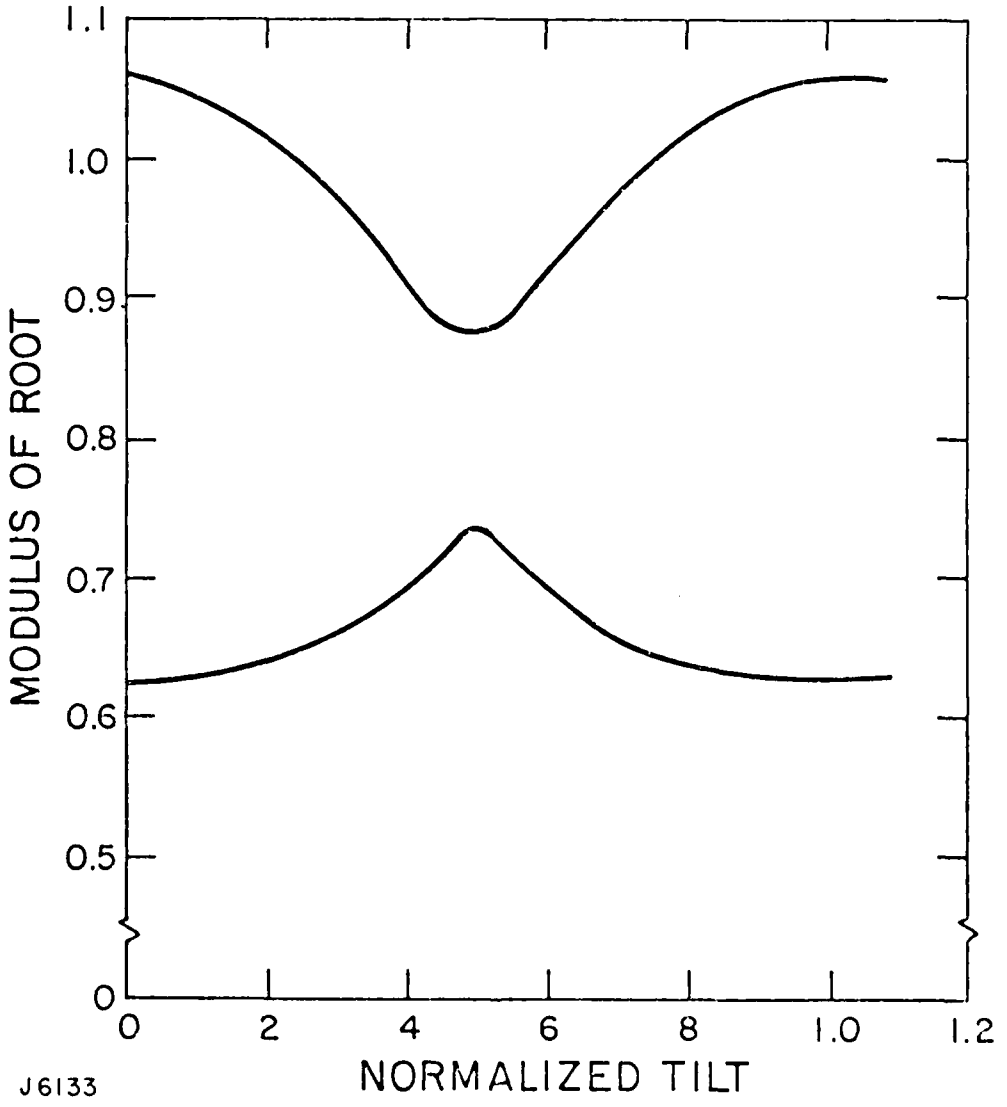

Figure 52. Modulus of λ vs Normalized Tilt for $F_{eff} = 9.378$. This is an exact calculation for a tilted resonator, but is approximated excellently by the "half-resonators" as in Figure 51.

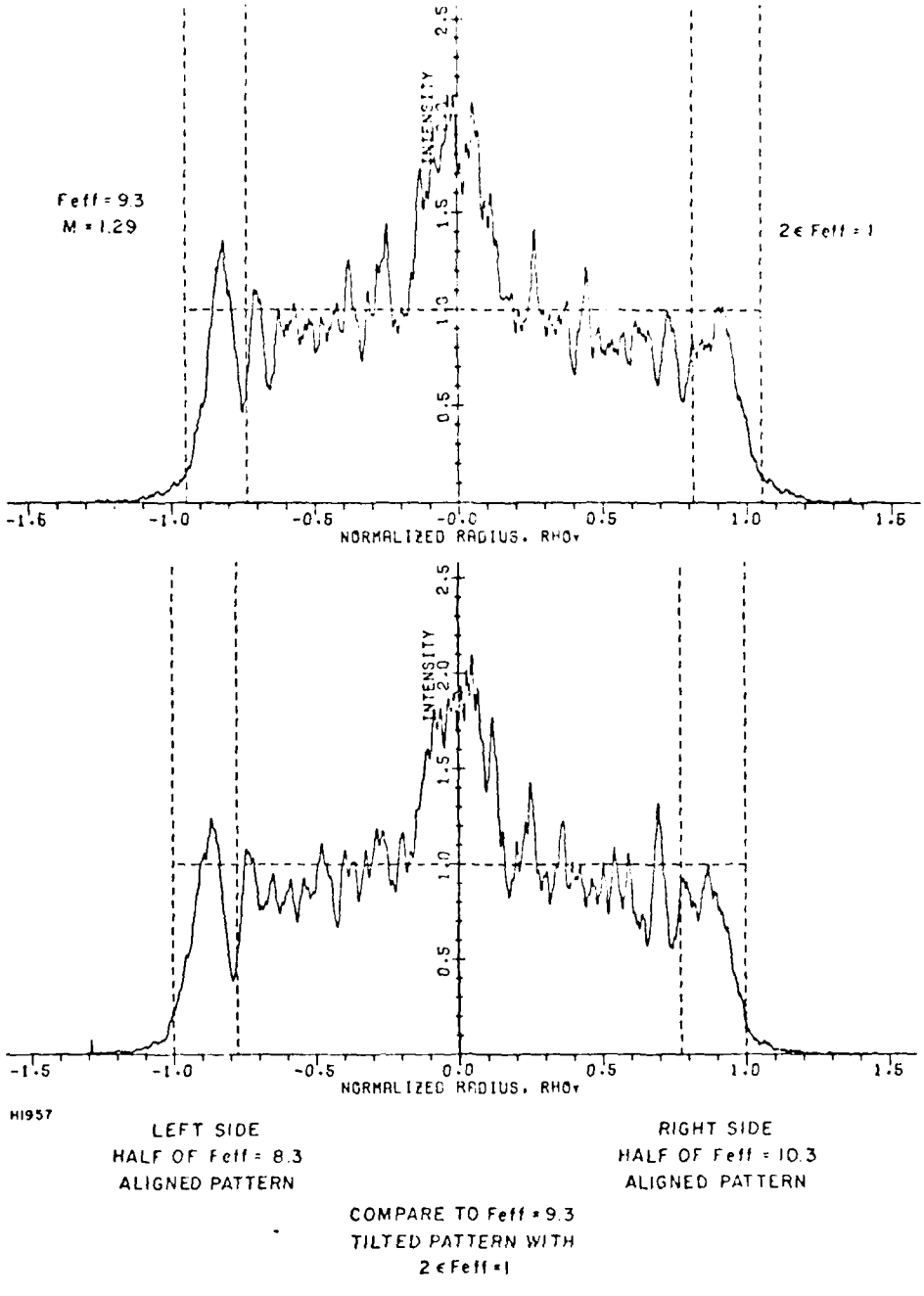

Figure 53. Comparison of Tilted Resonator Mode with Composite Formed by Two Untilted Half-Resonators with Differing F_{eff}

SECTION VI

STABILITY ANALYSIS OF A SUPERSONIC CHEMICAL LASER

A. INTRODUCTION

The objective of this study is to develop an analytic model of the stability characteristics of a supersonic laser; in particular that of a chemical laser. The flowfield and optical inhomogeneity of the chemical laser make it an extremely difficult problem to analyze, and it becomes necessary to simplify the laser characteristics in order to obtain a first-order model of mode-medium interaction inside the cavity.

The chemical laser generically consists of an array of flow nozzles from which alternate layers of fuel and oxidizer are ejected (Figure 54). This leads to a series of mixing and reaction zones across the laser cavity. The subsonic laser, as described previously, can couple to transverse acoustic waves and result in instability. The supersonic laser will generally not have such a mechanism, as the lateral transit time, D/c_s, is much longer than the axial flow time $1/\bar{u}$, such that acoustic disturbances will be swept out of the cavity (see the glossary of terms at the end of this section). For the purposes of this work the flowfield is treated as being one dimensional, and therefore any coupling of disturbances in the flowfield to the lasing will be primarily axial in form. This ignores the possible instability mechanisms introduced by the series of planar mixing layers acting as diffraction gratings or prisms which could then interact with the laser flux. This mechanism is considered to be outside the scope of the present analysis.

B. MODEL ASSUMPTIONS

As stated above, our model treats the laser as if it has a one-dimensional flowfield. This is obviously not true, but it leads to an overall simplification of the problem that may nonetheless be reasonably valid. The consequence of mixing is to reduce the overall rate of chemical reaction in the laser. Thus, a reaction of the form

$$A + B \overset{k_f}{\rightarrow} C$$

is described by

$$\frac{dX_C}{dt} = k_f \rho X_A X_B$$

where X denotes mass fraction, and ρ is gas density.

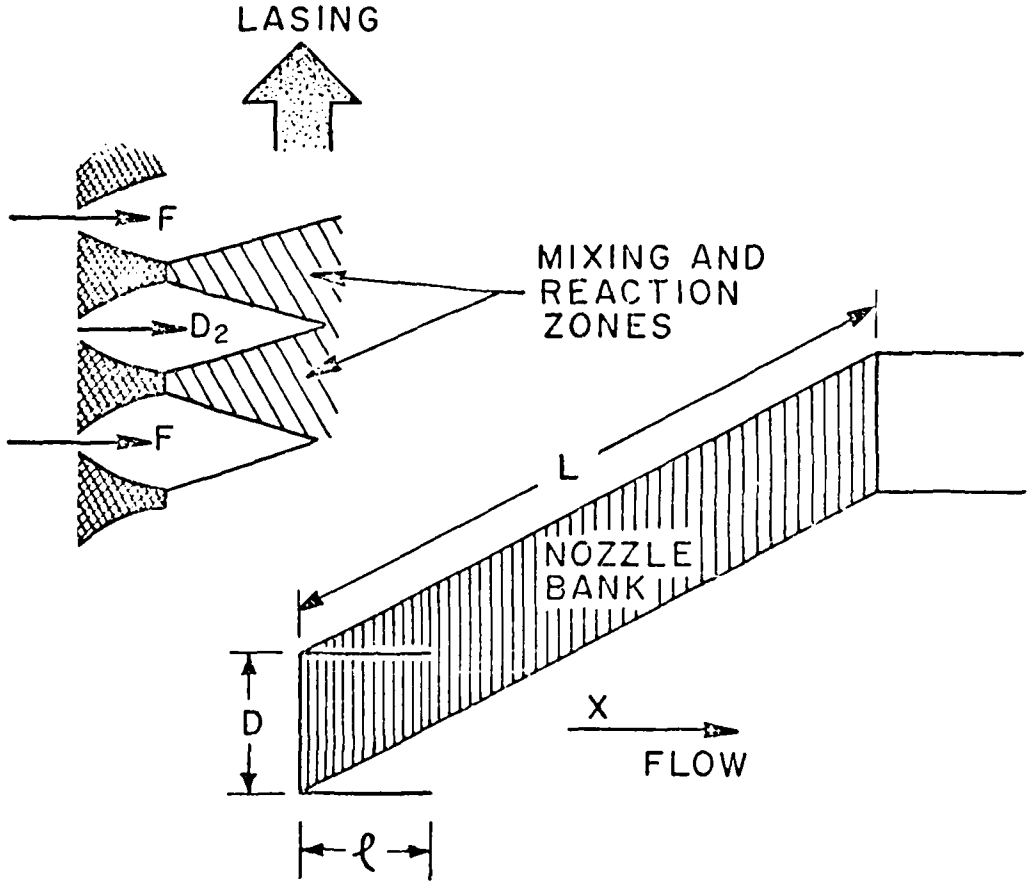

J6755

Figure 54. Schematic of Laser Geometry

Under turbulent mixing conditions the local values of the concentrations [A] and [B] may vary substantially with time, and their product more so. Although the dynamics of the mixing process are very complicated, and many workers have investigated such flowfields, it would appear feasible to use a simple model to estimate the reaction rates for a quasi one-dimensional treatment. In the model, the concentrations X_A, X_B of species A and B (averaged over a plane normal to the flow direction) are given by their mass-averaged flow rates and an effective reaction rate as follows:

$$\frac{d\bar{X}_c}{dt} = k_f \lambda X_A X_B \rho$$

where λ is a mixing parameter which is typically much less than unity, and $k_f\lambda$ is the effective reaction rate. The rate of disappearance of fuel/oxidizer species can be related to a lasing medium length in the flow direction. Thus for the DF laser, with the D_2 concentration significantly greater than F_2, we can write

$$X_F = X_{F_o} \exp\ (-k_f \rho \lambda X_{D_{2,o}} t)$$

where X_{F_o} is the initial fluorine concentration. Thus, we have an e-folding time for disappearance of fuel given by

$$\tau = \frac{1}{k_f \rho \lambda X_{D_{2,o}}}$$

The convective distance ℓ traversed during this time is thus given by

$$\ell = \bar{u}\tau$$

where $\bar{u}$ is the convective gas velocity. For a given mixing rate we can thus relate the length of the lasing mecium in the flow direction to the kinetic rate and the flow velocity, such that

$$\lambda \simeq \frac{\bar{u}}{k_f \ell \rho X_{D_{2,o}}}$$

In the following we denote the effective reaction rate by $k_f = k_f\lambda$.

A chemically pumped DF laser exhibits multiline operation such that laser action can occur on an many as three vibrational transitions and a total of 15-20 vibrational-rotational lines.(32)

32. Gross, R.W.F. and Spencer, D.J., "CW Hydrogen-Halide Lasers," Handbook of Chemical Lasers, R.W.F. Gross and J.F. Bott, ed., Wiley-Interscience, New York, NY, 1976, Chapter 4.

In order to accurately model such a system, the time evolution of all lasing states and the flux for each lasing transition should be followed. This leads to a system of approximately 20-30 coupled differential equations which must be integrated numerically. Such a large set of equations is too cumbersome to be of use for the present application; therefore, simplifying assumptions must be made in order to provide a manageable kinetics scheme.

The first assumption that we make is that three vibrational levels are sufficient to model the behavior of the lasing species. These levels are the upper lasing level, DF_u, the lower lasing level, DF_l, and the vibrational ground state, DF_g. We assume each level is in rotational thermal equilibrium.

In order to model the lasing action in the system, it is assumed that the multiline operation of the DF laser can be described by a single transition from DF_u to DF_l. Implicit in this assumption is the additional assumption that no lasing occurs to the ground state of DF. This allows us to use a steady-state approximation for describing the unperturbed lasing medium, since, with this assumption, the ground state of DF, whose population increases with time, is decoupled from the remaining kinetic equations. Since only ~ 20% of the laser energy in a DF laser arises from the $v = 1 \rightarrow v = 0$ transition,(32,33) this assumption is not unreasonable.

The reactions necessary to describe the DF laser are as follows:

(i) Formation:

$$F + D_2 \xrightarrow{k_{F_u}} DF_u + D$$

$$\xrightarrow{k_{F_l}} DF_l + D$$

No ground-state DF is formed by this reaction.

(ii) Deactivation:

$$DF_u + M \xrightarrow{k_{D_u}} DF_l + M$$

$$DF_l + M \xrightarrow{k_{D_l}} DF_g + M$$

33. "NACL Program Final Report" (U), LTM-292, TRW, July 8, 1976. Classified: CONFIDENTIAL.

M is the combined density of DF, D_2, D and F; deactivation by the carrier gas is assumed negligible.

(iii) Lasing:

$$DF_u + h\nu \overset{g}{\rightarrow} DF_l + 2\ h\nu$$

Three-body recombination is assumed neglibible and only single-quantum deactivations are considered. Estimates for the formation and deactivation-rate constants were obtained from the recommended values of Cohen(34) by assuming that the D_2/F ratio was 2-3 and 20-30% of the F atoms were reacted in the lasing region. Our estimated rate constants and the enthalpies for the various reactions are listed in Table 1.

One more quantity is necessary to model the behavior of the lasing medium and that is the gain per unit length, which can be written

$$g = \sigma_s \Delta N_{v,j}$$

where σ_s is the stimulated emission cross section and $\Delta N_{v,j}$ is the population inversion for the $v,j-1 \rightarrow v-1,j$ transition. Writing this equation in terms of the species discussed above yields

$$g = \sigma([DF_u] - \theta[DF_l])$$

where the brackets denote species concentration and σ is the product of the stimulated emission cross section and the fraction of the total DF_u population which is in the lasing rotational state. For a P-branch transition, $\theta = \exp(-2J/Q)$, where Q is the rotational partition function. Our estimated values for σ and θ, obtained using the spectroscopic data contained in Ref. 35, also are contained in Table 1.

Using the model discussed above, the time evolution of the chemical species and laser flux in a cw DF laser is described by the following equations:

---

34. Cohen, "A Brief Review of Rate Coefficients for Reactions in the D_2-F_2 Chemical System," TR-0074(4530)-9, Aerospace Corp., January 1974.

35. Emanuel, G., "Numerical Modeling of Chemical Lasers," Handbook of Chemical Lasers, op. cit., Chapter 8.

TABLE 1. CONSTANTS FOR SIMPLIFIED DF MODEL

Constant	Best Estimate	Probable Range	Heat of Reaction
k_{Fu}	8.3×10^{-12} cm^3/sec	5.9×10^{-12}-1.2×10^{-11}	-7.3 kcal/mole
k_{Fl}	9.4×10^{-13} cm^3/sec	6.6×10^{-13}-1.3×10^{-12}	-23.4 kcal/mole
k_{Du}	1.5×10^{-12} cm^3/sec	3.0×10^{-13}-4.5×10^{-12}	-8.0 kcal/mole
k_{Dl}	8.6×10^{-13} cm^3/sec	1.7×10^{-13}-2.6×10^{-12}	-8.3 kcal/mole
σ	5.0×10^{-17} cm^2	2.5×10^{-18}-2.5×10^{-16}	-----
θ	0.5	0.4 - 0.6	-----

$$\frac{d[DF_u]}{dt} = k_{F_u}[F][D_2] - k_{D_u}[DF_u][M] - \frac{\sigma\phi}{h\nu}([DF_u] - \theta[DF_1])$$

$$\frac{d[DF_1]}{dt} = k_{F_1}[F][D_2] + k_{D_u}[DF_u][M] - k_{D_1}[DF_1][M] + \frac{\sigma\phi}{h\nu}([DF_u] - \theta[DF_1])$$

$$\frac{d[DF_g]}{dt} = k_{D_1}[DF_1][M]$$

$$\frac{d\phi}{dt} = c\sigma([DF_u] - \theta[DF_1])\phi$$

where c is the speed of light, hν is the laser photon energy, and ϕ is the intracavity flux.

C. ANALYTIC MODEL

The laser cavity may be described by a set of one-dimensional flow equations plus gain and flux equation. The flowfield is assumed to be inviscid. Thus the continuity equations are:

Continuity $$\frac{\partial\rho}{\partial t} + \frac{\partial(\rho u)}{\partial x} = 0 \qquad (212)$$

Momentum $$\rho\frac{\partial u}{\partial t} + \rho u\frac{\partial u}{\partial x} = -\frac{\partial p}{\partial x} \qquad (213)$$

Energy $$\frac{Dh}{Dt} = [K_{F_u}\Delta H_{F_u} + K_{F_1}\Delta H_{F_1}]\rho X_{H_2} X_\Gamma + K_{D_u}\Delta H_{D_u}\rho X_m X_u \qquad (214)$$

$$+ K_{D_1}\Delta H_{D_1}\rho X_m X_1$$

where

$$\frac{D}{Dt} = \frac{\partial}{\partial t} + u\frac{\partial}{\partial x}$$

In addition, the gases are assumed perfect giving

$$p = \rho R_g T \tag{215}$$

The reacting species may be represented by the three DF states to give the species continuity equations

Upper State
$$\frac{DX_u}{Dt} = K_{F_u} \rho X_F X_{H_2} - K_{D_u} \rho X_m X_u - \frac{c\phi}{h\nu} (X_u - \theta X_l) \tag{216}$$

Lower State
$$\frac{DX_l}{Dt} = K_{F_l} \rho X_F X_{H_2} + K_{D_u} \rho X_m X_u + \frac{c\phi}{h\nu} (X_u - \theta X_l) \tag{217}$$

$$- K_{D_l} \rho X_m X_l$$

Ground State
$$\frac{DX_g}{Dt} = K_{D_l} \rho X_m X_l \tag{218}$$

The lasing may be described by the flux coupling equation described in Section II and the gain equation, such that

Flux
$$\frac{\partial \phi}{\partial t} = \frac{c\phi}{2L} [\int \alpha_R \rho' dx + \int \alpha_l g' dx] \tag{219}$$

Gain
$$g = \frac{\sigma \rho}{M_{DF}} (X_u - \theta X_l) \tag{220}$$

The magnitudes of the coefficients in Eq. (219) are given by

$$\alpha_R = 2\pi\beta \frac{\rho}{\rho_{ATM}} \frac{J}{\lambda}$$

$$\alpha_I = 1.0$$

These equations fully describe the flow inside the cavity. For the purposes of a stability analysis we are interested in the perturbation of the flow from a steady-state condition. Thus re-writing each variable as the sum of a steady state and a fluctuating part (i.e., $u = \bar{u} + u'$) we can derive perturbation equations from the above, neglecting higher order terms in fluctuating quantities. For the purposes of this analysis it becomes necessary to consider the mean-value steady-state properties of the flow variables to be constant throughout the cavity. There is one

exception to this case; the ground state mass fraction obviously increases with time whereas the other equations have both source and sink terms. The set of perturbation equations becomes:

Continuity

$$\frac{\partial \rho'}{\partial t} + \bar{u}\frac{\partial \rho'}{\partial x} + \bar{\rho}\frac{\partial u'}{\partial x} = 0 \tag{221}$$

Momentum

$$\bar{\rho}\frac{\partial u'}{\partial t} + \overline{\rho u}\frac{\partial u'}{\partial x} = -\frac{\partial p'}{\partial x} \tag{222}$$

Energy

$$-\frac{\bar{u}}{\bar{\rho}c_p}\frac{\partial p'}{\partial x} + \frac{DT'}{Dt} = \frac{1}{c_p}\left[K_{F_u}\Delta H_{F_u} + K_{F_l}\Delta H_{F_l}\right]\left\{X_{H_o} - \tfrac{1}{2}(\bar{X}_u + \bar{X}_l + \bar{X}_g)\right\}\left\{X_{F_o} - (\bar{X}_u + \bar{X}_l + \bar{X}_g)\right\}\rho'$$

$$- \frac{1}{c_p}\left[K_{F_u}\Delta H_{F_u} + K_{F_l}\Delta H_{F_l}\right]\left\{X_{H_o} + \tfrac{1}{2}X_{F_o} - (\bar{X}_u + \bar{X}_l + \bar{X}_g)\right\}(X_u' + X_l' + X_g')$$

$$+ \frac{1}{c_p}\left[K_{D_u}\Delta H_{D_u} + K_{D_l}\Delta H_{D_l}\right]X_m\left[\bar{\rho}X_u' + \bar{\rho}X_l' + \rho'(\bar{X}_u + \bar{X}_l)\right] \tag{223}$$

where X_{H_O} and X_{F_O} are the initial mass fractions of oxidizer and fuel respectively.

State

$$p' = \bar{\rho}R_s T' + \frac{c_s^2}{\gamma}\rho' \tag{224}$$

Species

Upper

$$\frac{DX'_u}{Dt} = K_{F_u}\left(X_{H_o} - \frac{1}{2}(\bar{X}_u + \bar{X}_1 + \bar{X}_g)\right)\left(X_{F_o} - (\bar{X}_u + \bar{X}_1 + \bar{X}_g)\right)\rho'$$

$$- K_{F_u}\bar{\rho}\left(X_{H_o} + \frac{1}{2}X_{F_o} - (\bar{X}_u + \bar{X}_1 + \bar{X}_g)\right)(X'_u + X'_1 + X'_g) \qquad (225)$$

$$- \frac{DX'_1}{Dt}$$

Lower

$$\frac{DX'_1}{Dt} = K_{F_1}\left(X_{H_o} - \frac{1}{2}(\bar{X}_u + \bar{X}_1 + \bar{X}_g)\right)\left(X_{F_o} - (\bar{X}_u + \bar{X}_1 + \bar{X}_g)\right)\rho'$$

$$- K_{F_1}\bar{\rho}\left(X_{H_o} + \frac{1}{2}X_{F_o} - (\bar{X}_u + \bar{X}_1 + \bar{X}_g)\right)(X'_u + X'_1 + X'_g)$$

$$+ K_{D_u}(\bar{X}_u + X_m)\rho' + K_{D_u}\bar{\rho}X_m X'_u \qquad (226)$$

$$+ \frac{\sigma}{h\nu}\left[(\bar{X}_u - \bar{\theta}\bar{X}_1)\phi' + \bar{\phi}(X'_u - \bar{\theta}X'_1) + \bar{\phi}\frac{\bar{\theta}\ln\bar{\theta}}{\bar{T}}T'\right]$$

$$- K_{D_1}(X_m\bar{X}_1)\rho' - K_{D_1}\bar{\rho}X_m X'_1$$

Ground

$$\frac{DX'_g}{Dt} = K_{D_1}\left[X_m\bar{X}_1\rho' + X_m\bar{\rho}X'_1\right] - u'\frac{\partial\bar{X}_g}{\partial x} \qquad (227)$$

Gain

$$g' = \frac{\sigma}{\dot{M}_{DF}}\left[(\bar{X}_u - \bar{\theta}\bar{X}_1)\rho' + \bar{\rho}X'_u - \bar{\rho}\bar{\theta}X'_1 + \frac{\bar{\rho}\bar{X}_1\bar{\theta}\ln\bar{\theta}}{\bar{T}}T'\right] \qquad (228)$$

Flux

$$\frac{\partial \phi'}{\partial t} = \frac{c\bar{\phi}}{2L} \left[\int_o^x \alpha_R \rho' dx + \int_o^x \alpha_I g' dx \right] \tag{229}$$

As we are considering supersonic flow, we need to only consider the flowfield downstream of the nozzle bank; thus a Laplace Transform treatment appears tractable. We apply a double transform in both space and time; i.e.,

$$\hat{f}(s,k) = \int_o^\infty \int_o^\infty e^{-st}\, e^{-kx} f(t,x)\, dx dt$$

This produces a set of linear equations from the above partial differential ones. Thus Eqs. (221)-(229) give

Continuity

$$(s + \bar{u}k)\,\hat{\rho} + \bar{\rho}\, k\hat{u} = 0 \tag{230}$$

Momentum

$$\rho(s + \bar{u}k)\hat{u} + k\hat{p} = 0 \tag{231}$$

Energy

$$-\{[K_{F_u} \Delta H_{F_u} + K_{F_l} \Delta H_{F_l}]\{X_{H_o} - \frac{1}{2}(\bar{X}_u + \bar{X}_l + \bar{X}_g)\}\{X_{F_o} - (\bar{X}_u + \bar{X}_l + \bar{X}_g)\}$$

$$+ [K_{D_u} \Delta H_{D_u} + K_{D_l} \Delta H_{D_l}][\bar{X}_u + \bar{X}_l]X_m\}\frac{1}{c_p}\hat{\rho}$$

$$+\{[K_{F_u} \Delta H_{F_u} + K_{F_l} \Delta H_{F_l}]\{X_{H_o} + \frac{1}{2} X_{F_o} - (\bar{X}_u + \bar{X}_l + \bar{X}_g)\} - [K_{D_u} \Delta H_{D_u} + K_{D_l} \Delta H_{D_l}]X_m\}$$

$$\times \frac{\bar{\rho}}{c_p}\{\hat{X}_u + \hat{X}_l\} \tag{232}$$

$$+ (s + \bar{u}k)\hat{T} - k\bar{u}/c_p\bar{\rho}\,\hat{p}$$

$$+ \frac{1}{c_p}[K_{F_u} \Delta H_{F_u} + K_{F_l} \Delta H_{F_l}]\{X_{H_o} + \frac{1}{2} X_{F_o} - (\bar{X}_u + \bar{X}_l + \bar{X}_g)\}\,\hat{X}_g$$

$$= 0$$

State

$$\frac{c_s^2}{\gamma}\hat{\rho} + \bar{\rho} R_g \hat{T} - \hat{p} = 0 \tag{233}$$

Species

Upper State

$$\begin{aligned}
&-K_{F_u}\bar{\rho}(X_{H_o} - \tfrac{1}{2}(\bar{X}_u + \bar{X}_1 + \bar{X}_g))(X_{F_o} - (\bar{X}_u + \bar{X}_1 + \bar{X}_g))\hat{\rho} \\
&+[(s+\bar{u}k) + K_{F_o}\bar{\rho}(X_{F_o} + \tfrac{1}{2}X_{F_o} - (\bar{X}_u + \bar{X}_1 + \bar{X}_g))]\hat{X}_u \\
&+[(s+\bar{u}k) + K_{F_u}\bar{\rho}(X_{F_o} + \tfrac{1}{2}X_{F_o} - (\bar{X}_u + \bar{X}_1 + \bar{X}_g))]\hat{X}_1 \\
&+K_{F_u}\bar{\rho}(X_{H_o} + \tfrac{1}{2}X_{F_o} - (\bar{X}_u + \bar{X}_1 + \bar{X}_g))\hat{X}_g
\end{aligned} \tag{234}$$

Lower State

$$\begin{aligned}
&-[K_{F_1}(X_{H_o} - \tfrac{1}{2}(\bar{X}_u + \bar{X}_1 + \bar{X}_g))(X_{F_o} - (\bar{X}_u + \bar{X}_1 + \bar{X}_g)) + K_{D_u}X_m\bar{X}_u - K_{D_1}X_m\bar{X}_1]\hat{\rho} \\
&+[K_{F_1}\bar{\rho}(X_{F_o} + \tfrac{1}{2}X_{F_o} - (\bar{X}_u + \bar{X}_1 + \bar{X}_g)) - K_{D_u}\bar{\rho}X_m - \frac{\sigma}{h\nu}\bar{\phi}]\hat{X}_u \\
&-\frac{\sigma}{h\nu}(\bar{X}_u - \theta\bar{X}_1)\hat{\phi} \\
&+[K_{F_1}\bar{\rho}(X_{H_o} + \tfrac{1}{2}X_{F_o} - (\bar{X}_u + \bar{X}_1 + \bar{X}_g)) + (s+\bar{u}k) + \frac{\sigma}{h\nu}\bar{\phi}\bar{\theta} + K_{D_1}\bar{\rho}X_m]\hat{X}_1 \\
&+[\frac{\sigma}{h\nu}\bar{\phi}\frac{\bar{\theta}\ln\bar{\theta}}{\bar{T}}]\hat{T} \\
&+K_{F_1}\bar{\rho}(X_{H_o} + \tfrac{1}{2}X_{F_o} - (\bar{X}_u + \bar{X}_1 + \bar{X}_g))\hat{X}_g
\end{aligned} \tag{235}$$

Ground State

$$-(s+2\bar{u}k)K_{D_1}X_m\bar{X}_1\hat{\rho} - K_{D_1}X_m\bar{\rho}\hat{X}_1\bar{u}k + \bar{u}k(s+\bar{u}k)\hat{X}_g = 0. \tag{236}$$

Gain

$$\hat{g} - \frac{\bar{\rho}}{M_{DF}}\left[(\bar{X}_u - \bar{\theta}X_1)\hat{\rho} + \bar{\rho}\,\hat{X}_u - \bar{\sigma}\bar{\theta}\hat{X}_1 + \frac{\bar{\sigma}\bar{X}_1\bar{\theta}\ln\bar{\sigma}}{\bar{T}}\hat{T}\right] = 0 \tag{237}$$

Flux

$$s\hat{\phi} - \frac{c\bar{\phi}}{2L}\{\alpha_R\hat{\rho} + \alpha_1\hat{g}\}/k = 0 \tag{238}$$

Eliminating $\hat{u}$ from Eqs. (230) and (231) and $\hat{g}$ from Eqs. (237) and (238) we obtain

Continuity-Momentum

$$(s + \bar{u}k)^2\hat{\rho} - k^2\hat{p} = 0 \tag{239}$$

Gain-Flux

$$\frac{c\bar{\phi}}{2L}[\alpha_R + \alpha_I\bar{\sigma}(\bar{X}_u - \bar{\theta}\bar{X}_1)]\hat{\rho} + \frac{\bar{\sigma}c\bar{\phi}}{2L}\alpha_I\bar{\rho}\,\hat{X}_u - ks\hat{\phi} \tag{240}$$

$$-\bar{\sigma}\frac{c\bar{\phi}}{2L}\alpha_I\bar{\rho}\bar{\theta}\,\hat{X}_1 + \bar{\sigma}\frac{c\bar{\phi}}{2L}\frac{\alpha_I\bar{\rho}\bar{X}1\bar{\theta}\ln\bar{\sigma}}{\bar{T}}\hat{T} = 0$$

where $\bar{\sigma} = \sigma/M_{DF}$.

The seven equations in variables, $\hat{\rho}$, $\hat{T}$, $\hat{p}$, $\hat{\phi}$, $\hat{X}_u$, $\hat{X}_1$, $\hat{X}_g$ can be written in matrix form

$$[A][\hat{x}] = 0 \tag{241}$$

Thus we have

Transformed Equations

$$\begin{bmatrix} \alpha_{11} & 0 & 0 & 0 & \alpha_{15} & \alpha_{16} & 0 \\ \alpha_{21} & \alpha_{22} & -ks & \alpha_{24} & \alpha_{25} & 0 & 0 \\ (s+\bar{u}k)^2 & 0 & 0 & 0 & 0 & -k^2 & 0 \\ \alpha_{41} & \alpha_{42} & 0 & \alpha_{44} & (s+\bar{u}k) & \alpha_{46}k & \alpha_{47} \\ \alpha_{51} & \alpha_{52} & \alpha_{53} & \alpha_{54}+(s+\bar{u}k) & \alpha_{55} & 0 & \alpha_{57} \\ \alpha_{61} & \alpha_{62}+(s+\bar{u}k) & 0 & \alpha_{64}+(s+\bar{u}k) & 0 & 0 & \alpha_{67} \\ \alpha_{71}(s+2\bar{u}k) & 0 & 0 & \alpha_{74}\bar{u}k & 0 & 0 & \bar{u}k(s+\bar{u}k) \end{bmatrix} \begin{bmatrix} \hat{\rho} \\ \hat{X}_u \\ \hat{\phi} \\ \hat{X}_1 \\ \hat{T} \\ \hat{p} \\ \hat{X}_g \end{bmatrix} = 0 \qquad (242)$$

where

$$\alpha_{11} = \frac{c_s^2}{\gamma}, \quad \alpha_{15} = \bar{\rho}R_g, \quad \alpha_{16} = -1$$

$$\alpha_{21} = \frac{c\bar{\phi}}{2L}\left[\alpha_R + \alpha_I\bar{\sigma}(\bar{X}_u - \theta\bar{X}_1)\right], \quad \alpha_{22} = \frac{\bar{\sigma}c\bar{\phi}}{2L}\ \alpha_I\bar{\rho}$$

$$\alpha_{24} = -\frac{c\bar{\phi}}{2L}\alpha_I\bar{\theta}\bar{\rho}\bar{\sigma}, \quad \alpha_{25} = \alpha_I\frac{c\phi}{2L}\bar{\alpha}\frac{\bar{\rho}\bar{X}_1\bar{\theta}\ln\bar{\vartheta}}{\bar{T}}$$

$$\alpha_{41} = -\frac{1}{c_p}\{[K_{F_u}\Delta H_{F_u} + K_{F_1}\Delta H_{F_1}]\{X_{H_o} - \tfrac{1}{2}(\bar{X}_u + \bar{X}_1 + \bar{X}_g)\}\{X_{F_o} - (\bar{X}_u + \bar{X}_1 + \bar{X}_g)\}$$

$$+\{K_{D_u}\Delta H_{D_u} + K_{D_1}\Delta H_{D_1}\}\{\bar{X}_u + \bar{X}_1 + \bar{X}_g\}X_m\}$$

$$\alpha_{42} = \alpha_{44} = \frac{\bar{\rho}}{c_p}\{[K_{F_u}\Delta H_{F_u} + K_{F_l}\Delta H_{F_l}]\{X_{H_o} + \frac{1}{2}X_{F_o} - (\bar{X}_u + \bar{X}_l + \bar{X}_g)\}$$

$$- [K_{D_u}\Delta H_{D_u} + K_{D_l}\Delta H_{D_l}]\bar{X}_m\}$$

$$\alpha_{46} = -\frac{\bar{u}}{\bar{\rho}c_p} \qquad \alpha_{47} = \frac{1}{c_p}\{X_{H_o} + \frac{1}{2}X_{F_o} - (\bar{X}_u + \bar{X}_l + \bar{X}_g)\}\{K_{F_u}\Delta H_{F_u} + K_{F_l}\Delta H_{F_l}\}$$

$$\alpha_{51} = -[K_{F_l}(X_{H_o} - \frac{1}{2}(\bar{X}_u + \bar{X}_l + \bar{X}_g))(X_{F_o} - (\bar{X}_u + \bar{X}_l + \bar{X}_g) + K_{D_u}X_m\bar{X}_u - K_{D_l}X_m\bar{X}_l]$$

$$\alpha_{52} = K_{F_l}\bar{\rho}(X_{H_o} + \frac{1}{2}X_{F_o} - (\bar{X}_u + \bar{X}_l + \bar{X}_g) - K_{D_o}\bar{\rho}X_m - \frac{\sigma\bar{\phi}}{h\nu}$$

$$\alpha_{53} = -\frac{\sigma}{h\nu}(\bar{X}_u - \bar{\theta}\bar{X}_l)$$

$$\alpha_{54} = K_{F_l}\bar{\rho}(X_{H_o} + \frac{1}{2}X_{F_o} - (\bar{X}_u + \bar{X}_l + \bar{X}_g)) + \frac{\alpha\bar{\phi}\bar{\theta}}{h\nu} + K_{D_l}\bar{\rho}X_m$$

$$\alpha_{55} = -\frac{\sigma\bar{\phi}}{h\nu}\frac{\bar{\theta}\ln\bar{\theta}}{\bar{T}}$$

$$\alpha_{57} = K_{F_l}\bar{\rho}(X_{H_o} + \frac{1}{2}X_{F_o} - (\bar{X}_u + \bar{X}_l + \bar{X}_g))$$

$$\alpha_{61} = -K_{F_u}\bar{\rho}(X_{H_o} - \frac{1}{2}(\bar{X}_u + \bar{X}_l + \bar{X}_g))(X_{F_o} - (\bar{X}_u + \bar{X}_l + \bar{X}_g))$$

$$\alpha_{62} = \alpha_{64} = \alpha_{67} = K_{F_u}\bar{\rho}(X_{H_o} + \frac{1}{2}X_{F_o} - (\bar{X}_u + \bar{X}_l + \bar{X}_g))$$

$$\alpha_{71} = -K_{D_l}X_m\bar{X}_{\cdot} \quad , \quad \alpha_{74} = -K_{D_l}X_m\bar{\rho}$$

The stability of the system can be examined in terms of the characteristic equation derived from Eq. (241); i.e.,

$$\det[A] = 0 \tag{243}$$

An analysis stability of the system is obtained from the Routh criterion for Eq. (243).(36)

The characteristic equation may be obtained from Eq. (242). After tedious algebra this reduces to

$$a_7 s^7 + a_6 s^6 + a_5 s^5 + a_4 s^4 + a_3 s^3 + a_2 s^2 + a_1 s^1 + a_0 = 0 \tag{244}$$

where

$$a_7 = A_6$$

$$a_6 = 6\eta A_6 + A_5$$

$$a_5 = 15\eta^2 A_6 + 5\eta A_5 + A_4 + B_5$$

$$a_4 = 20\eta^3 A_6 + 10\eta^2 A_5 + 4\eta A_4 + A_3 + 5\eta B_5 + B_4$$

$$a_3 = 15\eta^4 A_6 + 10\eta^3 A_5 + 6\eta A_4 + 3\eta A_3 + A_2 + 10\eta^2 B_5 + 4\eta B_4 + B_3$$

$$a_2 = 6\eta^5 A_6 + 5\eta^4 A_5 + 4\eta^3 A_4 + 3\eta^2 A_3 + 2\eta A_2 + A_1 + 10\eta^3 B_5 + 6\eta^2 B_4 + 3\eta B_3 + B_2$$

$$a_1 = \eta^6 A_6 + \eta^5 A_5 + \eta^4 A_4 + \eta^3 A_3 + \eta^2 A_a + \eta A_1 + A_0 + 5\eta^4 B_5 + 4\eta^3 B_4 + 3\eta^2 B_3 + 2\eta B_2 + B_1$$

$$a_0 = \eta^5 B_5 + \eta^4 B_4 + \eta^3 B_3 + \eta^2 B_2 + \eta B_1 + B_0$$

---

36. DiStefano, J.J., Stubberud, A.R., Williams, I.J., "Feedback and Control Systems," McGraw-Hill (1967).

and

$$A_6 = -\alpha_{16} k\eta$$

$$A_5 = \alpha_{15}\alpha_{46} k^2\eta - \alpha_{16}\alpha_{62} k\eta + \alpha_{16}(\alpha_{52} - \alpha_{54}) k\eta$$

$$B_5 = \alpha_{16}\alpha_{53} (\alpha_{22} - \alpha_{24})\eta$$

$$A_4 = -\alpha_{11} k^3\eta - \alpha_{15}\alpha_{46}(\alpha_{52} - \alpha_{54}) k^2\eta + \alpha_{16}\alpha_{62}(\alpha_{52} - \alpha_{54}) k\eta$$
$$+ \alpha_{16}\alpha_{57}\alpha_{74} k\eta$$

$$B_4 = \alpha_{53}(\alpha_{22} - \alpha_{24})\eta[-\alpha_{15}\alpha_{46} k + \alpha_{62}]$$

$$A_3 = \alpha_{11} k^3\eta[(\alpha_{52} - \alpha_{54}) - \alpha_{62}] + \alpha_{15}\alpha_{46}\alpha_{57}\alpha_{74} k^2\eta$$
$$+ \alpha_{15}\alpha_{47}\alpha_{71} k^3 - \alpha_{15}\alpha_{41}\eta k^3 + \alpha_{16}\alpha_{57}\alpha_{62}\alpha_{74} k\eta$$
$$- \alpha_{16}\alpha_{47}\alpha_{55}\alpha_{74} k\eta - \alpha_{16}\alpha_{52}\alpha_{62}\alpha_{74} k\eta$$

$$B_3 = \alpha_{11}\alpha_{53}(\alpha_{22} - \alpha_{24}) k^2\eta + \alpha_{15}\alpha_{46}\alpha_{53}\alpha_{62}(\alpha_{22} - \alpha_{24}) k\eta$$
$$- \alpha_{16}\alpha_{25}\alpha_{47}\alpha_{53}\alpha_{74}\eta - \alpha_{16}\alpha_{22}\alpha_{53}\alpha_{62}\alpha_{74}\eta$$

$$A_2 = \alpha_{11}\alpha_{62}(\alpha_{52} - \alpha_{54})k^3\eta + \alpha_{57}\alpha_{74}k^3\eta$$

$$+\alpha_{15}\alpha_{46}\alpha_{57}\alpha_{62}\alpha_{74}k^2\eta + \alpha_{15}\alpha_{47}\alpha_{62}\alpha_{71}k^3$$

$$-\alpha_{15}\alpha_{47}\alpha_{71}(\alpha_{52} - \alpha_{54})k^3 + \alpha_{15}\alpha_{47}\alpha_{71}k^3\eta - \alpha_{15}\alpha_{42}\alpha_{62}k^3\eta$$

$$+\alpha_{15}(\alpha_{41}\alpha_{52} - \alpha_{41}\alpha_{54})k^3\eta + \alpha_{15}\alpha_{46}\alpha_{52}\alpha_{62}\alpha_{74}k^2\eta$$

$$-\alpha_{15}\alpha_{42}\alpha_{62}\alpha_{71}k^2 + \alpha_{15}\alpha_{42}\alpha_{61}k^3\eta$$

$$+\alpha_{16}\alpha_{55}\alpha_{62}\alpha_{74}(\alpha_{42} - \alpha_{47})k\eta$$

$$B_2 = \alpha_{11}\alpha_{53}\alpha_{62}(\alpha_{22} - \alpha_{24})k^2\eta - \alpha_{15}\alpha_{47}\alpha_{53}\alpha_{71}(\alpha_{22} - \alpha_{24})k^2$$

$$+\alpha_{15}\alpha_{41}\alpha_{53}(\alpha_{22} - \alpha_{24})k^2\eta + \alpha_{15}\alpha_{22}\alpha_{46}\alpha_{53}\alpha_{74}k\eta$$

$$+\alpha_{16}\alpha_{25}\alpha_{53}\alpha_{62}\alpha_{74}(\alpha_{42} - \alpha_{47})\eta$$

$$A_1 = \alpha_{11}\alpha_{47}\alpha_{55}\alpha_{74}k^3\eta - \alpha_{11}\alpha_{52}\alpha_{62}\alpha_{74}k^3\eta$$

$$+\alpha_{15}\alpha_{47}\alpha_{62}\alpha_{71}k^3\eta - \alpha_{15}\alpha_{47}\alpha_{62}\alpha_{71}(\alpha_{52} - \alpha_{54})k^3$$

$$-\alpha_{15}\alpha_{47}\alpha_{71}(\alpha_{52} - \alpha_{54})k^3\eta + \alpha_{15}\alpha_{74}(\alpha_{41}\alpha_{57}\alpha_{51}\alpha_{47})k^3\eta$$

$$+\alpha_{15}\alpha_{62}\alpha_{41}(\alpha_{52} - \alpha_{54})k^3\eta - \alpha_{15}\alpha_{42}\alpha_{62}\alpha_{71}k^3\eta$$

$$+\alpha_{15}\alpha_{42}\alpha_{62}\alpha_{71}(\alpha_{52} - \alpha_{54})k^3 - \alpha_{15}\alpha_{42}\alpha_{61}(\alpha_{52}\alpha_{54})k^3\eta$$

$$B_1 = -\alpha_{11}\alpha_{25}\alpha_{47}\alpha_{53}\alpha_{74}k^2\eta - \alpha_{11}\alpha_{22}\alpha_{53}\alpha_{62}\alpha_{74}k^2\eta$$

$$-\alpha_{15}\alpha_{47}\alpha_{53}\alpha_{71}(\alpha_{22} - \alpha_{24})k^2\eta - \alpha_{15}\alpha_{47}\alpha_{53}\alpha_{62}\alpha_{71}(\alpha_{22} - \alpha_{24})k^2$$

$$-\alpha_{15}\alpha_{21}\alpha_{4}\alpha_{53}\alpha_{74}k^2\eta + \alpha_{15}\alpha_{41}\alpha_{53}\alpha_{62}(\alpha_{22} - \alpha_{24})k^2\eta$$

$$+\alpha_{15}\alpha_{42}\alpha_{53}\alpha_{61}(\alpha_{22} - \alpha_{24})k^2\eta + \alpha_{15}\alpha_{42}\alpha_{53}\alpha_{62}\alpha_{71}(\alpha_{22} - \alpha_{24})k^2$$

$$A_0 = -\alpha_{11}\alpha_{47}\alpha_{55}\alpha_{62}\alpha_{74}k^3\eta - \alpha_{15}\alpha_{47}\alpha_{62}\alpha_{71}(\alpha_{52} - \alpha_{54})k^3\eta$$

$$+\alpha_{15}\alpha_{62}\alpha_{74}(\alpha_{41}\alpha_{57} - \alpha_{51}\alpha_{47})k^3\eta$$

$$+\alpha_{11}\alpha_{42}\alpha_{55}\alpha_{62}\alpha_{74}k^3\eta - \alpha_{15}\alpha_{61}\alpha_{74}(\alpha_{42}\alpha_{57} - \alpha_{47}\alpha_{52})k^3\eta$$

$$-\alpha_{15}\alpha_{62}\alpha_{74}(\alpha_{41}\alpha_{52} - \alpha_{51}\alpha_{42})k^3\eta$$

$$+\alpha_{15}\alpha_{42}\alpha_{62}\alpha_{71}(\alpha_{52} - \alpha_{54})k^3\eta$$

$$B_0 = -\alpha_{11}\alpha_{25}\alpha_{47}\alpha_{53}\alpha_{62}\alpha_{74}k^2\eta - \alpha_{15}\alpha_{21}\alpha_{47}\alpha_{53}\alpha_{62}\alpha_{74}k^2\eta$$

$$-\alpha_{15}\alpha_{47}\alpha_{53}\alpha_{62}\alpha_{71}(\alpha_{22} - \alpha_{24})k^2\eta + \alpha_{11}\alpha_{25}\alpha_{42}\alpha_{53}\alpha_{62}\alpha_{74}k^2\eta$$

$$+\alpha_{15}\alpha_{53}\alpha_{74}[\alpha_{22}\alpha_{47}\alpha_{61} + \alpha_{62}(\alpha_{21}\alpha_{42} - \alpha_{22}\alpha_{41})]k^2\eta$$

$$+\alpha_{15}\alpha_{42}\alpha_{53}\alpha_{62}\alpha_{71}(\alpha_{22} - \alpha_{24})k^2\eta]$$

The value of the spatial wavenumber, k, is taken to be given by the cavity dimension in the flow direction, ℓ. Thus,

$$k \sim 1/\ell = .$$

Thus, we can now numerically specify all the coefficients of the characteristic equation.

D. STABILITY ANALYSIS OF DF LASER MODEL

The values of the laser parameters can be obtained from the "gain equals loss" condition and Eqs. (216) and (220). The "gain equals loss" condition specifies the gain in terms of cavity loss and cavity length such that

$$e^{2gL} = r_1 r_2$$

where r_1 and r_2 are the mirror reflectivities. Thus we obtain the population density of upper and lower states from

$$(\bar{X}_u - \bar{\theta}\bar{X}_1) = g/\bar{\sigma}\bar{\rho}$$

The flux can be obtained from Eq. (216) where we assume

$$\frac{\bar{D}\bar{X}_u}{Dt} \simeq 0 \simeq K_{F_u} \bar{\rho}\bar{X}_{F_o} \bar{X}_{D_{2,o}} - \frac{\sigma\phi}{h\nu} (\bar{X}_u - \theta\bar{X}_1)$$

Thus $\phi \simeq K_{F_u} \bar{\rho}^2 X_{F_o} X_{D_{2,0}} \bar{\sigma} h\nu/(\sigma g)$

Using these criteria, the parameters for a wide range of flow conditions were investigated. The laser conditions are listed in Table 2. Over the entire range of mixing rates, flow velocities, cavity lengths and pressures, use of the Routh criterion specifies that the laser is stable. This can be simply described by reference to the coefficients of Eq. (244). The only matrix coefficient containing contribution from a_R (the density fluctuation induced flux variation) is a_{21} which appears in coefficients B_1 and B_0; these affect only coefficients a_1 and a_0. In general, B_1 and B_0 are significantly smaller than the other terms in a_1 and a_0, resulting in both a_1 and a_0 being positive (if either of these coefficients were negative an unstable root would occur).

The response of the laser to upstream-induced noise disturbances may be described in terms of transfer functions derived from

$$[A][\hat{x}] = [F]$$

where [F] is the forcing function vector. The transfer function between parameter $\hat{x}_n$ and F_n is given by

$$\frac{\hat{x}_n}{F_n} = \frac{\det[A_F]}{\det[A]}$$

where $[A_F]$ is the matrix [A] with the n^{th} column replaced by [F].

TABLE 2. LASER CONDITIONS INVESTIGATED

Cavity length (L) 0.1 - 3.0 m

Mixing length ℓ 1.0 - 10.0 cms

Flow velocity 10^3 - 3 x 10^3 m/sec

Cavity pressure 1 - 10 torr

Cavity density 5 x 10^{-4} - 5 x 10^{-3} kg/m^3

Laser mix 10 He/5 D_2/0.8 F_2

$\bar{M}$ = 5.45

γ = 1.59

Mirror Reflectivities

r_1 = 0.98 r_2 = 0.88

The response of such a system is thus characterized by 1/det[A]. The normalized magnitudes of this function are illustrated in Figure 55. The response is essentially uniform up to frequencies of 10^5 rad/sec, and thereafter rapidly decreases in magnitude with a slope asymptoting to $-\omega^7$. The response reduces in magnitude as cavity pressure is increased.

Obviously, this is only part of the overall transfer function, and further analysis is necessary if the detailed system response is to be determined.

E. DETAILED SYSTEM RESPONSE

The model developed here is a simplification of the real laser behavior. A more detailed and correspondingly difficult approach is required if the full three-dimensional nature of the mode medium interaction is to be investigated. From the previous analysis a simple acoustic or gain fluctuation instability does not appear to occur in the chemical laser. However, the real flowfield may result in other significant mechanisms occuring.

The chemical laser consists of a series of quasi-planar flame sheets (Figure 54). The jets from the nozzle bank are normally in the transition range of Laminar to turbulent flow, where laminar instabilities of the flamesheet are apparent. These instabilities are akin to the Rayleigh-Taylor instability in mixing layers (see for example, Kimura[37] and Toong.[38] Fluctuations in the local gain and flow properties will result in modulation of laser output flux. Whether such a flowfield instablity can lead to an output instability is not clear. The coupling between the array of mixing layers is of importance; if the flowfield is driven by an upstream acoustic disturbance which is identical for all the shear layers, this may result in significant optical coupling. However, a random phasing of oscillation of the array of flame sheets may result in a quite different behavior.

F. SUMMARY

A simplified model of a supersonic chemical laser has been derived and a stability analysis performed. This indicates that the laser is stable across a wide range of operating conditions.

---

37. Kimura, I., Tenth Symposium (Int.) on Combustion, p. 1295-1300, The Combustion Institute (1965).

38. Toong, T.Y., Salant, R.F., Stopford, J.M., Anderson, G.Y., Tenth Symposium (Int.) on Combustion, p. 1301-1313, The Combustion Institute (1965).

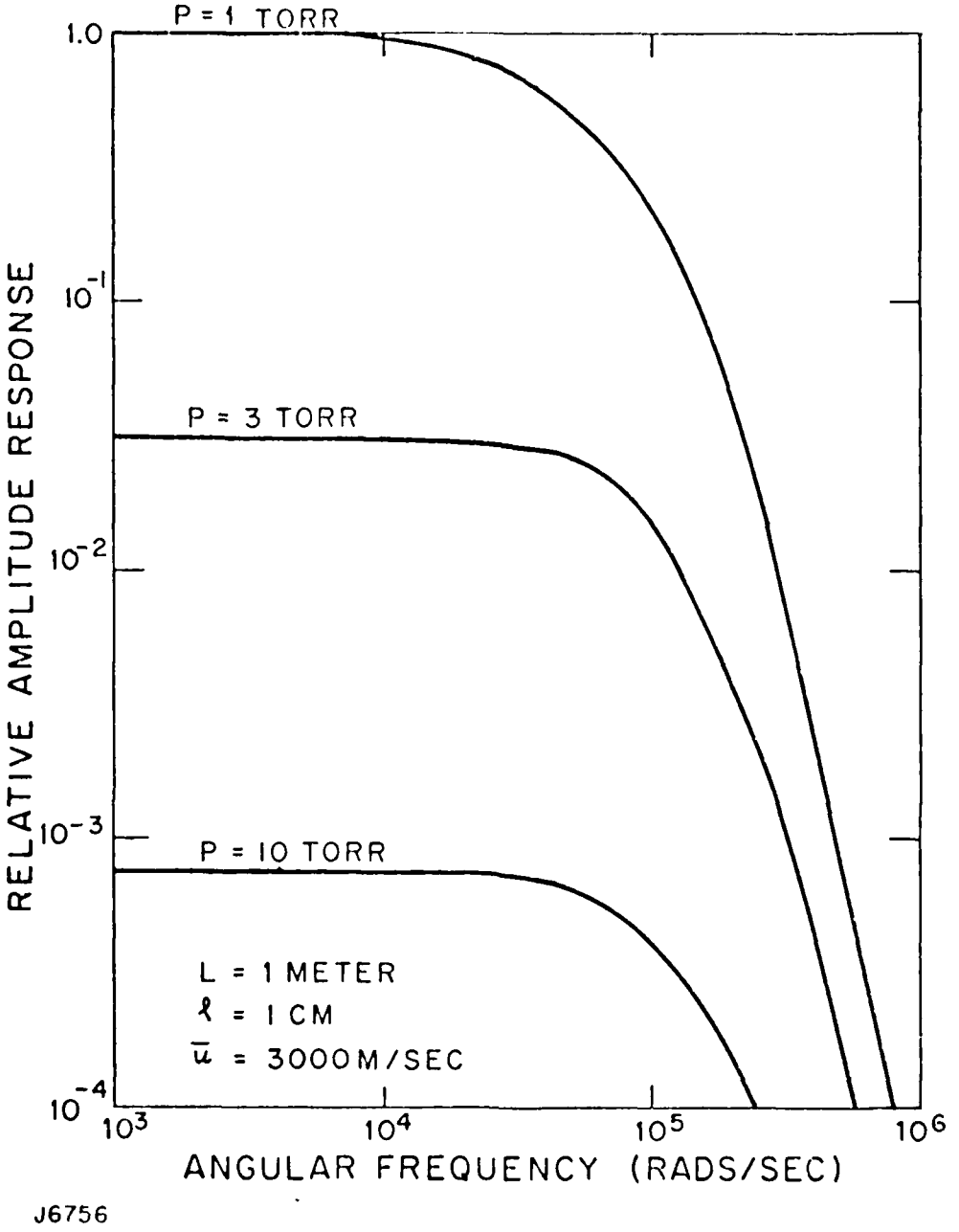

Figure 55. Frequency Response Function

However, the simplifying assumptions remove the possibility of a coupling occurring as a consequence of flame-sheet instability and as such would not appear in the solutions obtained in this work.

The above analysis provides a useful starting point in obtaining a description of possible mode-medium interactions in supersonic mixing lasers. However, it is far from complete and it is recommended that further exploration of the possible behavior of flame-sheet instabilities upon optical performance is necessary.

G. GLOSSARY OF TERMS

a	coefficients in Eq. (244)
A	coefficients in Eq. (244)
B	coefficients in Eq. (244)
c	speed of light
c_s	sound speed
c_p	specific heat
g	gain
h	enthalpy
k	space transform variable
k	kinetic rate coefficient
K	effective rate coefficient (= λk)
l	mixing length scale
L	cavity length
M_{DF}	molecular mass
r	mirror reflectivities
p	gas pressure
$\dot{s}_s$	[illegible]
u	gas velocity
t	time

s	time transform variable
T	temperature
x	axial coordinate
α_I, α_R	flux coupling coefficient in Eq. (219)
α	coefficient in matrix Eq. (242)
β	Gladstone Dale Constant
γ	ratio of specific heats
θ	degeneracy coefficient
λ	mixing parameter
λ	laser wavelength
ρ	gas density
ρ_{ATM}	density at a pressure of 1 atm
σ	lasing cross section
ϕ	intracavity flux
τ	reaction time constant
X	mass fraction
ΔH	enthalpy of reaction
$\bar{\sigma}$	σ/M_{DF}

Subscripts

u	upper state
l	lower state
g	ground state
F	formation rate
D	deactivation rate

SECTION VII

SUGGESTIONS FOR FUTURE RESEARCH

The dynamic models considered in Sections II, IV and VI have made simplifying assumptions on the nature of the laser cavity. In particular, uniform values of gain, density and flux have been assumed in the cavity. More quantitative results may be obtained by perturbing the actual steady-state modes.

The theory contained in Sections II-IV, and VI of this report deals not only with possible system instabilities, but also in the system transfer functions. Accordingly statistics of the system output can be predicted if external perturbations can be modeled. In particular, it would be useful to model the turbulent nature of the nonuniform flow field of the flowing gas. Once the correlation (or distribution) function of the density (i.e., refractive index) function is known, the statisities of the noise driver are known. The theory of this report then allows, via the transfer function, the calculation of the statistics of the laser flux output. In addition, the methods of the theory of light propagation through turbulence can be used to find the statisities of wave-front distortion of the output wave. This problem is especially acute for the chemical laser, where the imperfect mixing of the reactant gases can be modeled to predict the statistics of the system inhomogeneities.

Section V of this report describes a new technique for calculating the self-consistent modes of a saturated, unstable resonator. This is in fact the only reasonably fast technique that we know of for making such a calculation. Although we have only applied it to a strip-resonator geometry, it appears to be generalizable to a circular geometry as well. Calculations of this type can be used, for example, to determine the coupling between modes and the modification of the output coupling of individual modes induced by an external perturbation. We predict that this technique will find wide-ranging applications to laser-resonator problems in the future.

REFERENCES

1. Yoder, M.J. and Ahouse, D.R., Appl. Phys. Lett., 27, 673 (1975).

2. Kellen, P.F., Mattson, A.C., Ahouse, D.R., and Yoder, M.J., Optical Engineering 18, 340 (1979).

3. Korff, D., Glickler, S.L., and Daugherty, J.D., "Acoustic Instability Model for High Power cw EDL Lasers,: 30th Annual Gaseous Electronics Conference, Palo Alto, Cal., Oct. 18-24, 1977.

4. Kellen, P. and Smith, M., Opt. Eng., 18, pp. 157-160 (March/April 1979).

5. Yariv, Quantum Electronics, John Wiley & Sons, NY (1967).

6. Krylov, N., Bogoliubov, N.N., Intro. to Nonlinear Mechanics, Princeton U. Press, Princeton, NJ (1947).

7. Born, M., Wolf, E., Principles of Optics, Pergamon Press, NY (1959).

8. Yariv, A., Introduction to Optical Electronics, Holt, Rinehart, Winston, NY (1971).

9. Siegman, A.E., Proc. IEEE 53, p. 277 (1965).

10. Fox, A., and Li, T., Bell Syst. Tech. J. 40, pp. 453-488.

11. Streiffer, W., IEEE J. Quant. Elect. QE-9, pp. 1102-1113 (November 1973).

12. Berstein, L., Appl. Opt. 7, p. 495 (1968).

13. Chen, T., and Belsen, L., IEEE J. Quant. Elect. QE-9, pp. 1102-1113 (November 1973).

14. Horwitz, P., J. Opt. Sci. Am. 63, pp. 1528-1543 (December 1973).

15. Moore, G., and McCarthy, R., J. Opt. Soc. Am. 67, pp. 228-241 (February 1977).

16. Weiner, M., Appl. Opt. 18, pp. 1828-1834 (June 1979). The basic resonator equation is described in numerous papers, but this work is the only one to express it explicitly in terms of the effective Fresnel number.

17. Perkins, J., and Cason, C., Appl. Phys. Lett. 31, pp. 198-200 (August 1977).

18. Kellen, P., and Smith, M., Opt. Eng. 18, pp. 157-160 (March/April 1979).

19. Born, M., and Wolf, E., Principles of Optics, 5th Ed. (Pergamon, New York, 1975), pp. 752-754.

20. Anan'ev, Y., Sov. J. Quant. Elect. 5, pp. 615-617 (1975).

21. Moore, G., and McCarthy, R., J. Opt. Soc. Am. 67, pp. 221-227 (February 1977).

22. Rigrod, W., J. Appl. Phys. 36, pp. 2487-2490 (August 1975).

23. This formula assumes no interference between forward and backward traveling waves. If such interference exists, the effect is to shift the overall value of intensity by a small amount. See G. Agrawal and M. Lax, J. Opt. Soc. Am. 69, pp. 1717-1719 (December 1979).

24. Louisell, W., et al., Appl. Opt. 18, pp. 2730-2731 (15 August).

25. Sziklas, E., and Siegman, A., Appl. Opt. 14, pp. 1874-1889 (August 1975). The computer algorithm described in this paper is the archetype of a number of simulation codes in use today.

26. Rensch, D., and Chester, A., Appl. Opt. 12, pp. 997-1010 (May 1973).

27. Santana, C., and Felsen, L., Appl. Opt. 17, pp. 2239-2243 (15 July 1978).

28. McAllister, G., et al., IEEE J. Quant. Elect. QE-10, pp. 346-355 (March 1974).

29. Butts, R., and Avizonis, P., J. Opt. Soc. Am. 68, pp. 1072-1078 (August 1978).

30. The observation that the next-to-lowest-loss eigenvalue has a geometric optics asymptote of $M^{0.25}$ has not been noted previously, but is apparent from a close examination of the $|\lambda|$ vs Feff plots.

31. A more rigorous exposition of the contributing diffractive effects of the two edges can be found in C. Santana and L. Felsen, Appl. Opt. 17, pp. 2352-2356 (1 August 1978). Cursiously enough, that paper considers a fixed nonzero tilt (ε) with varying F_{eff}, but does not take up the complementary case, although the formalizm for doing so is present.

32. Gross, R.W.F. and Spencer, D.J., "CW Hydrogen-Halide Lasers," Handbook of Chemical Lasers, R.W.F. Gross and J.F. Bott, ed., Wiley-Interscience, New York, NY, 1976, Chapter 4.

33. "NACL Program Final Report (U)," LTM-292, TRW, July 8, 1976. Classified: CONFIDENTIAL.

34. Cohen, "A Brief Review of Rate Coefficients for Reactions in the D_2-F_2 Chemical System," TR-0074(4530)-9, Aerospace Corp., January 1974.

35. Emanuel, G., "Numerical Modeling of Chemical Lasers," Handbook of Chemical Lasers, op. cit., Chapter 8.

36. DiStefano, J.J., Stubberud, A.R., Williams, I.J., "Feedback and Control Systems," McGraw-Hill (1967).

37. Kimura, I., Tenth Symposium (Int.) on Combustion, p. 1295-1300, The Combustion Institute (1965).

38. Toong, T.Y., Salant, R.F., Stopford, J.M., Anderson, G.Y., Tenth Symposium (Int.) on Combustion, p. 1301-1313, The Combustion Institute (1965).

APPENDIX A

THE PERTURBED RESONATOR

In this appendix we will treat the perturbation expansion of Section II somewhat more rigorously, thereby clarifying the physical meaning of the acoustically induced perturbation of the electromagnetic wave in the resonator.

Writing the part of the electromagnetic wave which propagates to the right as

$$E(\vec{x},t) = u(\vec{x},t)\, e^{i(k_o z - \omega_o t)} + c.c. \qquad (A-1)$$

we find that u satisfies

$$u(\vec{x},t + \tau_o) = \int K(\vec{x},\vec{x}',t)\, u(\vec{x}',t)\, dx' \qquad (A-2)$$

where $K = K_o + K_1$; K_o is the unperturbed propagator (i.e., the propagator in the absence of the acoustic wave); K_1 is the perturbation due to fluctuations in the density (acoustic wave) and gain of the medium (see Section II); $\vec{x}$ and $\vec{x}'$ represent (vector) positions in an x-y plane between the mirrors; and $\tau_o = 2L/c$ is the round-trip time. In the following we write x to denote $\vec{x} = (x,y)$.

The time dependence in K_1 is due to an acoustic oscillation whose frequency is very low compared to $1/\tau_o \cong 5 \times 10^7$ sec^{-1}. This means that

$$\frac{\partial K_1}{\partial t}\, \tau_o << K_1 \qquad (A-3)$$

and we therefore may construct an equation for $\partial u/\partial t$ (x,t) as follows:

$$\frac{\partial u}{\partial t} \cong \frac{1}{\tau_o} [u(x,t + \tau_o) - u(x,t)] = - i \left[\int V_o(x,x')\, u(x',t)\, dx' + \int V_1(x,x',t)\, u(x',t)\, dx'\right] \qquad (A-4)$$

where

$$V_o \equiv \frac{i}{\tau_o} [K_o(x,x') - \delta(x-x')] \qquad (A-5)$$

and

$$V_1 \equiv \frac{i}{\tau_o} K_1(x,x',t) \qquad (A-6)$$

Equation (A-4) has been written in a form which makes it identical with the Schrodinger equation. Thus, we may solve this equation by the well known perturbation-theory techniques used in quantum mechanics.

The integral operator V_o represents an unperturbed, time-independent "Hamiltonian" of the system, while V_1 is the perturbation. To calculate the behavior of $u(x,t)$ (analogous to the wave function of quantum mechanics) we may expand $u(x,t)$ in any complete set $\{\Psi_n(x)\}$ of space-dependent functions:

$$u(x,t) = \sum_n a_n(t) \Psi_n(x) \qquad (A-7)$$

As the set $\{\Psi_n\}$ we choose the eigenfunctions of the unperturbed Hamiltonian V_o, so that

$$\lambda_n \Psi_n(x) = \int V_o(x,x') \Psi_n(x') dx' \qquad (A-8)$$

i.e., Ψ_n is the eigenfunction of eigenvalue λ_n. Equation (A-8) may be shown to be equivalent to

$$\Psi_n(x) = (1 + i\lambda_n\tau_o) \int K_o(x,x') \Psi_n(x') dx' \qquad (A-9)$$

or, for $|\lambda_n\tau_o| << 1$

$$e^{-i\lambda_n\tau_o}\Psi_n(x) = \int K_o(x,x')\Psi_n(x') dx' \qquad (A-10)$$

which is the usual integral form of the eigenvalue equation of a laser resonator. It will be shown below that the natural optical frequency of mode n is

$$\omega_n = \omega_o + \text{Re } \lambda_n$$

i.e., Re λ_n represents the frequency offset of mode n from that of the pure longitudinal mode of frequency ω_o. On the other hand, -2 Imλ_n represents the fractional energy loss per second of mode n.

Substituting Eqs. (A-7) and (A-8) into Eq. (A-4) gives

$$i \sum_m \left[\frac{da_m}{dt} + i\lambda_m a_m \right] \Psi_m(x) = \sum_m a_m(t) \int V_1(x,x',t) \Psi_m(x') \, dx'$$

We now assume that the modes $\{\Psi_n\}$ form a complete orthonormal set. This assumption could be rigorously justified if the unperturbed Hamiltonian V_o were Hermitian; the eigenvalue λ_n would then be real, corresponding to an unperturbed cavity in which all modes have the same value of net loss (loss minus gain). This will clearly not be the situation in an actual unstable resonator. However, the only modes which are interesting are the initially oscillating mode and those modes whose net losses are nearly equal to that of this initial mode; other modes (with significantly higher net losses) will be strongly damped and will therefore never be excited by the acoustic coupling. Thus, it should be a good approximation to assume that for the modes of interest

$$\text{Im}\lambda_n \cong 0 \qquad \text{(A-12)}$$

and therefore

$$\int \Psi_n^* \Psi_m \, dx \cong \delta_{nm} \qquad \text{(A-13)}$$

Equation (A-12) implies that multimode oscillation is possible in our model laser. In fact, such multimode behavior has been observed in cw EDL Lasers.[1] Multiplying both sides of Eq. (A-11) by $\Psi_n^*(x)$ and integrating over all x then yields, with the aid of Eq. (A-13)

---

1. R. Patrick, AERL, private communication.

$$\frac{da_n}{dt} + i\lambda_n a_n = - i \sum_m W_{nm}(t)\ a_m(t) \qquad \text{(A-14)}$$

where

$$W_{nm}(t) = \int\int \Psi_n^*(x)\ V_1(x,x',t)\ \Psi_m(x')\ dxdx' \qquad \text{(A-15)}$$

It will be noted that no use has been made so far of perturbation theory; within the limits of our assumption that the modes of interest are orthonormal Eq. (A-14) is exact.

The meaning of Eq. (A-14) may be elucidated by first examining its solution in the absence of the perturbation (i.e., with $W_{nm} = 0$). We then find that each amplitude a_n satisfies

$$\frac{da_n}{dt} = - i\lambda_n a_n \qquad \text{(A-16)}$$

with the solution

$$a_n = a_n(0) e^{-i\lambda_n t} \qquad \text{(A-17)}$$

so that the electromagnetic wave propagating to the right in the cavity is, from Eqs. (A-1) and (A-7)

$$E(x,t) = \sum_n a_n(0)\ e^{i(k_o z - \omega_n t)}\ \Psi_n(x) + c.c \qquad \text{(A-18)}$$

where ω_n, the natural frequency of mode n, is given by

$$\omega_n = \omega_o + Re(\lambda_n) = \omega_o + \lambda_n \qquad \text{(A-19)}$$

This is clearly what one would expect: each mode which is present initially (at $t = 0$) continues to oscillate freely at its natrual frequency. Because we have not allowed for any damping, none of these modes decays with time; since we have not allowed for any coupling between them, they do not affect one another, either.

Consider the direct effect of the perturbation on an initially oscillating mode. We denote the initial mode by the subscript 0, and take $\lambda_o = 0$. (This is equivalent to defining ω_o to be the frequency of the initial mode.) First-order perturbation theory allows us to ignore the amplitudes of all the other modes to a first approximation. We thus have, from Eq. (A-14)

$$\frac{da_o}{dt} = - i W_{oo}(t)\, a_o \qquad \text{(A-20)}$$

The real part of W_{oo} (defined in Eq. (A-15)) corresponds to a shift in the frequency of the initial mode, while the imaginary part corresponds to a change in the net cavity loss (or gain) per unit time of this mode. Such a loss change could come about as a standing transverse acoustic wave oscillates in amplitude; we would then expect the cavity loss to be modulated at twice the frequency of the acoustic wave. Loss modulation of this type is, in fact, used to mode lock lasers. It could in principle lead to an instability if the initial mode is not uniform in intensity within the cavity, since the heating associated with the cavity loss modulation is then nonuniform and can create an acoustic disturbance. Indeed, our calculations of the modes of an unstable resonator (Section V) show explicitly that a nonuniform mode intensity distribution is to be expected, so this is a possible candidate for an acoustic instability.

Let us now consider the effect of the acoustic perturbation on the other modes of the cavity. Again, we may assume to first order that the amplitude a_o of the initial mode is much larger than that of any other mode. We may thus ignore all amplitudes a_m other than a_o on the right of Eq. (A-14), and set a_o equal to unity. This approximation is, of course, only self consistent as long as the equations predict that $|a_n| \ll 1$ for all $n \neq 0$, i.e., in the initial stages of any buildup of other cavity modes. The a_n's then satisfy

$$\frac{da_n}{dt} + i\lambda_n a_n = - i W_{no}(t)\, a_o(t) \qquad \text{(A-21)}$$

It is useful at this point to consider two types of modes, which we label N and M for definiteness. Mode N is degenerate in frequency with the initially present mode ($\omega_N = 0$), while mode M is offset in frequency by an amount $\omega_M \neq 0$. The mode amplitudes satisfy

$$\frac{da_N}{dt} = - i W_{NO}(t) \qquad \text{(A-22)}$$

$$\frac{da_M}{dt} + i\lambda_M a_M = - i W_{MO}(t) \qquad (A-23)$$

Associated with a_N will be the perturbation in the field, $a_N(t)\mathcal{F}_N(x)$, which we denote by $u_1(x,t)$. It is seen immediately that u_1 satisfies

$$\frac{\partial u_1}{\partial t}(x,t) = - i W_{NO}(t)\, \mathcal{F}_N(x) \qquad (A-24)$$

The perturbation $W_{NO}(t)$ will generally oscillate at an acoustic frequency ω_A, so Eq. (A-24) predicts that u_1 will oscillate at this frequency as well. This means that the perturbation in the actual field E will oscillate at $\omega_o \pm \omega_A$, even though the cavity mode being excited would oscillate naturally (i.e., in the absence of the perturbation) at the frequency ω_o (since it is degenerate in frequency with the initially present mode). This result is expected: the mode N is in a state of forced oscillation, and it oscillates at the driven frequency $\omega_o \pm \omega_A$.

Equation (A-24) is in the form of the starting equation for the flux perturbation in our treatment in Section II. It is thus seen that this treatment pertains to the flux disturbance associated with the buildup of a cavity mode whose unperturbed frequency is degenerate with that of the initial mode. We show in Section II that this buildup does indeed lead to an instability.

On the other hand, we now consider the buildup of a mode of type M, satisfying Eq. (A-23). Since W_{MO} oscillates at frequency ω_A, Eq. (A-23) predicts that the buildup of a_M will be resonantly enhanced when

$$\lambda_M \cong \omega_A \qquad (A-24)$$

We show in Section IV that the buildup of a mode of this type can also lead to an instability, at least in the low-fluence limit.

Finally, we comment on the probability of finding cavity modes which are degenerate or nearly degenerate ($\omega_A/2\pi \sim 10$-20 kHz in LDL experiments). Because of the gas flow, the FDL gas density varies with position in the upstream-downstream direction. The nonuniformity implies that the discrete longitudinal mode frequencies are not well defined, and it should not surprise us to find a continuum of possible eigenfrequencies for such a realistic laser cavity. As a result, a model based on degenerate, or nearly degenerate modes appears to be realistic. On the other hand, calculating the modes of such a loaded resonator is not expected to be an easy task.

APPENDIX B

PROPERTIES OF DEGENERATE MODES AND CONDITIONS FOR THEIR REINFORCEMENT

We wish to derive several results stated without proof in Section II.

First, we calculate the conditions under which two resonator modes may be degenerate in their eigenfrequencies. Consider for simplicity light modes contained in a box of length L and width W. The eigenfrequencies ν_{mn} (measured in cm^{-1}) satisfy

$$\nu_{mn} = \left[\left(\frac{m}{2L}\right)^2 + \left(\frac{n}{2W}\right)^2\right]^{1/2} \tag{B-1}$$

where m and n are integers. For $\nu_{mo} = m/2L >> n/2W$ we may write this as

$$\nu_{mn} \cong \nu_{mo} + \frac{1}{2\nu_{mo}}\left(\frac{n}{2W}\right)^2 \tag{B-2}$$

In order for $\nu_{m-1,0}$ to equal ν_{mn} n must satisfy

$$\frac{1}{2L} = \frac{1}{2\nu_{mo}}\left(\frac{n}{2W}\right)^2 \tag{B-3}$$

i.e.,

$$n = \sqrt{\frac{4W^2}{\lambda L}} \tag{B-4}$$

where $\lambda = \nu_{mo}^{-1}$ is the wavelength of the light.

Equation B-4 suggests an integer n on the order of 10 will permit the frequency ν_{mn} of a transverse mode to be degenerate with that of a longitudinal mode. For example, let W = 5 cm, L = 400 cm, and $\lambda = 10^{-3}$ cm. We obtain

$$n \cong 16. \tag{B-5}$$

From this value we may also determine the number n' of transverse oscillations which are to be expected in an acoustic wave of wave vector k_A which satisfies the phase-matching condition

$$\vec{k}_{m-1,0} + \vec{k}_A = \vec{k}_{m,n} \tag{B-6}$$

For an acoustic mode contained in the transverse dimension of the idealized resonator of this appendix we then have

$$k_A = \frac{2\pi}{\lambda_A} = \frac{2\pi n'}{W} \tag{B-7}$$

so that

$$n' = n/2 \simeq 8. \tag{B-8}$$

This is, of course, only a qualitative result, meant to indicate the approximate number of fringes to be expected. If the approximate conditions of the model (uniform steady state properties for flux density and gain) were rigorously true, n' would have to be a integer to match the acoustic boundary conditions at the walls. In the actual case Eq. (B-8) is only approximate.

Next we show that the wave scattered by the phase grating (standing acoustic wave) produces a flux perturbation of the same shape as the acoustic wave.

The theory of scattering of light by an acoustic wave (Debye-Sears) predicts scattered or diffracted waves at angles of

$$\phi = \pm \frac{\lambda}{\lambda_a} = \pm \frac{\lambda k_a}{2\pi} = \pm \frac{k_a}{k} \tag{B-9}$$

with respect to the initial wave. These waves, at least for a confocal unstable resonator, will after one round trip, return at the same angles.

The interference between these waves and the unperturbed waves will be of the form

$$u_o^* u_1 + u_1 u_o^* = e^{ik_1 \left(\frac{k_a}{k}\right) X} + e^{-ik_1 \left(\frac{k_a}{k}\right) X} = \cos k_a X \tag{B-10}$$

if u_1 has the same unperturbed frequency (i.e., if $k_1 \simeq k$) as the original wave. The situation is illustrated in Figure B-1.

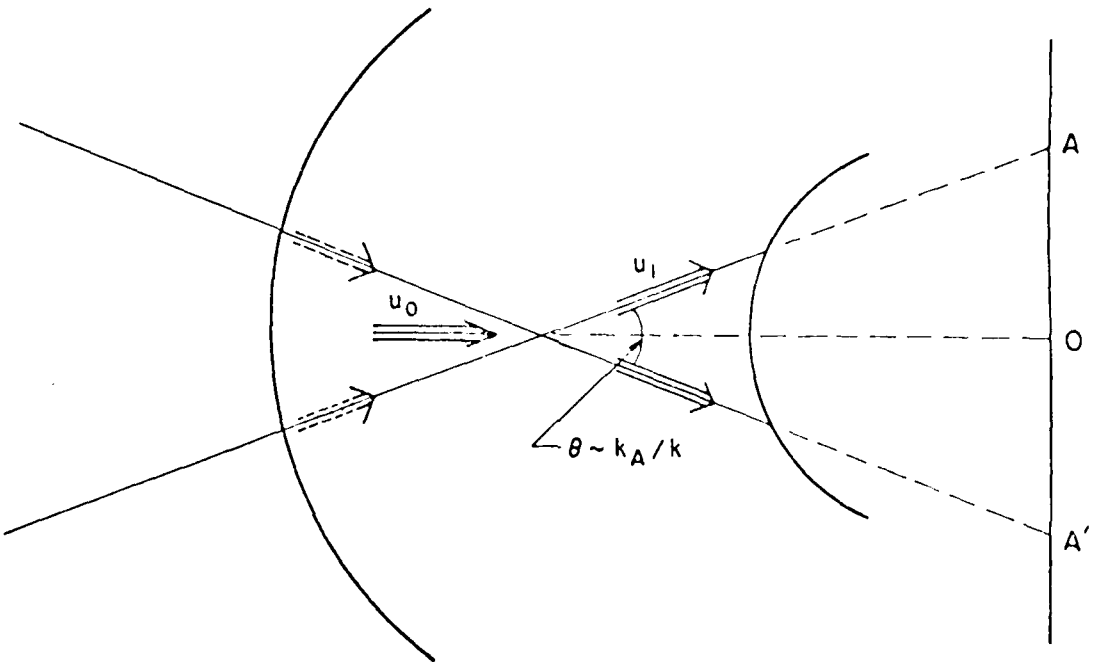

Figure B-1. Illustration of the Reproducibility of the Scattered Wave. The unperturbed wave focuses (virtually) at the point O in the common focal plane of the two mirrors. The scattered waves also focus in this plane but at slightly displaced points A and A'. The return waves after one round trip will then be in the same direction as the original scattered waves.

Finally, we justify our assertion that the density perturbation is independent of z, the light propagation direction. If in the notation of Section II u_1, and hence ϕ_1, has, in fact, a different $k_\parallel$ than ϕ_0, then, after the common factor $\exp i(kz - \omega t)$ is factored out, $\phi_{1\ell}$ can be written

$$\phi_{1\ell} \sim \cos\left[k_a x - \frac{\pi z}{L}\right] \tag{B-11}$$

Now the gain and heating equations will be inconsistent unless $g_{1\ell}$ and $\rho_{1\ell}$ have this same additional z behavior. However, since the thickness of the medium is of the order of half the separation of the mirrors (or less) in a typical case, the z-variation will be insufficient to cancel out the effects of the mode-medium interaction and we are justified in neglecting it.

APPENDIX C

In this appendix, we present a semi-heuristic justification for Eq. (60) of the text.

Let us assume the heating is one dimensional (flow direction) and uniform in the region $(-b/2) \leq x \leq (b/2)$. In this case, Fourier and Laplace transforming Eq. (57) leads to

$$\rho_1(k,s) = \frac{-2(\gamma-1)\, F_1(s)\, k \sin k\frac{b}{2}}{(s+ivk)\left[(s+ivk)^2 + c_s^2 k^2\right]} \tag{C-1}$$

where $F_1(s)$ represents the temporal history of the heating and we have used the F-transform of a step function. Then, by contour integration we obtain

$$\rho_1(x=0,s) = \frac{(\gamma-1)\, F(s)}{c_s^2 s}\left[e^{-\frac{sb}{2v}} - e^{-\frac{sb}{2c_s}\Big/\left(1-\frac{v^2}{c_s^2}\right)} \cosh \frac{sb}{2c_s}\left\{\frac{v/c_s}{1-\frac{v^2}{c_s^2}}\right\}\right] \tag{C-2}$$

Expanding about $s = 0$ we find that the first two terms in the brackets are the same as the expansion of

$$\rho_1(x=0,s) \approx \frac{-(\gamma-1)\, F(s)}{c_s^2}\,\frac{v_1}{s+v_2} \tag{C-3}$$

where

$$v_1 = \frac{1 - \frac{v}{c_s} - \frac{v^2}{c_s^2}}{1 + \frac{v}{c_s} - \frac{v^2}{c_s^2}} \tag{C-4}$$

and

$$v_2 = \frac{2v}{b} \cdot \frac{1 - \frac{v^2}{c_s^2}}{1 + \frac{v}{c_s} - \frac{v^2}{c_s^2}} \qquad \text{(C-5)}$$

We may arrive at a result similar to Eq. (C-3) by making the substitution

$$s + ivk \to s + v_2 \qquad \text{(C-6)}$$

For $v/c_s \sim 0.5$, we have

$$s + v_2 \approx s + 1.25\,\frac{v}{b} \qquad \text{(C-7)}$$

In the text we have taken, somewhat arbitrary $s + v/b$ as the damping term on intuitive grounds for all values of v/c_s, since we expect the convective damping to be of the order of (flush time)$^{-1}$.

APPENDIX D

RESONATORS

1. EMPTY RESONATOR (STABLE)

There are many ways in which the equations satisfied by the eigenfunctions of an empty, stable resonator can be formulated. In this appendix a derivation based on classical potential theory will be presented, since that provides the most lucid extension to the analysis to be presented later on.

The steady-state wave equation for a transverse electromagnetic wave (Helmholtz equation) is given by $\nabla^2 E + k^2 E = 0$ where $k^2 = \omega^2/c^2$, ω is the wave frequency, c is the speed of light and E is the Laplace-transformed transverse component of the electric field. The solution to this equation can be written in terms of the Huygens-Fresnel-Kirchhoff integral by means of Green's identities(1)

$$E(x,y,z) = \frac{1}{4\pi} \int_A \left(E_s \frac{\partial G}{\partial n} - G \frac{\partial E_s}{\partial n} \right) dA \qquad (D\text{-}1)$$

where G is the appropriate Green's function, A is the area of interest, E_s and $\partial E_s/\partial n$ are the electric field and its normal derivative on the surface respectively. Thus, once the field and its normal derivatives on the bounding surfaces are given, the field everywhere can be determined. This approach has the disadvantage that it requires the specification of both the electric field and its normal derivative on the surface. In general, either the function or its normal derivative will be specified. These are the Dirichlet and Neumann boundary conditions, respectively. Note that mixed conditions are allowed where Dirichlet is specified over part of the bounding surface and Neumann over the rest of it but not both at the same time over the same surface. Thus, it is necessary to reformulate the solution in terms of so called dipole and singlet charge distribution. For the Dirichlet problem this implies that(2)

---

(1) Born, M. and Wolf, E., Principles of Optics, Pergamon Press, NY (1959).

(2) Mikhlin, S.G., Integral Equations, Pergamon Press, NY (1957).

$$E(x,y,z) = \frac{1}{4\pi} \int_A \mu(x') \frac{\partial}{\partial n} G(x,x') \, dA \qquad (D-2)$$

and the dipole layer μ satisfies

$$E^- = \mu + \int_A \mu \frac{\partial G}{\partial n} \, dA \qquad (D-3)$$

where E^- is the value of the electric field on the boundary, n is the normal direction, A is the surface area and G is the appropriate Green's function for the problem at hand. For three-dimensional problems it is

$$G(x,x') = \frac{e^{ik \cdot r}}{r} \qquad (D-4)$$

Consider applying this procedure to the stable resonator shown in Figure D-1 which consists of the two mirrors with unequal radii of curvature separated by a distance D. In the Fox-Li calcualtions for the stable resonator only the fields on the mirrors are determined, that is only μ is solved for. Since fields on the mirrors vanish Eq. (D-3) reduces to

$$\mu_1 + \int_{M_1} \mu_1 \frac{\partial}{\partial n_{11}} \frac{e^{ikS_{11}}}{S_{11}} + \int_{M_2} \mu_2 \frac{\partial}{\partial n_{21}} \frac{e^{ikS_{12}}}{S_{12}} = 0 \qquad (D-5)$$

$$\mu_2 + \int_{M_1} \mu_1 \frac{\partial}{\partial n_{21}} \frac{e^{ikS_{21}}}{S_{21}} + \int_{M_2} \mu_2 \frac{\partial}{\partial n_{22}} \frac{e^{ikS_{22}}}{S_{22}} = 0 \qquad (D-6)$$

where μ_1, μ_2, M_1, M_2 are the dipole layers and minor areas of mirrors 1, 2, respectively; S_{12}, S_{11}, S_{22} are the distances between the mirrors including curvature terms and the distances of different points on the same mirror. Writing the first two terms in Eq. (D-6) as $\gamma_1 \mu_1$ and the first and last term in Eq. (D-6) as $\gamma_2 \mu_2$ these equations can be rewritten as

$$\gamma_1 \mu_1 = \int_{M_2} \mu_2 \frac{\partial}{\partial n_{21}} \frac{e^{ikS_{12}}}{S_{12}} = 0 \qquad (D-7)$$

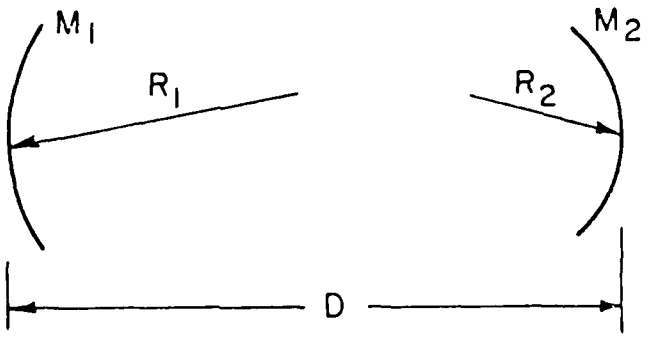

J6767

Figure D-1. Empty Stable Resonator

$$\gamma_2 \mu_2 + \int_{M_1} \mu_1 \frac{\partial}{\partial n_{21}} \frac{e^{ikS_{21}}}{S_{21}} = 0 \qquad \text{(D-8)}$$

Substituting Eq. (D-8) into (D-7) results in the conventional integral equations for the Fox-Li problem.(3) In order to solve these equations the paraxial approximation is made, that is, the term proportional to S^{-2} in Eqs. (D-7) and (D-8) is neglected. The question of what happens when the resonator is loaded will now be addressed.

2. LOADED RESONATOR (STABLE)

The Maxwell equations appropriate to the loaded resonator are,

$$\nabla \cdot \varepsilon_o \bar{E} = - \nabla \cdot \bar{\mathbb{P}} \qquad \text{(D-9)}$$

$$\nabla \cdot \bar{B} = 0 \qquad \text{(D-10)}$$

$$\nabla \times \bar{E} = - \frac{\partial B}{\partial t} \qquad \text{(D-11)}$$

$$\nabla \times H = \varepsilon_o \frac{\partial \bar{E}}{\partial t} + \frac{\partial \bar{\mathbb{P}}}{\partial t} \qquad \text{(D-12)}$$

where it has been assumed that there are no free-charge currents flowing, but the medium responds to electromagnetic waves through the polarization term.

Equations (D-9) and (D-10) can be combined into a single wave equation,

$$\nabla^2 E - \frac{1}{c^2} \frac{\partial^2}{\partial t^2} E = \mu_o \frac{\partial^2}{\partial t^2} \mathbb{P} - \frac{1}{\varepsilon_o} \nabla \nabla \cdot \mathbb{P} \qquad \text{(D-13)}$$

For transverse electromagnetic waves the last term vanishes. The polarization term is assumed to be given by

---

(3) Fox, A.G., Li, T., Bell Syst. Tech. J 40, 453 (1961).

$$\vec{P} = \epsilon_o (\chi \vec{E}_k + c.c) \qquad (D-14)$$

where χ is the complex dielectric susceptibility. Its form in terms of more fundamental quantities is given in Appendix E. Substituting Eq. (D-14) into the Laplace transform of Eq. (D-13) results in

$$\nabla^2 \vec{E} + k^2 E = 0 \qquad (D-15)$$

where

$$k^2 = \frac{\omega^2}{c^2} \left(1 + \chi_r + i\chi_i + i \frac{\sigma_r}{\epsilon_o \omega}\right) \qquad (D-16)$$

where σ_r denotes a phenomenological loss term due to output coupling from the resonator ($\chi_i < 0$ for lasing medium). The solution to Eq. (D-16) can be written in the same form as Eq. (D-1). However, since again only the field or the normal derivative would normally be specified it is necessary to recast the problem in terms of one for the singlet or doublet charge layers. However because of the amplification by the medium it is now necessary to calculate the fields between the mirrors as well. The only difference in the doublet equation (Eq. [D-3]) would be that the Green's function has a growing (decaying) part to it because of the complex values of k. Hence special attention has to be paid to the convergence properties of the various functions if equations of the form of Eqs. (D-7) and (D-8) are to be derived. Most of the difficulties are swept into finding the appropriate Green's function.

At this point an alternative procedure could be used. This is the method of multiple scaling. This technique is used to essentially eliminate the rapid variation in the $\hat{z}$ direction (direction normal to the mirrors) from the equations. To implement this the fields are assumed to have e^{ikz} variations in the $\hat{z}$ direction. Substituting this form into Eq. (D-15) and averaging over the fast variation results in

$$\nabla_T^2 E + 2ik_z \frac{\partial}{\partial z} E + k'^2 E = -i \frac{\omega^2}{c^2} \chi_i E - i\omega\mu_o \sigma_r E \qquad (D-17)$$

where

$$k'^2 = \frac{\omega^2}{c^2}\left(1 - \frac{k_z^2 c^2}{\omega^2} + \chi_r\right) \qquad \text{(D-18)}$$

∇_T^2 is the transverse Laplacian operator.

The solution to Eq. (D-17) can in principle be found by the following procedure:

$$E(r) = \left(-i\frac{\omega^2}{c^2}\chi_i - i\omega\mu_o\sigma_r\right)\int d^3r\, E(r')\, G(\bar{r},\bar{r}') \qquad \text{(D-19)}$$

(for a homogeneous medium) and G satisfies,

$$\nabla_T^2 G + 2ik_z\frac{\partial}{\partial z}G + k'^2 G = \delta(\bar{r}-\bar{r}') \qquad \text{(D-20)}$$

Note that E and G have to be found in the entire region between the mirrors, not just on the mirrors themselves as had been the case for the empty resonator.

Even assuming that the Green's function can be found Eq. (D-19) is still an integral equation which has to be solved, either numerically or in a perturbation series (Born appproximation). Solving the coupled set of Eqs. (D-19) and (D-20) is more akin to a scattering calculation than it is using the Green's theorem of the previous section.

3. LOADED RESONATOR (UNSTABLE)

The unstable resonator is even more complicated. Figure D-2 illustrates why this is the case. The wave Eq. (D-17) still applies. However, it has to be solved in a number of regions and the solutions have to be matched across the boundaries.(4) Region I contains both a right-going and a left-going wave. Region II contains only a right-going wave with gain. Region III contains a right going wave but with no gain ($\sigma_r = 0$). In the analysis where the equations are solved in all the regions, $\sigma_r = 0$ because the loss is calculated explicitly. The procedure for solving Eq. (D-17) is to assume a right-going cylindrical wave and a left-going spherical wave in Region I, to assume only a cylindrical wave with different propagation constants in Regimes II and III, and then matching the wave solutions across the different boundaries. Thus, the field in Region I is given by (for the lowest-order mode)

(4) Moore, G.T. and McCarthy, R.J., J. Opt. Soc. AM, 67, 228 (1977).

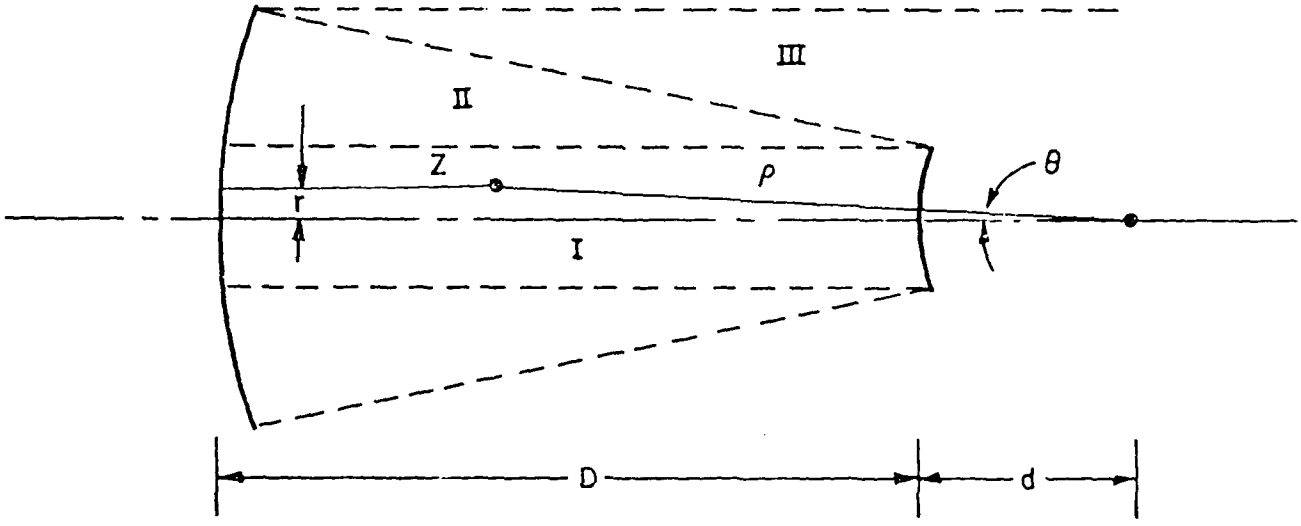

J6766

Figure D-2. Confocal Unstable Resonator

$$E = f\ (r,\theta)\ e^{ik_{\parallel}(z + d + D)} - G(\rho,\theta)\ \frac{e^{ik_{\perp}\rho}}{\rho} \qquad \text{(D-21)}$$

where f and G are to be determined. The boundary condition E = 0 on the two mirrors lead to

$$f(o,r) = \frac{G(d + D, r/(D + d))}{D + d} \qquad \text{(D-22)}$$

$$f(D,r) = \frac{G(d, r/d)}{d} \qquad \text{(D-23)}$$

where the magnification is given by M = (D + d)/d and the longitudinal mode number, $k_{\parallel} = n\pi/D$. Substituting Eq. (D-21) into (D-17) leads to

$$\frac{\partial f}{\partial z} + \frac{\nabla_T^2 f}{2ik_{\perp}} = \frac{g}{2} f \qquad \text{(D-24)}$$

$$\frac{\partial G}{\partial \rho} + \frac{\nabla_T^2}{2ik_{\perp}} = \frac{g}{2} f \qquad \text{(D-25)}$$

where ∇_T^2 is the transverse Laplacian in cylindrical and spherical coordinates in the two equations and $g = -(\ldots^2/k_{\perp}{}^2 e^2)k_{\ldots i}$ is the gain. Equations (D-24), and (D-25) were solved by Moore and McCarthy[4] using an assumed gain profile. The self-consistent gain profile is given by the Rigrod equation,

$$V \cdot gV = -\frac{g}{\tau} - \frac{g}{\tau}\frac{\ldots}{\ldots_s} + P \qquad \text{(D-26)}$$

where V is the flow velocity of the medium τ, is the deactivation time, $\ldots$, $\ldots_s$ are the optical and saturation flux and P is the pumping rate. Since $\ldots \sim E^2$ this implies that the equations for the fields [(D-24), (D-25)] are coupled through the gain Eq. (D-26). Since the two fields are described in different coordinate systems, this makes the self-consistent problem particularly complex. A complete numerical analysis of these Eqs. (D-24), (D-25) and (D-26) is described in Section V.

In the integral formulation of the mode-medium instability the solution to the equilibrium problem is written as $u_o = \int K_o u_o dr$ where K_o is the appropriate Huygens-Fresnel operator.

APPENDIX E

DERIVATION OF THE POLARIZATION TERM

In the simple approach taken here the electrons are treated semiclassically. Since the medium treated is a low-density gas the electric field seen by the individual molecules is the same as the external field. (In a denser medium like a solid the effective field would be $E_{eff} = E + P/3$ where P is the polarization shielding.)(1)

Thus individual electrons obey the following equation,

$$\ddot{X} + \gamma\dot{X} + \omega_B^2 X = -\frac{e}{m}E \qquad (E\text{-}1)$$

where γ, ω_B are the damping (growth) rate, the orbital binding frequency and E is the stimulating electric field. Solving Eq. (E-1) leads to

$$X = \left[\frac{e}{m}\frac{E_K e^{-i\omega_o t}}{\omega_o^2 - \omega_B^2 - i\gamma\omega_o} + c\cdot c\right] \qquad (E\text{-}2)$$

where c·c is the complex conjugate. The dipole moment of the molecule is given by

$$p = -ex \qquad (E\text{-}3)$$

Finally the macroscopic polarization for a density of N molecules per cubic centimeter is given

$$P = Nex$$

or

$$P = -N\frac{e^2}{m}\left[\frac{E_K e^{-i\omega_o t}}{\omega_o^2 - \omega_B^2 - i\gamma\omega_o} + c\cdot c\right] \qquad (E\text{-}4)$$

The effects of a spatially varying wave are included in a similar fashion. The Fourier transformed polarization has real and imaginary parts given by,

---

1. Panofsky, W.K.H., Phillips, M., Classical Electricity and Magnetism, Addison-Wesley, Mass. (1955).

$$\mathbb{P}_{kr} = - \frac{Ne^2}{m} \frac{\omega_o^2 - \omega_B^2}{R} E_k \qquad \text{(E-5)}$$

$$\mathbb{P}_{ki} = - \frac{Ne^2}{m} \frac{\gamma\omega_o}{R} E_k \qquad \text{(E-6)}$$

where $R = (\omega_o^2 - \omega_B^2)^2 + \gamma^2\omega_o^2$. Thus the real part modifies the index of refraction while the imaginary part produces stimulated emission of absorption depending upon the population inversion. In Section IV $\mathbb{P}$ is written as follows:

$$\mathbb{P} = \varepsilon_o \chi_r E + i\varepsilon_o \chi_i E \qquad \text{(E-7)}$$

Comparing Eq. (E-7) with Eqs. (E-5) and (E-6) leads to

$$\chi_r = - \frac{Ne^2}{\varepsilon_o m} \frac{\omega_o^2 - \omega_B^2}{R} \qquad \text{(E-8)}$$

$$\chi_i = - \frac{Ne^2}{\varepsilon_o m} \frac{\gamma\omega_o}{R} \qquad \text{(E-9)}$$

In addition $\mathbb{P}$ was defined in terms of χ. Equations (E-8) and (E-9) give a simple definition of the frequency dependence of χ.

In the semiclassical treatment growth (stimulated emission) is obtained by letting γ be negative.(2) In addition, the effects of saturation enter γ by making it amplitude dependent. Thus a relationship between the semiclassical treatment and the quantum treatment is obtained by identifying χ_i with the gain of the medium. The gain is given by

$$g = - \frac{\omega_o^2}{k_o^2 c^2} N_o \chi_i k_o \qquad \text{(E-10)}$$

Hence

$$g = \frac{e^2}{m\varepsilon_o} \frac{\omega_o^2}{k_o^2 c^2} \frac{\gamma\omega_o}{R} N k_o \qquad \text{(E-11)}$$

Finally this allows the polarization to be written in terms of the gains as,

---

2. Yariv, A., Quantum Electronics, John Wiley & Sons, NY (1967).

$$\mathbb{P}_k = \varepsilon_o \alpha_R \, N\mathbb{E}_k - i\varepsilon_o \frac{k_o^2 c^2}{\omega_o^2} \frac{q}{k_o} \mathbb{E}_k \qquad \text{(E-12)}$$

This result is derived on the basis of assuming that N and q remained constant over the time period of interest. The generalization allows both of these to change and is treated in Section IV. Note that even in equilibrium q is allowed to vary because of saturation dependence on the fields. That is γ depends on the fields, but α_R is assumed to have a weak dependence on the fields at best. For single frequency electric fields the polarization in real space and time is given by

$$\mathbb{P}(r,t) = \mathbb{P}_k + \mathbb{P}_k^* \qquad \text{(E-13)}$$

where $\mathbb{P}_k$ is given by Eq. (E-12). For more complicated electric fields the Fourier-Laplace inversion of Eq. (E-12) has to be performed. This leads to a convolution integral of the form,

$$\mathbb{P}(r,t) = \int dr'dt' \; \chi(r',t') \; \mathbb{E}(r-r',t-t') \qquad \text{(E-14)}$$

where χ is given by Eqs. (E-8) and (E-9).

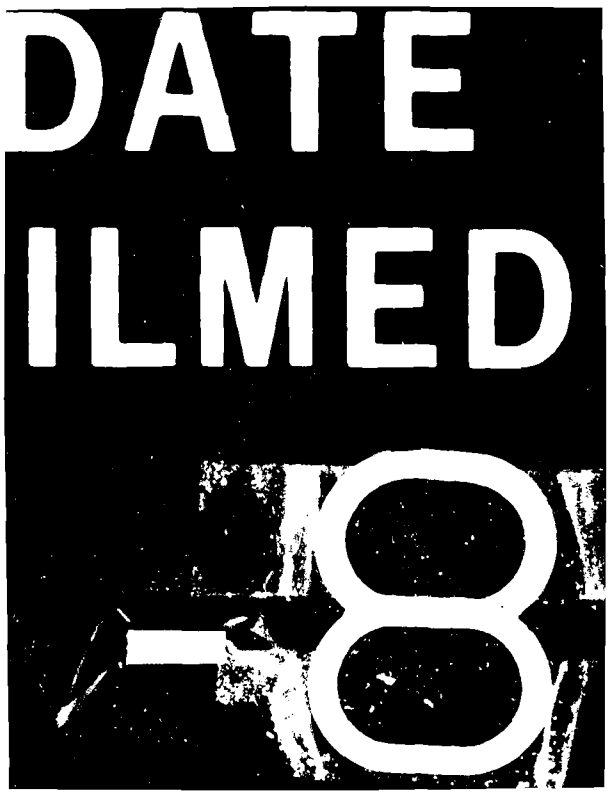
DATE
ILMED
-8